The University of Adelaide
School of Mechanical Engineering

Investigation of Welding Fume Plumes Using Laser Diagnostics

Owen Lucas

20th of August 2008

Chapter 1

Introduction

Since early civilisation, metals have been an important building material for humans. Metals exhibit a number of unique material properties that lend themselves to an endless list of applications. For this reason, metals now form a critical part of modern life. Therefore there is not only a reliance on the production of metals but also the processes that are involved in manufacturing the raw product into its functional form. Welding is one of a number of common metal fabrication processes used by industry. The process of welding is used to fuse two pieces of material together by temporarily melting or plasticly deforming an area at the joint interface. When done correctly, this process results in a permanent uniform joint with good mechanical properties. It is the strength and low cost of a welded joint that makes welding attractive among a number of other joining methods such as gluing, bolting, or riveting.

One popular method of welding involves using an electrical arc to briefly melt a small portion of the materials in the area being joined. The molten material from the pieces being joined amalgamates and later solidifies bonding both parts together. While there is an increased use of automation in arc welding processes, many applications, particularly in the areas of construction and maintenance, require direct human intervention to control them. It is the close proximity of the operator to the arc that exposes them to a number of different occupational hazards. One of these hazards is the exposure to gases and fine particles created by arc welding which are collectively known as fume. Inhaling these airborne byproducts can potentially cause a number of short and long term health complications. These can have a detrimental effect on the operator's productivity and quality of life. It is therefore a requirement of the employer to minimise exposure, not only to maintain productivity but, to satisfy legislation that protects workers.

The exposure of employees to welding fumes can be controlled in a number of ways. At the current time one of the best methods of minimising fume exposure is through provision of adequate ventilation. This ventilation is often provided by the use of mechanical fans and ducting. The purpose of this equipment is to provide fresh clean

air to the welder while removing the fume from the work place before it can be inhaled. Despite being the primary method of fume exposure control little is currently known on how fume dissipates from source into the workplace.

Previous research has encountered difficulties investigating fume plumes close to the welding arc. This has necessitated the use of water and numerical models to simulate the dissipation. Applications of laser diagnostics in the field of combustion research and fluid dynamics indicated that they may be useful in determining some of the processes involved in welding fume dissipation. Laser diagnostics utilise the unique properties of coherent light to provide a number of advantages over other measurement techniques. The use of lasers allow for the relatively non-intrusive detection of a number of properties with good temporal and spacial resolution.

The aim of the work presented here is to consider some of the laser techniques used in combustion research and implement them in a welding environment to investigate the plume close to the welding arc. Using these techniques it is hoped that additional understanding of the fume plume dissipation can be gained. Such information is of significance in the design of welding equipment and fume extraction systems. Improvements in fume extraction and ventilation would reduce worker exposure and minimise the health impact from the occupation.

Chapter 2

Literature review

2.1 Welding

Modern products rely on a several different joining processes for construction. These joining processes can be divided into the following groups (Norrish 1992):

- mechanical joining
- adhesive bonding
- brazing and soldering
- welding

Welding processes utilise heat or pressure or a combination of the two to form a joint where there is a continuity of nature between the parts. In obtaining this continuity the material at the joint interface is liquefied or plastically deformed in some way.

Welding processes come in a diversity of forms to accommodate different applications and materials. One branch of welding processes for joining metals involves an electrical arc as a source of heat to temporarily melt the material at the joint. The popularity of arc welding can be attributed to a number of advantages including its productivity, controllability, quality of weld and range of metals to which it can be applied.

Arc welding utilises an electrical discharge between an electrode and the parent material of the metal workpiece where the join is to be formed. The electrical discharge in arc welding is created by applying a voltage potential between the workpiece and the welding electrode. When the tip of the electrode is brought into close proximity with the workpiece the region between them becomes ionised. The current carrying capability of the ionised gas completes the electrical circuit formed by the welding torch, power supply and workpiece allowing a flow of electrons. In welding processes the density of flowing charge carriers is sufficient to generate arc temperatures capable of locally

melting most metals. Using this localised heating, material on both sides of the joint is melted to form a pool of molten metal. In most welding processes additional material is deposited into the molten pool to improve the resulting metallurgy and weld geometry. When the arc is either extinguished or moved the molten weld pool cools to a point where it solidifies to form a solid joint.

Arc welding incorporates a number of processes with variations for different applications. In relation to occupational exposure to fume, arc welding processes that require the direct intervention of an operator are of most interest. The work presented in this thesis will focus on Gas Metal Arc Welding (GMAW) and Flux Cored Arc Welding (FCAW). The interest in these welding processes arise due to the proximity of the operator and the amount of fume produced. Both GMAW and FCAW are extensively used throughout a range of different industries due to their high productivity.

2.1.1 Gas metal arc welding

Gas metal arc welding (GMAW) has become one of the most widely used welding processes in industry. The popularity can be attributed to a number of advantages that GMAW has over traditional welding processes such as manual metal arc welding (MMAW). One of the most significant advantages of GMAW is the high productivity obtainable on the majority of common engineering metals. The high productivity achievable with GMAW can be attributed to the continuous consumable wire electrode by which metal is added to the weld pool. As a result metal can be rapidly deposited and the welding operator does not need to regularly stop to replace the electrode. A cut away image of the tip of a GMAW torch can be seen in Figure 2.1.

Figure 2.1: Gas metal arc welding (Norrish 1992)

In GMAW the arc is struck between the metal onto which the weld is deposited and the wire electrode fed axially through the welding torch. This wire electrode is fed into the torch from a wire spool during welding by a mechanical drive system. A coaxial flow of shielding gas is used to protect the arc and the molten metal surfaces from the atmosphere. This shielding gas also plays an important role as the ionisation medium in which the arc conducts. Common shielding gases include pure inert gases or mixtures of argon, helium, oxygen and carbon dioxide. Metal from the wire electrode is melted and vaporised by heat arising from the arc and is transfered into the molten weld pool formed at the joint interface. The welding torch is moved along the joint depositing metal into the weld pool which later solidifies to form a permanent joint. Commonly the deposited metal leads to a raised profile at the joint known as a weld bead. Figure 2.2 shows a person using GMAW in a workshop environment. In this application the worker holds the torch to move the arc along the joint depositing metal.

Figure 2.2: GMAW in a workshop

2.1.1.1 Welding arcs

The welding arc arises from current flowing through the ionised gases between the wire electrode and the work piece to complete an electrical circuit. The characteristics of the arc and the resultant weld are governed by a number of complex chemical, electrical and thermal interactions. In total arc welding processes are subject to more than 20 variables, many of which are interdependent (Yeomans 1994).

Prior to arc initiation the gaseous medium between the electrode and the workpiece has a very high electrical resistance. In GMAW this resistance is overcome by the electrode contacting the workpiece to form a short circuit, producing metal vapour and a medium through which charge carrying particles can move. Once initiated the heat generated by the arc is sufficient to maintain the ionised current carrying region. This

region consists of molecules, atoms and ions from the shielding gas and the metals involved.

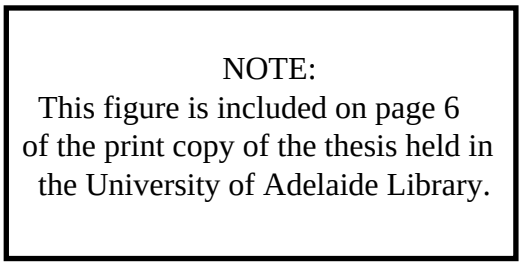

Figure 2.3: GMAW voltage potential (Yeomans 1994)

Traditional GMAW is typically operated with a direct current electrode positive (DCEP) polarity. In such a configuration the positive wire electrode becomes the anode and the workpiece becomes the cathode. Therefore the current carrying arc allows for the transfer of electrons to the electrode and positively charged ions to the workpiece. A schematic of the voltage potential across a DCEP GMAW arc is shown in Figure 2.3. The total voltage potential V_T across the arc is the sum of the individual components V_R, V_A, V_{PC} and V_C (Yeomans 1994). The total current I_T through the welding arc is the sum of the current due to the electrons I_E and the positively charged ions I_P. The total power dissipated by the arc is the product of $I_T \times V_T$ the majority of which is dissipated in the form of heat. It should be noted however that this heat is not dissipated uniformly through the arc resulting in areas of different temperature. A numerical model of the temperature distribution in a GMAW arc is displayed in Figure 2.4. In GMAW the characteristics of the arc are time dependent as metal transfers through the arc from the electrode to the workpiece. The resulting arc is therefore less stable than that generated in welding processes with non consumable electrodes such as gas tungsten arc welding (GTAW).

It was previously stated that many of the variables that govern arc properties are interdependent. Based on this interdependence it is not unexpected that the relationship between the arc voltage V_T and the current I_T is non linear. The actual operation of the arc occurs when the voltage and current match that of the output of the power supply used to drive the electrical circuit.

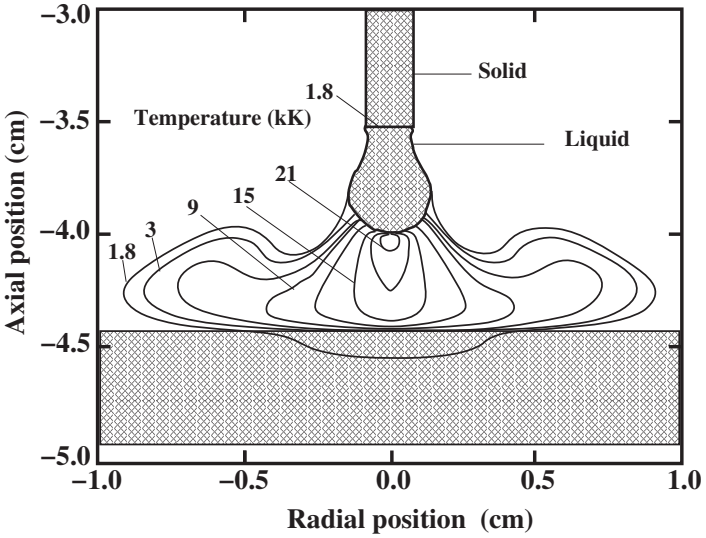

Figure 2.4: Calculated temperature contours within a GMAW arc and electrode with a mild steel wire of 1.6mm diameter at a current of 200A (Haidar 1998)

2.1.1.2 Power supply

The power supply used for GMAW has a strong influence on the properties of the arc produced. Traditionally for GMAW a voltage controlled power supply is used. In this case the voltage is regulated to produce a near uniform output. This characteristic is a requirement to control the arc length making it suitable for operation with an automated wire feed system. This self adjusting arc length occurs because as the wire feed reduces the arc length the resistance across the arc reduces. Fixed voltage and decreasing resistance results in an increased current as depicted in Figure 2.5. The higher current with near constant voltage increases the heat input and the rate at which the electrode melts which will in turn increases the arc length. The voltage generated by the power supply can therefore be used as a control of arc length. The wire feed rate can also be used to obtain some control on the arc current. A wide range of voltage and current are used depending on the application. GMAW operation may utilise voltages between 15 to 40 Volts and currents between 50 to 500 Amps.

Physically this voltage controlled power supply can be implemented in several ways. Common modern power supplies generate the low voltage high current output used for welding by using solid state electronics. These electronics produce a high frequency mains voltage which reduces the size, weight and cost of the transformer required while obtaining higher efficiency. Such inverter power supplies have reasonable responsiveness to welding transients and can be used to provide a number of output wave forms with modern digital control electronics.

Power supplies operate from either single or three phase mains. The majority of industrial power supplies use three phase due to the high power demands and the smoother DC output that can be rectified from it. The output from the power supply is trigger activated only being energised during the welding process.

Figure 2.5: GMAW power source characteristics (Yeomans 1994)

The output from the power supply is connected to the contact tip in the welding torch via a cable contained in the torch lead. The contact tip transfers power to the electrode wire running through it. The contact between the contact tip and the wire is one of many critical factors in determining the stability of the welding arc (Fanning et al. 2004). To complete the electrical circuit the work piece is connected back to the power supply via the return lead. Electrical resistance in the cables result in voltage drops in the welding circuit. For this reason the voltage at the power supply is not the same as that at the welding torch. Likewise the voltage of the workpiece is not the same as the return at the power supply.

2.1.1.3 Droplet transfer

GMAW obtains high deposition rates through the use of an automatically feed wire electrode from which metal is transfered into the weld pool. The movement of this metal is interrelated with the properties of the arc and impacts on resultant weld properties (Zhu & Simpson 2005). This metal transfer can occur in several different ways termed droplet transfer modes resulting from the forces and heat transfer in and around the arc. Four general droplet transfer modes are dip, globular, spray and streaming, however there are many other phenomena observable.

Dip transfer occurs when the heating of the electrode by the arc and the forces involved are insufficient to detach molten droplets from the wire. The result is that the moving electrode contacts the workpiece extinguishing the arc, as depicted at time C in Figure 2.6. Having formed a direct link the short circuit produced increases the current in the electrode. The high current increases the ohmic heating in the wire forming a molten portion that detaches from the wire and enters the weld pool. The removal

of this material from the wire reestablishes the gap between the workpiece and the electrode reinstating the arc. The welding variables and power supply characteristics are critical in controlling the current during the short circuit event and amount of spatter generated. Dip transfer has a relatively low heat input resulting in a small molten weld pool. Dip transfer is widely used when welding on inclined or overhead surfaces and where heat input may be detrimental to the metallurgy.

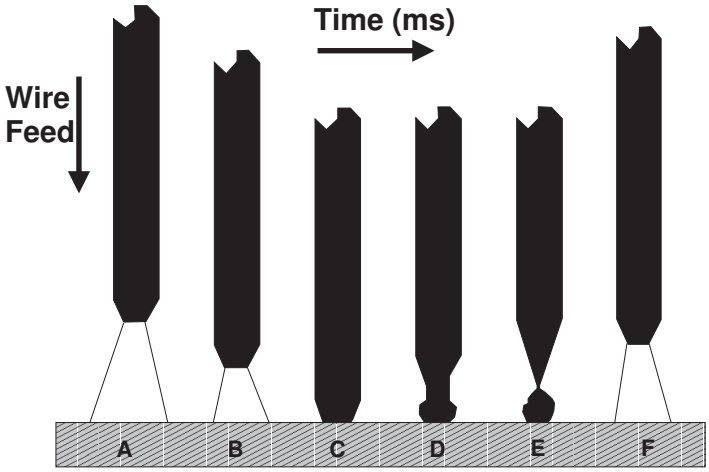

Figure 2.6: Mechanism of dip transfer (Norrish 1992)

Globular transfer is a free flight transfer mode. That is to say that the electrode does not come in direct contact with the workpiece, rather the metal is transfered in droplets and the arc is not extinguished as in dip transfer. Globular transfer is characterised by large droplet formation on the electrode before detaching primarily due to gravitational forces. The formation of the large droplets means the detachment rate is low and only one droplet is ever in flight. Generally globular transfer occurs at higher voltages than that of dip transfer but still relatively low currents. Globular transfer is rarely used in practical GMAW due to low productivity and poor surface finish on the resulting weld bead.

Spray transfer is characterised by detached droplets of similar size or slightly smaller than the electrode diameter. While the droplets are smaller than in globular transfer the detachment rate is much higher. Spray transfer occurs above a transition current where the electromagnetic forces start to play a dominant role in droplet detachment. The higher current driving spray transfer results in good weld penetration and high deposition rates. For this reason it is widely used in industry, particularly for welding on horizontal surfaces. Table 2.1 displays typical transition currents from globular to spray transfer for different wire diameters and shielding gases for plain carbon steel.

Streaming transfer occurs at currents above that required for spray transfer. This results in an extended necked molten region at the end of the electrode wire. The droplets that detach from this region are smaller in diameter than that of the electrode wire. The high frequency of droplet detachment along with usually high voltages means that more than one droplet may be in flight between the electrode and the weld pool

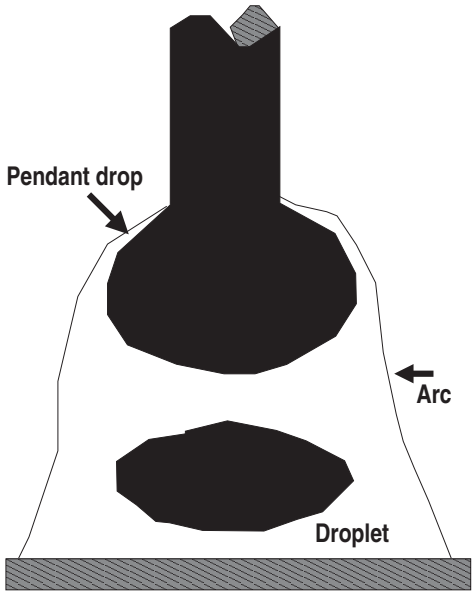

Figure 2.7: Mechanism of globular transfer (Norrish 1992)

Wire diameter (mm)	Argon/5%CO_2	Argon/10%CO_2	Argon/15%CO_2
0.8	140	155	160
1.0	180	200	200
1.2	240	260	275
1.6	280	280	280

Table 2.1: Spray transition currents (Amps) for plain carbon steel wire diameters with various shielding gas mixtures (Norrish 1992)

at any one time. Due to the high heat input this transfer mode is often used to weld thick sections and where high deposition rates are desirable.

The detachment of droplets from the electrode are governed by the forces acting on the molten portion; these include gravitational force, aerodynamic drag, electromagnetic, surface tension and vapour jet forces. In free flight modes the droplet will break away from the electrode when the forces propelling the droplet exceed those retaining the droplet. The magnitude and even direction of these individual forces is dependent on wide number of welding parameters. Change of these welding parameters can result in a change in droplet mode. This change however is not clearly defined and some welding variables can result in mixed mode droplet transfer in between clearly defined modes.

Modern power supplies and wire feed units can be used to implement control strategies to assist desirable droplet transfer. For instance modulation of the voltage in a pulsed operation can be used to generate spray transfer by increasing peak current to promote droplet detachment, while keeping the mean current and heat input relatively low. This additional control can be used to improve weld metallurgy, bead profile and ease of operation.

2.1.1.4 Shielding gas

The shielding gases used for GMAW provide several critical functions and is therefore an important consideration. The primary functions of the shielding gas are to protect the weld from the atmosphere and to act as an ionising medium in which the arc is formed. Inert gases, particularly argon, were initially used leading to the name by which the process is still commonly termed, Metal Inert Gas (MIG) welding. Inert gases such as argon and helium, or mixtures thereof, are still used for welding of reactive metals such as Titanium, Magnesium and Aluminium. However it has become common practise to use active gases or additions for welding many ferrous alloys. Widely used mixtures include argon and carbon dioxide with small additions of oxygen. These active additions are intended to control arc stability, droplet transfer, penetration, heat input and weld bead profile. Active gases however can increase the loss of alloying elements and in the case of carbon dioxide increase the carbon content of the weld metal. Many proprietary gas mixtures can be obtained for particular welding applications.

The shielding gas flow rate is another welding variable of consideration. The flow rate needs to be sufficient to provide protection of the arc and the weld pool from the atmosphere. However excessive gas usage is undesirable given cost considerations. Very high gas flow rates may have a detrimental effect on arc stability and weld bead profile. Many welding units provide variable pre and post weld gas flow times to improve shielding.

2.1.1.5 Welding wire

The consumable electrode wire is yet another critical consideration in GMAW. This wire is fed from a spool along a conduit and axially through the torch. The chemical composition of the welding wire is typically similar to the metal being joined. Additional alloying components may be added to account for elemental loss during the welding process. Additions may also be made to the electrode to control the fluidity of the weld pool and improve the microstructure of the resultant weld metal. The majority of ferrous wires are copper coated. Copper coating intends to reduce the sliding friction of the wire making it easier to feed through the torch and reducing wear of the conduit through which it is fed. In addition copper coating assists the conduction between the contact tip and the wire. Copper coating may also prevent surface oxidation of the wire. Some wires may have additional coatings to protect the surface, reduce friction or as a result of production. In some cases such additional coating is considered undesirable.

Welding wires come in a number of diameters. Diameters frequently found in industry are 0.9, 1.2 and 1.6 mm. Choice of wire diameter is made in consideration of the required deposition rate and penetration. The speed at which the wire is fed is used to control arc current.

The welding wire can be fed from the spool to the welding torch in a number of ways. The smoothness of this feed is also critical in determining arc stability. In many instances rollers mounted on the wire feed unit are used to push the welding wire through the welding torch lead along a spiral liner. Some welding torches have a drive unit mounted at the operator end to pull the wire through the torch lead resulting in a smoother wire feed at the contact tip. However due to the added complexity, weight and cost the use of such torches is avoided where possible. The use of such torches is more common in nonferrous than ferrous welding. Recent advanced welding processes utilise a modulated extend and retract wire feed synchronised with a pulsed power supply waveform to deposit metal at very low heat inputs (Bruckner 2005).

2.1.2 Flux cored arc welding

Flux cored arc welding (FCAW) is becoming increasingly popular as it offers the high productivity available with GMAW while providing additional benefits and flexibility. The hardware involved in FCAW is similar to that of GMAW. As the name suggest FCAW utilises a consumable wire which contains flux powder which is incorporated axially into the wire during production. The proportion of flux in the wire is usually only 15 to 20% with the outer metal sheath making up the remainder (Yeomans 1994). The composition of this flux varies greatly depending on the intended application. The flux may contain alloying elements, deoxidants, arc stabilisers and slag forming compounds. The presence of such compounds significantly influence the properties of the arc and the resultant weld.

The composition of the flux can be configured to produce a self shielding wire. In this case the decomposition of flux powder provides sufficient shielding of the weld pool that additional shielding gas is not required. This is useful for applications where transporting and storing shielding gas bottles is difficult such as in field maintenance operations. The flux in this case contains high levels of deoxidants such as aluminium. High concentrations of deoxidants and vapour forming compounds result in a weld metallurgy that is not as good as that obtainable from gas shielded welding (Yeomans 1994). Flux cored wires designed for operation with gas shielding can produce very high quality welds due to the combined effect of the shielding gas and the flux. The slag overlay produced from flux compounds protect the cooling weld bead from the environment. With correct selection of welding variables FCAW can, in some situations, provide metal deposition rates higher than that obtainable from GMAW. Since labour is the major cost in weld production higher deposition rates can offset the additional cost of the flux cored wire (Norrish 1992). FCAW wires can contain high levels of alloying elements in the core to produce alloy deposits. Such wires are widely utilised in mining and mineral processing to deposit hard overlays on wear surfaces.

While flux cored wires provide a number of advantages and additional process flexibility

there are a number of drawbacks. Firstly the production of a slag overlay requires removal which is particularly critical to maintain an acceptable metallurgy and minimise slag inclusions with multi-pass weld runs. The presence of flux in the wire imposes additional constraints on the welding variables. Selection of voltage, current, stand off, stick out and traverse rate are critical to the decomposition of the flux powders to produce desirable results. Getting these settings correct and maintaining them for a particular wire and application can be time consuming and costly. Another drawback can be the large amount of welding fume generated by the FCAW process that poses an occupational hazard to operators.

2.2 Welding fume

Welders face a diverse range of serious occupational hazards. One of these hazards is the exposure to the airborne gases and aerosols known as fume formed from welding processes. The quantity and chemical complexity of welding fume resulting from arc welding processes is of particular concern. Variables such as type of process, filler metal, welding current, arc length and shielding gas flow are involved in determining the composition and concentration of the fume produced (Farwer 1989).

2.2.1 Components of welding fume

Welding fume comprises of a number of gaseous and particulate compounds. The range of compounds found in welding fume is a result of the physical and chemical processes in and surrounding the high temperature welding arc. The energy dissipated in the electrical arc forms a high temperature plasma. From measurements and numerical calculations, as shown in Figure 2.4, temperatures over 20000°K are reached at some points within the arc. Arc temperature is an important property as it produces the environment necessary for chemical reactions between elements in the parent material, filler wire, atmosphere and shielding gases or fluxes.

2.2.1.1 Gases

In GMAW and shielded FCAW the shielding gas used makes up the majority of the gaseous fume. However due to the relatively low toxicity of such fume it is believed to present minimal adverse long term health effects. While lower in concentration gases, such as ozone, phosgene and nitrogen oxides produced by the welding process are considered to be of greater potential risk due to the high toxicity of these substances.

Nitric oxide NO is formed when air comes in contact with hot gases, from the arc or the hot surface of the workpiece being welded (Anderson & Wiktorowicz 1995*a*). The

formation of nitric oxide is therefore dependent on the heat input of the welding process and the effectiveness of the gas shielding that protects the arc from the atmosphere. It is suggested that processes such as FCAW that have a high heat input and rely solely on the shielding provided by the decomposition of flux, have the highest levels of nitric oxide formation (Anderson & Wiktorowicz 1995*b*).

Ozone O_3 is considered to be a particularly hazardous gas to inhale as it is a powerful oxidiser. Unlike most other fume constituents ozone does not necessarily form immediately adjacent to the arc. This is because ozone is formed photochemically due to the interaction between ultraviolet (UV) light emitted by the welding arc and atmospheric oxygen O_2 (Sipek 1980). It is believed that UV light in the wavelengths from 130nm to 242nm are primarily responsible for this photochemical reaction (Anderson & Wiktorowicz 1995*a*). Due to the effect of UV the light spectrum emitted from the arc is important in ozone formation. The spectrum of light emitted is dependent on the chemical composition of the arc. It is believed that the spectrum emitted from the welding of aluminium and stainless steel is responsible for higher ozone production on these metals.

Due to the reactiveness of ozone it can break down into other chemical species. One well known reaction takes place between ozone and nitric oxide to form nitrous oxide NO_2 and oxygen O_2 (Farwer 1989). This reaction and other reactions in the destruction of ozone can be assisted by the catalytic effects of the particulate fume component (Anderson & Wiktorowicz 1995*a*).

Other gaseous welding fume components arise from other substances used in the manufacturing process. Chemicals such as phosphine can be formed from the break down of protective rust proofing layers applied to steels. Similarly phosgene can be formed by the break down of metal cleaning solvents on the material surface or as vapours in the work place (Australian National Occupational Health and Safety Commission 1990). Proper metal preparation and work shop practises can minimise the formation of these highly toxic compounds.

2.2.1.2 Solid particles

The particulate matter in welding fume can originate in several separate ways and can have a variety of compositions. The composition of these particles is dependent on the type of material being welded, the type of filler metal being used and the type of flux or shielding gas. In welding processes that use no flux, such as GMAW, the solid particles produced comprise almost entirely of metal and metal oxides. In GMAW there are two main processes through which these metal particles form resulting in two classifications of fume, being microsplatter and fine fume (Deam, Bosworth, McAllister, Norrish, Brooks, Zhou, Haidar, Lowke, Farmer & Simpson 2000). Microsplatter is formed from small molten droplets that detach from the metal transfered from the

consumable electrode to the weld pool. The small molten droplets that make up microsplatter remain in a liquid state during the formation process and quench in the atmosphere surrounding the arc. Due to the surface tension of the molten material the droplets and the resulting fume particles are greater than 1 micron in diameter. In most practical applications of GMAW only a small portion of the total particulate fume formation is microsplatter (Deam, Simpson & Haidar 2000). The other classification, fine fume, generally makes up the majority of particulate matter formed by GMAW and presents the greater health risk. A large proportion of fine fume is formed by the condensation of metal vapour at the edges of the welding arc. In addition fine fume can also be formed from vapour evaporating from splatter ejected from the welding process (Jenkins & Edgar 2005). At formation fine fume particles range from a few nanometres to about 500nm in diameter. These fine fume particles can amalgamate after formation to produce chains, networks and clusters of fume particles (Deam et al. 1997). The composition of the particulate welding fume is similar to that of the parent and electrodes being used. However due to the dependence on vaporisation in the formation process there is a tendency for the particulate matter to have slightly higher concentrations of metals that vaporise more readily. The particulates formed from the welding process typically dissipate into the workplace by way of a plume that is initially thermally buoyant. If proper ventilation is not provided much of the fume dissipation occurs through a region where the operator is breathing.

2.2.2 Health effects of welding fume

The inhalation of welding fume can produce a number of short and long term health complications. Effects of exposure to welding fume depend on many welding and environmental variables. These include the welding process, consumable and parent material involved. Environmental factors such as ventilation and exposure duration also contribute to the health effects of fume on welders.

When assessing the impact of welding fume it is useful to break the effects into acute and chronic, although with some diseases it is difficult to differentiate between them. The differentiation between acute and chronic is made difficult due mainly to the causes of the latter being poorly understood. A summary of some potential health effects from inhaling welding fume is displayed in Table 2.2.

2.2.2.1 Acute effects

Acute effects are generally exhibited quickly and are often caused by significant doses of inhaled fume. Due to the short time span between significant exposure and the onset of symptoms the two can be easily linked and have been well, but not conclusively, researched. Usually acute illnesses involve the respiratory system and a reduction in

Table 2.2: Some health effects and their reported causes in welders (Hewitt 1996)

pulmonary function. In many cases acute symptoms are the precursor to future chronic effects.

A common acute health effect is metal fume fever which has been estimated to affect up to 30% of welders (Liss 1996). It is characterised by influenza like symptoms produced from an immune reaction. This illness is primarily attributed to the inhalation of freshly formed oxides, particularly those of copper, magnesium, cadmium and zinc (Hewitt 1996). In many cases the fume originates from a surface coating on the material being welded. The symptoms of metal fume fever usually abate within a day of exposure but it is suspected that the effect of prolonged exposure could lead to chronic conditions of the immune system (Liss 1996).

Another common symptom is irritation of the respiratory tract which exhibits as a dryness of the throat, tickling, coughing, tightness of the chest and difficulty in breathing (Health and Safety Executive 1990). Many of these symptoms usually disappear within several hours after the exposure has ended. This irritation can be associated with changes in lung function which in extreme cases cause lung fibrosis and oedema (Hewitt 1996). These changes in part can be attributed to the exposure of oxides of nitrogen, carbon, metal and other oxidising agents.

2.2.2.2 Chronic effects

One of the most serious though rare chronic respiratory effects is that of asphyxiation caused by working in confined poorly ventilated work areas (Hewitt 1996). The lack of ventilation allows fume and shielding gases to build up to a point where they displace the available oxygen that sustains the operator.

More typically chronic effects exhibit as a number of health complications caused by accumulative effects of extended occupational exposure. The exact causes are generally poorly understood often due to the time over which the welder is exposed and the time between exposure and the onset of symptoms. This time makes it hard to relate a symptom to a number of different potentially harmful exposures.

Chronic respiratory diseases where a link to welding fume is suspected include bronchitis, emphysema and asthma (Hewitt 1996). These diseases have a higher occurrence in welders than the general population but it is difficult to eliminate other possible causes to form a direct link to the inhalation of welding fume (Liss 1996). Other possible causes include the occupational exposure to a number of different materials such as solvents, asbestos and airborne particles from other metal working processes. There is also a number of recreational causes such as smoking that further complicate the formation of a direct link.

The inability to form a direct link can also be found when considering whether welding fume is carcinogenic (IARC 1990). In 1984 the International Institute on Welding (IIW) published a statement on a possible excess cancer risk among stainless steel workers (*Welding in the World* vol.22, No. 7/8 p.184) (Zschiesche 1993). This possible excess risk however could not be directly linked to welding due to a lack of published data on the topic. On the 27th of February 1992 commission VIII of the IIW which monitors publications in relation to health and safety in welding issued a further statement which included the following.

> Since the 1984 statement many studies have been completed. Commission VIII now concludes that, on the balance of the evidence from these studies, welders as a group have a slightly greater risk of developing lung cancer than the general population. This risk, although slight can not be neglected.
>
> The cause of the excess risk has not been completely identified. While tobacco and asbestos exposure, often more common in the welders studied than in the population generally, are known causes of lung cancer they do not provide a complete explanation. The role of welding processes must be considered. The studies do not show welding processes in general or of a specific type to be a definite cause of the excess.

The statement then went on to suggest that compounds found to be carcinogenic in other situations such as chromium and nickel, which are both found as alloying elements in many steels, may be likely causes.

Chronic illnesses caused by the toxicity of welding fume are not localised to the respiratory system affecting other parts of the body, particularly organs. In a study of the cytotoxicity of welding fume it was found that the welding of stainless steel was more hazardous than that of mild steel (Liss 1996). The increased toxicity of fume from stainless steel is primarily attributed to the content of chromium compounds (IARC 1990, Liss 1996).

The extended exposure to welding fume has been linked to a condition referred to as siderosis (Hewitt 1996). This is caused by the buildup of fine fume particles in the lungs which can damage lung tissue and reduce lung function. The buildup of these

metal particles in the lungs exhibit as a light clouding on chest X-rays and can be found several years after exposure (Hewitt 1996).

2.2.3 Fume exposure reduction

Considering the health effects that welding fumes cause it is important to limit the exposure of humans as much as possible. This is of significant importance in occupational situations where the accumulative effects of long term exposure are more likely to result in adverse health effects. When considering the reduction of a hazard it is common to consider the following control strategies.

- Elimination, substitution and process modification
- Administrative controls
- Use of personal protective equipment
- Engineering controls

2.2.3.1 Elimination, substitution and process modification

Reducing the exposure to humans can be made through process elimination, substitution or modification. Elimination of the need to join or deposit metal would eliminate the risks of welding entirely but since this is such an important operation in production this is unobtainable. The substitution of welding with another joining processes such as gluing, bolting or riveting would eliminate welding fume but may be more costly, less effective or introduce their own unique hazards. Different welding processes produce less fumes than others but often with limitations on the productivity, effectiveness, cost and materials to which they can be applied. Process modification can be used to reduce the exposure of the operator to fume but are often limited by process requirements other than the minimisation of fume. Good work shop practises such as the proper preparation of the material and selection of welding variables can significantly reduce but not eliminate exposure.

2.2.3.2 Administrative controls

There are several forms of administrative controls that can be applied in a welding environment. One way of limiting the exposure of the operator to welding fume is to control the time that the operator spends welding. This means that the welder can work up to the point where they have reached a certain level of exposure. The obvious draw back of such a process is that it limits the productivity of the welder. Such strategies require the rate at which the worker is exposed to be known which is difficult in most

industrial situations. This also assumes that the maximum level of exposure is a safe level of exposure producing no health effects. Due to these drawbacks limiting welder exposure in this way is not considered effective or appropriate. Another more popular form of administrative control is through education of operators to avoid positioning themselves directly in the path of the fume plume. Such education on the effects of welding fume and how to avoid exposure are important but may be treated with complacency by some workers. General administrative procedures such as monitoring the health of workers can be an useful tool in assessing their exposure and adequacy of other control measures.

2.2.3.3 Personal protective equipment

The use of personal protective equipment (PPE) can be an effective measure for fume exposure control. Ventilated welding masks from a battery driven compressors worn on the belt have found applications in industry where fume removal with ventilation is insufficient. This system only provides protection while the welding mask is being worn and requires the air intake to be of suitable quality for breathing. The belt worn compressor can be uncomfortable to wear, requiring maintenance and battery changes. Cloth type dust masks that do not require power impede breathing and do not remove all fume constituents. Fully contained positive pressure breathing apparatus operating from remote compressors or air tanks guarantee clean air but are costly to purchase and maintain. Such devices are also uncomfortable to wear, require special training and therefore only find application in welding the most toxic of metals. In general while PPE can be important in exposure control disadvantages such as cost, productivity and comfort make them less than the complete solution.

2.2.3.4 Engineering controls

Engineering controls are currently one of the most widely implemented and effective exposure reduction measures. Atmospheric contaminates in the work place can be greatly reduced by the use of an appropriate mechanical ventilation and fume extraction system. These mechanical extraction systems remove the fume from around the welding operation and exhaust it into a less hazardous location. Such ventilation systems intercept much of the fume travelling from the welding process to the breathing zone of the operator. Mechanical ventilation systems require additional infrastructure to be constructed and maintained in the workplace. Where the welding occurs in a fixed location such as in a workshop the installation of an appropriate system is a once off cost. However the installation of ventilation systems in temporary locations, as would be found in construction or shipbuilding, can be costly and inconvenient. Further problems can be found in confined spaces where there is insufficient space for fans

and ventilation ducts or a safe exhaust point is a long distance away (Thornton & Stares 1994).

2.3 Particulate fume

Welding fume comprises of both gaseous and solid particulate components. Due to the capabilities of the laser techniques that will be introduced in later sections the particulate component of the welding fume will be the primary focus of this thesis.

2.3.1 Formation mechanisms

Gray et al. (1982) proposed that seven mechanisms are responsible for the formation of particulate fume from GMAW. These seven mechanisms are displayed in Figure 2.8 created by Gael Ulrich (Quimby & Ulrich 2000). The quantity of fume from each of these individual mechanisms is dependent on a number of welding variables. Also each mechanism results in particles of different characteristics, particularly size, shape and composition. The formation of particulate fume in welding processes such as FCAW are similar to those of GMAW but are complicated by the presence of substances contained within the flux (Gray & Hewitt 1982).

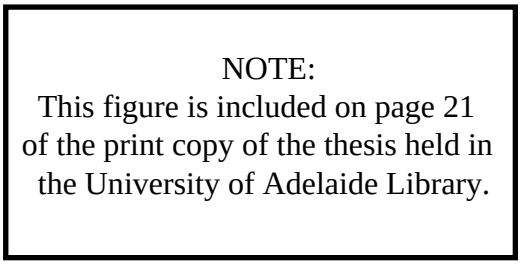

Figure 2.8: Fume formation mechanisms (Quimby & Ulrich 2000)

2.3.1.1 Droplet evaporation

Droplets are formed from the wire electrode melting due to the electrical heat input. The heat input into the droplet is a combination of ohmic heating from the current passing through the wire, and thermal conduction from the arc. In the majority of practical GMAW applications the entire mass of the electrode wire feed is rendered molten prior to entry into the weld pool. The movement of metal between the electrode and the weld pool is primarily done via droplet transfer and to a lesser extent vapour transfer. The amount of vapour generated off these droplets depends on several factors including surface temperature, area and the velocity of surrounding gas. These factors in turn are closely linked with droplet transfer mode and heat input. Evaporation of elements from the surface of the droplets occurs at a ratio which can be explained by partial pressures. For this reason the fume generated by this mechanism is likely to be higher in the elements that have a tendency to vaporise more readily.

A number of numerical fume formation models have been created that focus on this mechanism. While of varying complexity, these models undertake heat and mass balance calculations to determine vapour generation. The temperature of the droplet can be determined from a thermal equilibrium between the heat input and heat losses. Droplet temperature and surface area are controlled by the droplet transfer mode and therefore linked to a number of welding parameters.

It was found experimentally that metal transfer modes with larger droplets produce more fume than those with smaller droplets for the same wire feed rate (Bosworth & Deam 2000). Large droplets take longer to form and therefore remain attached to the electrode for longer periods. Due to the geometry of the larger droplets, higher surface temperatures were obtained increasing vapour generation. Even though the larger droplets have a lower ratio of surface area to mass, the increase in vapour generation and lengthened time of droplet attachment to the electrode resulted in larger fume formation rates (Deam, Simpson & Haidar 2000).

2.3.1.2 Arc root evaporation

Regions in contact with the arc root experience the highest temperatures. Arc root evaporation is also influenced by ion and electron movement.

2.3.1.3 Explosive evaporation

Explosive evaporation is caused by ohmic heating in the neck region of the molten material during droplet detachment. As the cross sectional area of the neck is reduced the resistance increases resulting in rapid heating and vaporisation. The heat input is sufficiently high to rapidly vaporise material in the necked segment at detachment

resulting in fume of similar composition to the electrode wire. The amount of fume generated from this mode is dependent on the current, resistance of the material, frequency and geometry of detachment. The explosive vaporisation mode of fume formation is particularly evident in dip transfer mode as a result of the increased current during short circuiting that drives droplet detachment. It is also evident at currents above that required for streaming transfer as the magnetic forces result in a frequent and lengthened necked region.

2.3.1.4 Micro splatter (Spatter and fine spray)

This mode is linked to the physical process of detachment from the electrode and entry into the weld pool. It is also closely linked to the rapid expansion of gases due to the explosive evaporation mechanism as outlined above. The rapid expansion due to vaporisation ejects molten particles of similar elemental composition to that of the electrode. Micro splatter fume particles are larger in size larger than those formed from mechanisms that involve vapour condensation. Due to the large size; these particles make up a significant proportion of particulate fume by mass while remaining relatively few in number.

2.3.1.5 Combustion of micro splatter

The entry of micro splatter into a oxidising environment can lead to combustion and oxygen assisted vaporisation. This can result in the production of finer fume particles due to the condensation of vapour from these larger particles arising from molten metal. As this mode is linked to the formation of splatter and microsplatter it is therefore also linked back to explosive vaporisation.

2.3.1.6 Weld pool evaporation

Minimal metal vapour is created from the weld pool as the temperature is limited by the heat dissipation, through conduction, to the surrounding solid material. Due to the relatively lower temperature of the weld pool much of the metal vapour generated in the arc ends up condensing into the weld pool and onto surrounding parent material. In this way it is only the portion of metal vapour that avoids condensation back into the weld pool or onto the workpiece that forms the fine metal fume. Fume generated from the weld pool is likely to have a different composition than that from the electrode due to the overall lower temperature of the weld pool and the dilution of the electrode composition in that of the parent material. The small contribution of the weld pool to fume formation is evident in gas tungsten arc welding, a process where the only molten material is the weld pool and therefore lacks most of the fume formation mechanisms

described above (Gray & Hewitt 1982). In total it is believed that 10 to 15% of the particulate fume originates from the workpiece (Gray & Hewitt 1982).

2.3.1.7 Bead evaporation

In GMAW negligible quantities of particulate fume are formed from the vaporisation of metals from the weld bead. This is due to the relatively low temperature of the bead resulting from thermal conduction to the surrounding metal.

2.3.2 Formation rate

Particulate welding fume arises both from solidified vapour generated in the arc and ejected particles. Fume formation rate (FFR) is a measure of the entire mass of fume formed from a particular welding process. The FFR of a particular process can be represented in a number of ways. Often it is reported as mass per unit time having the units of grams of fume per minute or hour of welding. Alternatively FFR may be represented as the proportion of fume to metal deposited, perhaps having the units of grams of fume per kilogram of wire feed. The latter representation accommodates for weld productivity however the former is more commonly found in the literature. The traditional way of measuring FFR is by collecting fume with the use of a hood or chamber that encapsulates the welding process such as that in Figure 2.9.

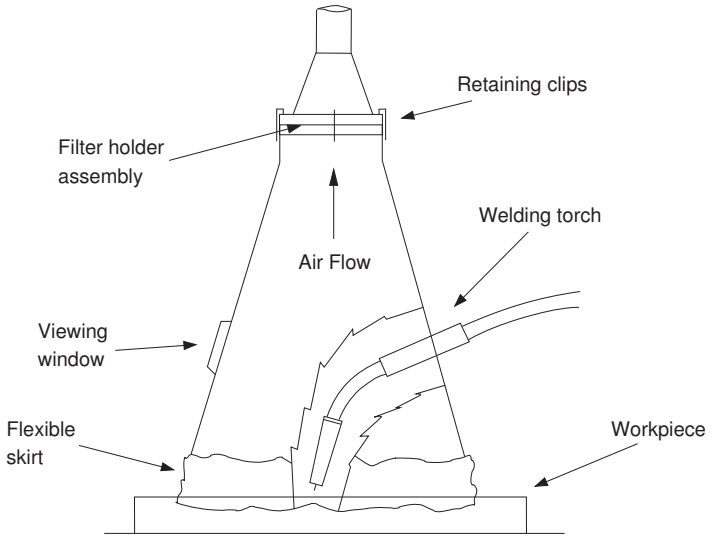

Figure 2.9: Fume collection chamber (Ioffe et al. 1995, Thornton & Stares 1994)

Particulate fume is collected by exhausting the volume of the chamber through a filter with the assistance of mechanical ventilation. The particulate matter collected results in an increase in the mass of the filter medium which is weighed before and after welding. The filter weight change divided by the welding time is then considered the FFR.

The results of one such fume box study by Quimby & Ulrich (1999) demonstrated the relationship between fume formation rate, welding arc voltage and wire feed speed. A summary of the welding variables used in this study is shown in Table 2.3. Figure 2.10 displays fume formation rates across a range of voltages for two of the wire feed speeds used by Quimby & Ulrich (1999). These results parallel those of previous research and discussions of Gray et al. (1982). The change in the droplet transfer modes and the associated fume formation modes, across the voltage range were used to explain the shape of the curve. The basic trend observed was a rise in FFR through dip to globular transfer, a reduction during spray transfer, rising again during steaming transfer.

	GMAW	Units
Electrode Wire	1.2mm ER70S3	
Voltage	18-32 (DCEP)	Volts
Wire Feed	4.5, 7.6	m/min
Current	170,225	Amps
Shielding gas	Ar 92, CO_2 8	%
Gas Flow rate	16.5	l/min
Weld traverse rate	360	mm/min
Standoff	19	mm

Table 2.3: Summary of some of the GMAW variables used by Quimby & Ulrich (1999)

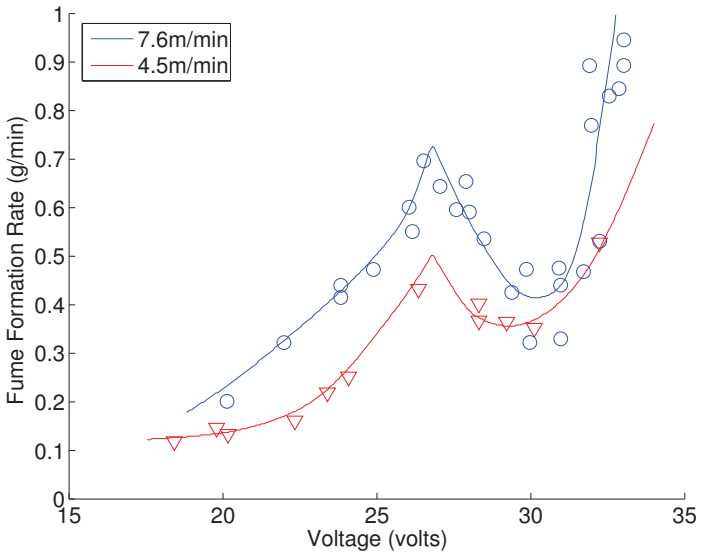

Figure 2.10: FFR from fume box measurements (Quimby & Ulrich 1999)

The rise in the FFR during dip transfer mode can be attributed to the presence of the explosive evaporation due to the short circuit at the time of droplet detachment. Higher voltages increase the current during short circuiting resulting in greater explosive evaporation and associated fume modes such as microsplatter. Droplet evaporation is also likely to increase slightly with voltage. However due to the relatively low heat input and small size of the droplet, formation of metal from the surface is minimal. When the voltage becomes sufficiently high, the droplet transfer mode becomes globular. That is the droplet grows and detaches without short circuiting with the workpiece. The

lack of short circuit reduces the peak current however due to the necking between the large droplet and the electrode at detachment, explosive evaporation is still significant. The large droplet size results in higher vapour generation from droplet evaporation (Deam, Simpson & Haidar 2000). The combination of all these formation mechanisms results in a peak in fume formation rate. In the case of the work done by Quimby & Ulrich (1999) in Figure 2.10 this peak due to the onset of globular transfer occurs at about 27 volts. In the transition between globular and spray transfer the droplet size decreases, reducing droplet surface temperature and evaporation. The reduction in droplet size also results in the arc enveloping the droplet and making contact with the solid electrode (Quimby & Ulrich 1999). The combination of the different current path and the propulsion of the smaller droplets from the electrode reduces explosive evaporation. The overall effect is a reduction in the FFR to a trough at spray transfer, occurring at a voltage between 29 and 31 volts in Figure 2.10. Voltages above that required for spray transfer produce streaming transfer and result in an increase in the FFR. This is attributed to explosive evaporation once again becoming significant as magnetic forces lengthening the molten necked region and the increasing frequency of droplet detachment. The higher current also increases arc convection forces on the droplets which lead to greater droplet evaporation.

Figure 2.10 displays the FFR for two different wire feed speeds. Extrapolating the results from a number of FFR measurements for different voltages and wire feed speeds Quimby & Ulrich (2000) produced the three dimensional plot shown in Figure 2.11.

By simply weighing the filter material used in fume boxes only FFR can be determined. However fume particles collected on the filter material can be further analysed for composition and size using various techniques.

The main advantage of fume box measurements is that they give a reasonably quantitative value of the FFR for a particular process. In the work undertaken by Quimby & Ulrich (2000) the reported standard deviation in FFR measurements was $\pm 5\%$ being a significant improvement over that from other fume box research which was reported to be typically in the order of $\pm 20\%$. Some variation is likely to occur since the mass of fume being collected is relatively small compared to the overall mass of the filter. Extending the time over which the fume is collected can result in a greater mass change and a more accurate FFR measurement. However if the collection time is too long it will result in excessive clogging of the filter medium and a variation due to a change in the extraction flow rate. Due to the complexity of welding processes much of the variation found in FFR measurements may arises as a result of the welding process itself rather then being a measurement error as such.

As with every fume measurement technique some difficulty exists in directly linking the FFR results from different studies. Primarily this is due to the large number of welding variables that affect the FFR, that make it difficult to determine exactly what is being compared. Variations also occur in the design and operation of each fume

Figure 2.11: FFR from fume box measurements (Quimby & Ulrich 2000)

box and how the fume particles are collected. The type of filter material, its support, distance and orientation are all important, along with the movement of air through the confined chamber. Due to the confinement in the chamber there is potential that the fume formation will be altered by the unrealistically confined environment. This is particularly true for fume formation mechanisms involving splatter that are dependent on the surrounding environment (Gray et al. 1980). Relating the filter mass change to the FFR makes the assumption that all the fume is collected and that the particulates collected are the same as those which may be inhaled by the welder. Some fume may become attached to the walls of the fume chamber or be fine enough to pass through the filter material. Coarse particles entrained by the fume box extraction may also be collected by the filter that may not be readily inhaled in practical welding situations. The actual time required to undertake the weld for measurable amount of fume for collection limits the temporal resolution that can investigated.

Each FFR measurement undertaken requires a new filter, often constructed from fibre glass matting. To accurately measure the FFR the filter material must be carefully handled and weighted. This may include drying the matting before and after collection. As a result undertaking a number of measurements can be time consuming. This is problematic when investigating the large number of welding variables that affect fume

formation.

The obvious limitation of fume boxes is that they collect the entire quantity of the fume generated. This is useful in determining the fume generation of the welding process in a confined space but does not determine worker exposure. This is by the simple fact that the welder does not inhale the entire volume of the welding fume but rather only the portion that reaches their breathing zone.

To obtain a better judgement of occupational exposure point measurements can be taken in the breathing zone. These are undertaken in industry to judge actual welder exposure (AS3853.1-1991 1991, Moreton 1982). In the case of a research environment some of these measurements attempt to replicate the welder with a manikin and obtain samples behind a welding helmet (Slater 2004). These measurements are useful in determining occupational exposure and the effectiveness of fume extraction systems. However due to environmental factors, such as ventilation, it is difficult to compare results obtained from different research groups. Measuring only a single point provides little information about the spacial dissipation of fume into the workplace. This is particularly true due to the long collection period required for a useful weight of fume to be collected on the filter from a single point.

2.3.3 Size

Particulate matter ejected from welding processes has a wide size distribution. Particle sizes range from only a few nanometres in diameter up to millimetre sized globules of metal and flux. Not all of these particles are readily inhaled. Of those that are inhaled particles of different sizes interact differently with the human respiratory track. This interaction is important in classifying which of the particles ejected from the welding process are of concern or can be classified as fume.

Large particles have sufficient mass and or momentum to not become entrained in the flow and transported to the welder's breathing zone. The upper limit on particles that do not drop from suspension in the plume and are therefore of concern is about $100\mu m$ in diameter (Deam et al. 1997). Inhaled particles greater than $1\mu m$ in diameter become attached to the lining of the respiratory track. As such they do not enter the lungs but can still be absorbed by the body or ingested. Of the smaller particles that are inhaled into the lungs a portion will enter and attach to the lining of the lungs while some will be subsequently exhaled. Although the interactions of inhaled particles with the respiratory track is dependent on size the general approach is to assume that any particles that have reached the breathing zone could be inhaled and present some level of risk to the operator.

Three different categories of welding fume were described by Jenkins et al. (2005). The smallest of these categories was individual particles formed from metal vapour

from a few nanometres up to $\sim 0.1\mu m$ in diameter. The second category comprised of agglomerates of individual particles. While the agglomerates were non spherical they were described of being in the order of $\sim 0.1\mu m$ to $\sim 1\mu m$ in size. The the third category described was coarse unagglomerated particles of microsplatter in the range of $\sim 1\mu m$ to $\sim 20\mu m$ in diameter.

Figure 2.12 shows a scanning electron microscope image of microsplatter collected by Jenkins et al. (2005) from a FCAW process. Two transmission electron microscope images of agglomerated fine fume can be seen in Figure 2.13.

Figure 2.12: Scanning electron microscope image of coarse fume particles from FCAW (Jenkins et al. 2005)

(a) Fume from GMAW with 2% O_2 Ar shielded 1.2mm ER70S-3 30V 200A.

(b) Fume from FCAW 1.2mm E71T-GS 30V 170A.

Figure 2.13: Transmission electron microscope image of fine fume particles (Jenkins & Eagar 2005)

The particle size distribution depends on a large number of welding and environmental variables. These include metal composition, droplet transfer mode, shielding gas composition and coverage. Since particles from different fume formation mechanisms

have different sizes it is logical that as these mechanisms change in significance, in response to droplet transfer, so does the size distribution of the bulk fume. The extent of fume agglomeration has been linked with FFR and the composition of the particles (Jenkins et al. 2005).

Due to the large range of particle sizes a number of different measurement techniques are used to determine size. This is because different techniques have various limitation on size range and overall accuracy. One method used to separate different fume size ranges is with a particle impacter. This device operates by drawing particulate laden air through a number of chambers separating particles according to inertia and ability to remain entrained in the flow. Particles unable to negotiate a particular passage impact and become attached to a plate. In this way the the welding fume is separated by way of its aerodynamic diameter. The geometric diameter of the particle is different to that of the aerodynamic diameter which represents a particle with equivalent inertial properties that has a density of $1000kg/m^3$. Equivalent aerodynamic measurement is thought of as a useful measurement for fume particles. Firstly because the fume particles or agglomerates are not necessarily spherical in shape making the diameter difficult to determine from a geometric measurement. Secondly aerodynamic diameter is closely related to how the particles negotiate through the respiratory track and collect in the lungs. Particle impactors can separate different size ranges, however can not provide fine resolution on the size distribution. This is problematic as the finer fume particles and agglomerates can not be separated.

A particle impactor was used by Jenkins et al. (2005) to investigate the relative proportion of the three different fume categories collected from a fume box. The impactor was used to roughly sort the fume which was then analysed further with an electron microscope and image processing. Due to the bin size range for each stage of the particle impactor this study was only able to clearly differentiate between fine fume and micro splatter. This study determined that for the particular GMAW parameters used, microsplatter by mass made up less than 6% of the fume for spray transfer and less than 10% for globular transfer. The amount of microsplatter from the self shielded FCAW process used was said to be no more than 30% of the overall fume mass.

While impactors can not differentiate between finer particles other measurement processes can. Due to the processes behind the operation of scanning mobility particle sizers, large particles cannot be measured and may interfere with its operation. Zimmer & Biswas (2001) used a scanning mobility particle sizer to measure fine fume concentration and size distribution. Figure 2.14 shows the particle distribution at 192mm above the arc for GMAW and FCAW processes. This plot shows that there is a different distribution for the two processes measured. The mean particle diameter by number for GMAW from Figure 2.14 produced by Zimmer & Biswas (2001) is approximately $160nm$.

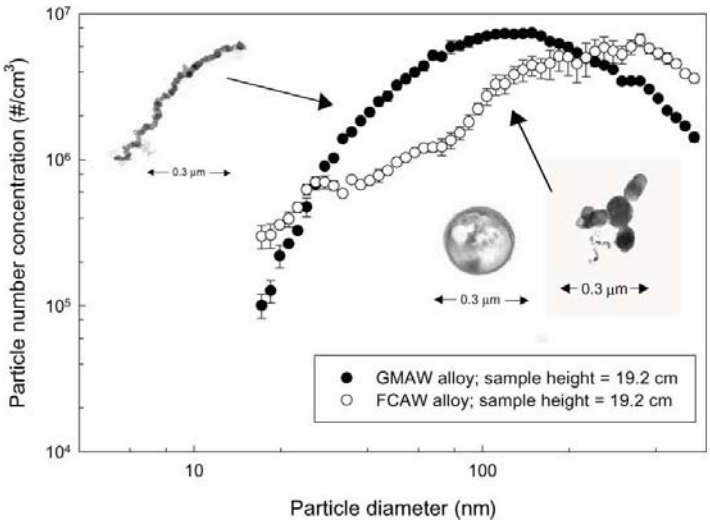

Figure 2.14: Fume size distribution measured with a scanning mobility particle sizer (Zimmer & Biswas 2001)

2.3.4 Composition

The composition of fume particles results from the materials involved in the welding process and the numerous welding values. Typically fume particles to be analysed are collected with fume boxes. The composition of collected particles can be determined by several different analytical procedures (Jenkins & Eagar 2005). A large proportion of the fume material comes from the welding electrode. This is due to droplet evaporation, explosive vaporisation and microsplatter mechanisms during droplet formation and transfer. Resultantly the composition of the fume is primarily linked to the composition of the electrode. Elements with lower partial pressures are the first to vaporise in response to droplet superheat. This results in higher concentrations of elements with lower partial pressures arising from fume mechanisms such as droplet evaporation. Conversely this evaporation leads to a leaching of low partial pressure elements from the weld metal. Often the amount of these elements have been increased in the electrode to compensate for this loss to obtain the required weld metal composition. As such fine fume particles can have higher concentrations of particular elements then that found in either the workpiece or consumable electrode. Such a case is displayed in Figure 2.15 by Albert (1996). The top plot in Figure 2.15 displays the FFR and exhibits a similar shape and link to droplet transfer mode as that in Figure 2.10. The lower plot in Figure 2.15 displays the bulk composition of the fume. The horizontal dotted lines represents the bulk composition of the welding wire. On the whole it can be seen that Manganese and Chromium occur in the fume at a percentage higher than they constitute in the electrode. This percentage is also higher than that found in 304 grade stainless steel parent material, while Nickel and Iron concentrations in the fume are lower than that found in the electrode. The trend of the bulk fume composition across the voltage range can be attributed to the ratio of fume generated from different formation mechanisms. A voltage of 37Volts on this plot relates to a streaming transfer mode indicated by

the dip in FFR. The reduction in explosive evaporation and associated microsplatter at streaming transfer results in the larger relative contribution of fume from droplet evaporation, which is richer in the elements of lower partial pressure.

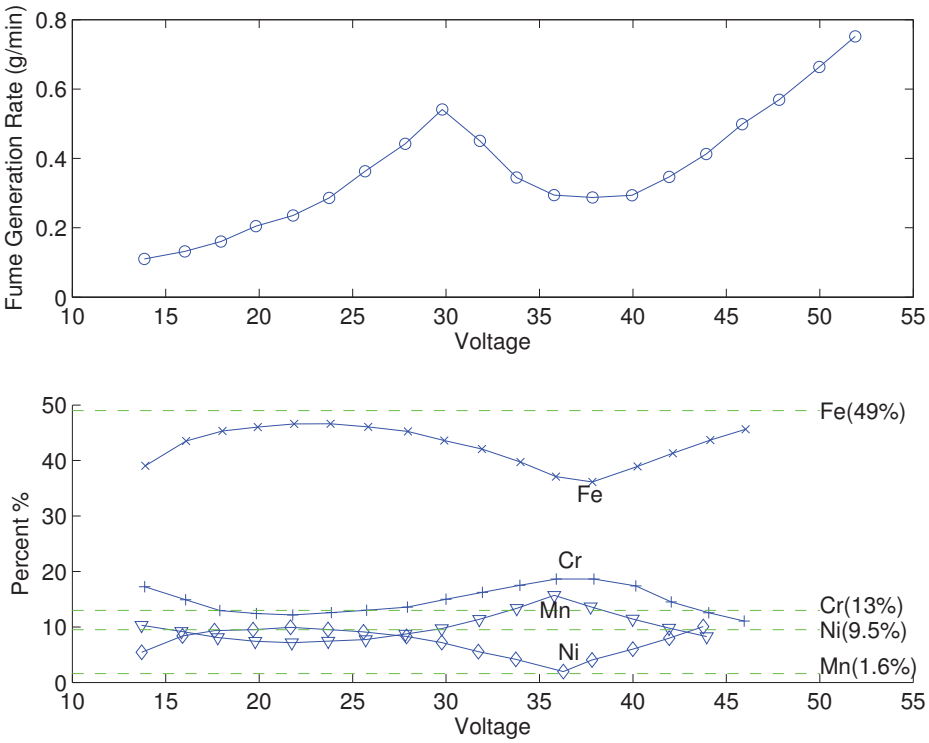

Figure 2.15: FFR and metal composition for GMAW 304 stainless steel welding fume (Albert 1996)

Element	Ni	Fe	Cr	Mn
Boiling point $°K$	3186	3134	2944	2334

Table 2.4: Boiling points of different metals at 1 atmosphere

The elements in the fume particles can form different compounds. Due to the temperature and small size most metallic elements in the fume readily oxidise when exposed to the atmosphere or shielding gases containing a component of oxygen.

2.3.5 Effect of welding variables on fume formation

It has been determined that the formation of fume is the result of thermal, chemical and mechanical interactions. These in turn are related to a large number of possibly interrelated welding variables. So changing one welding variable may alter several others. The resulting change in fume formation is quite complex and non linear. In an attempt to summarise a number of different welding variables an unquantifiable concept of arc stability is considered by some. This approach is convenient as obtaining an improving arc stability has several practical advantages and can be gauged visually and audibly. For DC GMAW arc stability relates to consistency of arc length, current

and contact point on the electrode and workpiece. Arc stability is closely linked with droplet transfer, with high stability generally associated with the frequent and regular detachment of small droplets. Improving arc stability generally reduces FFR and improves the surface finish of the weld bead. The lower FFR on stable arcs can be associated with a number of factors such as small droplet size, reduced splatter, lower peak current and arc convection forces. Anything that alters droplet transfer or arc stability will alter the fume formation.

Voltage Voltage has a significant influence on fume formation. Changing the voltage will alter the droplet transfer mode and arc length. Since changing the voltage will also change the heat input it is also likely to change the size of the weld pool and the geometry of the weld bead. As indicated by Figures 2.10 and 2.11 a complex relationship exists between voltage and FFR.

Wire feed speed Wire feed speed is used as the primary control on current. Increasing the wire feed increases the current in response to a higher required melt rate. This alters the size and frequency of droplet detachment. It will also change the heat input and as in the case of voltage the weld pool and weld bead geometry. Generally higher wire feed rates result in higher FFR per unit time.

Shielding gas The composition of the gas is significant in determining the properties of the arc and the droplet transfer mode. The change in droplet transfer mode, current and arc shape will therefore result in marked variation in FFR. Shielding gas flow rate has minimal impact on FFR as long as the gas flow rate is sufficient to protect the arc from the atmosphere. It is possible that very high gas flow rates can alter arc stability but this is rarely the case in practical applications due to the desire to keep gas flow as low as possible for cost reasons.

Traverse rate Traverse rate, it is believed, has minimal impact on the FFR other than what occurs due to the changes in weld pool and weld bead geometry. It has been reported that doubling the traverse rate changes the FFR by 5% (Quimby & Ulrich 1999).

Wire feed system The smoothness that electrode wire can be feed into the arc is one limiting factor on the arc stability that can be obtained. Many things determine the smoothness of the wire feed including the drive motor, contact rollers, torch liner, torch lead path and contact tip. The smoothness and ease at which the wire is fed is termed feedability. If the wire is not smoothly fed through the system the droplet transfer and current vary reducing arc stability.

An area of recent interest has been in the design of the contact tip which transfers power from the torch lead on to the wire electrode. With normal contact tips the electrode slides through a free running fit through the length of the tip. The actual point where the contact is made and current transfered between the two is not fixed, changing ohmic heating in the electrode, and resulting in a source of instability. It has also been suggested the arcing across the gap between the wire and the tip as the point of contact moves can result in the two becoming temporarily fused reducing the smoothness at which the wire is feed into the actual arc. A number of contact tips have been designed to try and improve conduction and consistency of point of contact. The CSIRO has patented a contact tip that uses a spring loaded brush that the welding wire slides past (Fanning et al. 2004). This design fixes the point of contact, reducing current variation and temporary fusion. The result is greatly improved arc stability for spray and streaming transfer and reduced FFR.

Electrode The electrode wire is also critical in determining arc properties and droplet transfer mode. As previously discussed the composition of the fume is related to that of the welding wire. Beyond this seemingly similar wire specifications have been found to produce measurably different FFR. One recent source of interest has been the variation in FFR between copper and non-copper coated wires made by the same manufacturer. Slater (2004) reported that from breathing zone measurements the concentration of fume from non-copper coated wire was approximately 25% less than the copper coated equivalent. The exact reason for this is unclear as the mass of the copper coating is far less than the difference in fume formation. It has been suggested that the reduction may have more to do with the proprietary coating the manufacture has placed on the non-copper coated wire that improves wire feed and arc stability. Along a similar line variations in FFR exist in wires that come from different manufactures that have the same designation as shown in Figure 2.16. This may be due to such factors as dimensional tolerance of the wire, the presence of gas forming elements in the wire and any additional surface coatings.

Power supply The operating voltage and current is a match between the arc impedance and the power supply output. Resultantly different power supplies will produce arcs with different properties and FFR. Of particularly interest is how the power supply responds to transient variations in arc impedance from droplet transfer across the arc. This is a major consideration for globular transfer where the response of the power supply to the short circuit event created by the droplet contacting the workpiece will determine how the droplet detaches and the magnitude of the explosive vaporisation. The response to such short circuit events depends on the inductance of the power supply and feedback on the control circuitry used. On many modern power supplies the transient response can be adjusted by way of feedback control often

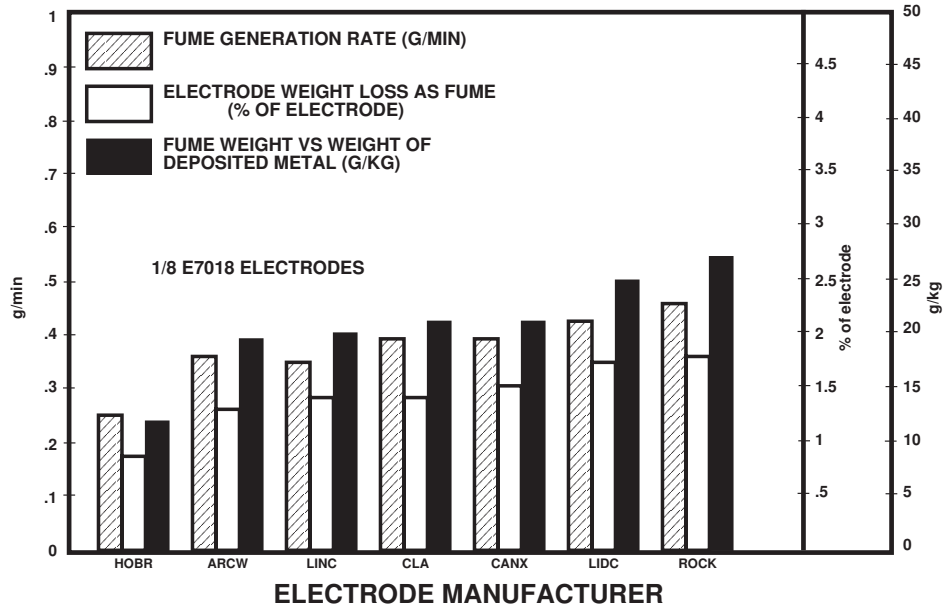

Figure 2.16: Fume box measurements of fume formation from different manufacturer's electrodes (Tinkler & Ditschun 1984)

referred to as arc force. The current and voltage can be rerecorded in such a way that the waveform is useful for determining arc properties and droplet transfer (Zhu & Simpson 2005, Lin et al. 2001).

2.4 Fume plumes

With the exception of a small proportion of fume generated by way of evaporation or combustion of ejected spatter, the particulate fume originates either in or immediately adjacent to the arc. The main occupational concern with welding fume is through its inhalation. Therefore the transportation mechanism of the fume between the arc and the welder's air intake is important in determining exposure. Without extraction or cross draft ventilation the dissipation of this fume is primarily by way of a thermally buoyant plume that rises from the weld.

2.4.1 Jets and Plumes

Many contaminants dissipate and are disposed of by way of a jet or a plume into the surrounding environment. Examples of such are the underwater outfall from sewage treatment plants, the emission stack of a power plant or the exhaust of a motor vehicle as seen in Figure 2.17. In these cases the hope is that the dilution of the contaminant in the environment will be sufficient to result in an immediate impact on society small enough that it can be justified by the immediate benefit. The discharge of the emission and its subsequent dissipation can be characterised by the velocity, and density of the substance.

Figure 2.17: Plume from a moving source (Photo: Paul Medwell 2005)

It is the velocity and density that determines whether the dissipation is classified as a pure jet, pure plume or more likely some combination of the two. A pure jet has a velocity at the origin of the discharge and no differential in density with the environment. Dissipation of the material is therefore dominated by the momentum arising from its velocity at source. A pure plume however results from a differential in density with the environment and no initial velocity. As such the dissipation of the pure plume occurs by way of buoyancy with the ambient environment and possesses no momentum at source. In the case of the welding discharge there is both a differential in density and velocity at source, a combination referred to as a forced plume.

Forced plumes are found in a number of situations where material is being exhausted into the atmosphere. Welding plumes however differ from the classical case due to the geometry involved in the process. Shielding gas used in GMAW, the bulk often comprising of argon or carbon dioxide, is denser than the atmosphere at the same temperature. As a result the discharge of shielding gas from the nozzle, being denser than air, would have a tendency to settle once released. In operation however the shielding gas is heated by energy dissipated in the welding process. Heat transfer to the shielding gas occurs from the welding torch, arc and parent material. The increase in temperature reduces the density in most cases to a point where the shielding gas becomes positively buoyant in the surrounding environment and has the tendency to rise.

In a typical welding situation where the torch is pointed down, the momentum of shielding gases is initially downward while the buoyancy of the heated gas is upward. Neglecting the presence of the parent material the result described by Slater (2004) is an inverted fountain such as depicted in the left hand image of Figure 2.18. In this case the plume turns and rises when the effect of buoyancy upwards overcomes the initial momentum downwards from the nozzle. Considering the parent material in the welding situation is close to the nozzle, the downward momentum results in the gas flow impinging on this surface. This impingement results in the vertical momentum of the gas being deflected horizontally across the surface and radial spread of the plume, depicted in the right hand image of Figure 2.18. While the plume is positively buoyant

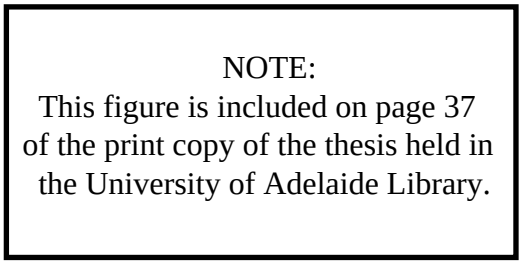

Figure 2.18: Turbulent fountain in a homogeneous environment and impinging on a horizontal plate (Cooper & Hunt 2004)

the boundary layer attachment, due to Coanda effects, cause the horizontal movement of the gas across the surface. This movement occurs as a radial jet until separation, depicted in Figure 2.18 as occurring at radial distance R_{sp}.

As the plume rises and dissipates, entrainment of ambient air results in dilution. Dilution of the plume increases the total volume of the plume with corresponding reductions in the concentration of the contaminant and the temperature of the heated plume. The plume continues to rise up to such a point cooling of the plume increases the density until it matches that of the surrounding air and becomes neutrally buoyant. Figure 2.19 displays a schematic of plume development sketched by Jin (1992) from direct imaging of the plume.

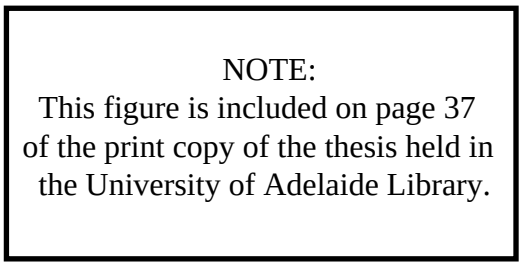

Figure 2.19: Schematic of welding fume plume development (Jin 1992)

2.4.1.1 Direct imaging of fume plumes

Plume shape can be determined visually as shown in Figure 2.20. While this is a simple technique to determine plume extent, it has several limitations. One of the major limitations is that the outer components of the plume camouflage the internal

structure of the plume. The other limitation is the uniformity of light from the arc reflected by the fume particles. That is to say areas of the plume that are not as well lit do not show up as significantly as those that are. This is inherent as the light intensity drops off with distance from the arc and due to shadows projected by the gas shroud. For this reason the plume low down near the torch is likely to be exaggerated over that higher up or further out. Also changes in welding variables change the intensity of the arc light. For example the light intensity from globular transfer is likely to be much less than that from spray transfer where the arc length is longer.

Figure 2.20: Direct viewing of FCAW plume (Norrish et al. 2005)

Figure 2.20 show the differences between the plumes generated by shielded and unshielded FCAW. The left hand image, being unshielded FCAW, represents the pure plume case where the fume dissipation is driven by thermal buoyancy alone. The right hand case, having shielding gas, depicts the forced plume where both buoyancy and initial momentum exist. The initial downward momentum leading to greater radial spread across the surface of the plate than the unshielded pure plume case. The mean diameter of spread determined by Slater (2004) was about 75mm and 180mm for the unshielded and shielded cases respectively.

2.4.1.2 Physical modelling

Water models have been used to detach the multiple welding variables involved from the fluid mechanics of the plume by using liquids of different densities. The advantages of undertaking modelling is that it avoids the complexity and variation that is inherent in welding, allowing the fluid mechanics to be investigated in a more controlled environment. Slater (2004) used saltwater in fresh water to investigate fluid mechanics of welding plumes. Scaling was used to determine the required salt content of the liquid used to represent the shielding gas. The salt water being denser than the freshwater representing the ambient environment results in the plume being negatively buoyant. This is the opposite to what is encountered in the actual welding case so the whole water model was inverted. That is to say the initial momentum from the water nozzle was up

and the buoyancy was down. Coloured dye was added to the salt water representing the shielding gas and the fountain effect directly imaged. As in the case of direct viewing of the actual welding plume the external components of the plume camouflage the internal structure.

Cooper & Hunt (2004) used a water model to investigate the radial spread of impinging positively buoyant jets. In this case the water representing the ambient was saltwater and the jet freshwater. A fluorescent dye was added to the freshwater to allow cross sectional images to be obtained with light excitation, a common technique used in modern fluid visualisation. By using the light induced fluorescence the internal structure of the plume can be observed unlike the direct imaging cases. Figure 2.21 displays a false colour image representing intensity of induced fluorescence from the left half of the plume.

Figure 2.21: Light induced fluorescence image of impinging jet water model (left half) (Cooper & Hunt 2004)

The images obtained by Cooper & Hunt (2004) were used to observe the internal structure of the impinging jet. The images were also used to measure the radial spread of the plume across the plate before separation under a number of different flow conditions.

These water models, being only that, have a multitude of limitations when considering the true fume plume circumstance. One of the main disadvantages is that the plume properties are decoupled from welding variables. As such these models could not be used to link changes in actual welding variables with the resulting changes in plume properties. What connection there is between the welding plume and the fluid model arises from scaling which may or may not be accurate since there are a number of factors involved. Resultantly scaling can not compensate simultaneously for all variable involved such as, plume density, gas viscosity, specific heat, and thermal conduction. For instance the salt content used by Slater (2004) was calculated to obtain similar buoyancy by matching the calculated reduced gravity of the fume plume

and the buoyancy was down. Coloured dye was added to the salt water representing the shielding gas and the fountain effect directly imaged. As in the case of direct viewing of the actual welding plume the external components of the plume camouflage the internal structure.

Cooper & Hunt (2004) used a water model to investigate the radial spread of impinging positively buoyant jets. In this case the water representing the ambient was saltwater and the jet freshwater. A fluorescent dye was added to the freshwater to allow cross sectional images to be obtained with light excitation, a common technique used in modern fluid visualisation. By using the light induced fluorescence the internal structure of the plume can be observed unlike the direct imaging cases. Figure 2.21 displays a false colour image representing intensity of induced fluorescence from the left half of the plume.

Figure 2.21: Light induced fluorescence image of impinging jet water model (left half) (Cooper & Hunt 2004)

The images obtained by Cooper & Hunt (2004) were used to observe the internal structure of the impinging jet. The images were also used to measure the radial spread of the plume across the plate before separation under a number of different flow conditions.

These water models, being only that, have a multitude of limitations when considering the true fume plume circumstance. One of the main disadvantages is that the plume properties are decoupled from welding variables. As such these models could not be used to link changes in actual welding variables with the resulting changes in plume properties. What connection there is between the welding plume and the fluid model arises from scaling which may or may not be accurate since there are a number of factors involved. Resultantly scaling can not compensate simultaneously for all variable involved such as, plume density, gas viscosity, specific heat, and thermal conduction. For instance the salt content used by Slater (2004) was calculated to obtain similar buoyancy by matching the calculated reduced gravity of the fume plume

in the environment with the increased gravity of the saltwater plume in the freshwater tank. The fluid models used a homogeneous discharge to represent the plume. This is probably a reasonable assumption when investigating the plume at some distance from the torch. However the fume particulates are entrained mostly from gas flowing over molten surfaces so may not be evenly distributed in the plume close to the source. Another disadvantage with these fluid models is that they require a discharge of fluid at source that generates momentum to represent the difference in density. As such these models would not accurately emulate unshielded welding cases where the plume dissipation is purely thermally driven convection.

Actual welding equipment was used by Johnson et al. (2006) to investigate the flow of shielding gas from a non operating welding torch. In this case oil particles were entrained in the flow of shielding gas as a tracer. Scatter from a sheet of laser light off these particles was imaged to obtain a cross sections such as shown in Figure 2.22. In addition to visualisation, a technique that collects two images in rapid succession was used to determine flow velocity profile. Johnson et al. (2006) investigated a number of different flow conditions and welding torch configurations. Different welding travel speeds were investigated by moving the plate representing the parent material. It was observed that separation of the shielding gas from the plate occurred closer to the torch in the downstream direction. This effect became more pronounced with increasing travel speed. This would suggest that the actual welding case may not be axis symmetric.

Figure 2.22: Cold flow cross section of oil seeded shielding gas flow. Recessed contact tip Re=1260 (Johnson et al. 2006)

The obvious limitation with this method of visualisation is that it can only be undertaken in cold flow as the oil particles would quickly evaporate and burn if actually undertaking welding. Since it can only be undertaken cold, oil seeding is not useful for investigating the thermally buoyant fume plume. Also since not undertaken in an actual welding situation the effect of the weld bead, weld pool and arc forces on the

gas flow can not be assessed.

To undertake a similar method in actual welding would require the plume to be seeded with non combustible particles for use as a tracer. Indeed such particles are inherently generated in GMAW in the form of particulate fume. Similar welding byproducts were used by Dahmen et al. (1993) to investigate the flow of shielding gas in laser welding. In this case a secondary laser was used to form a sheet of light that passed through the weld beam. The light scatter from the secondary laser beam off the particles generated by the welding process was then imaged with a camera. An optical band pass filter was used to separate the scattered laser light, of known wavelength, from other optical emissions.

2.4.1.3 Numerical modelling

Computational fluid dynamic (CFD) simulations of GMAW plumes close to the welding arc have been undertaken by Godbole et al. (2007). The published work aimed to investigate the design of on-torch fume extraction. These systems use a co-annular suction device on the gas shroud in an attempt to capture the fume close to the point of formation. Such extraction systems are not commonly found in industry due to the extra complexity, awkwardness in operation, cost and general poor effectiveness in operation.

Figure 2.23: Computational fluid dynamic vector field for an impinging fountain (Godbole et al. 2007)

Numerical modelling was used to determine concentration and plume velocity. Figure 2.23 displays a CFD model of an impinging fountain similar to that displayed in Figure 2.21. A series of water models from Cooper & Hunt (2004) were used as validation of the CFD model with excellent correlation. However Godbole et al. (2007) noted that GMAW processes introduce a number of additional factors in particular arc

forces and heating. In the subsequent CFD of GMAW the arc was modelled as a cone directly beneath the welding torch which supplied a heat input. Godbole et al. (2007) also noted the lack of detailed experimental data in regards to flow fields in this region to which the GMAW CFD could be compared. This was attributed to the difficulty in carrying out experimental measurements due to the extreme heat and light conditions close to the arc.

2.4.2 Plume variable definitions

The principle of mathematical modelling is to generate equations that provide a useful simulation of the physical event. Typically there are a number of different ways to model a particular process using different mathematical techniques. In plume modelling the approach is to consider the volumetric flux Q, the specific momentum flux $M$and the buoyancy B and how each of these relate to each other throughout the dissipated plume.

The volumetric flux is obtained by integrating the plume velocity u across the extent of the plume.

$$Q = \int u dA \tag{2.1}$$

The momentum generated by the plume is then the volumetric flow rate Q multiplied by density ρ, to obtain mass, multiplied by the plume velocity u. However in order to obtain specific momentum M, being momentum per unit mass, the actual momentum is divided by the density. The specific momentum is then simply the volumetric flow rate Q multiplied by the velocity integrated across the plume.

$$M = \int u^2 dA \tag{2.2}$$

The buoyancy is defined as the the plume velocity u multiplied by the reduce gravity g' integrated cross the plume. The reduced gravity representing the gravitational effect on the volume due to its difference in density with the ambient.

$$B = \int u g' dA \tag{2.3}$$

$$g' = g\left(\frac{\rho_\infty - \rho}{\rho}\right) \tag{2.4}$$

Where ρ is the density of the plume ρ_∞ is the density of the ambient environment and g is gravitational acceleration.

A summary of some pure plume and jet equations are included in Appendix B. In the case of a forced plume, where the momentum and buoyancy are in the same direction, both pure jet and pure plume equations can be used to model the dissipation. Close to the origin dissipation is assumed to be momentum dominated and therefore approximated by pure jet equations within the momentum length scale l_s as determined by Equation 2.5. After this distance l_s the effect of buoyancy becomes more significant then the initial momentum and pure plume equations can be used.

$$l_s = \frac{M_o^{\frac{3}{4}}}{B_o^{\frac{1}{2}}} \tag{2.5}$$

2.4.3 Welding plume modelling

Slater (2004) undertook modelling of a welding plume using classical plume theories. The classical plume theories however assume a finite source diameter released in to free space with momentum and buoyancy in the same direction. In the welding situation impingement of the gas on the workpiece results in radial spread and not a finite source from which the plume dissipates. The approach by Slatter, and others, to account for this initial diameter at source was to use a virtual origin z_o below the true source as shown in Figure 2.24.

After making this assumption that the plume emanated from a virtual origin below the true origin Slatter modelled the fume as a round pure plume with velocity constant across the radius. Initially Slatter determined the heat input driving the plume. He did this by first calculating the volumetric melt rate MR_v of the wire electrode used, based on the current I_T and the voltage V_T. The actual requirement for Slatter to calculate volumetric melt rate is unclear given the free flight transfer mode and that the wire feed rate was physically measured by on line instrumentation. The calculated melt rate, lower than that actually measured, was then used to determine the heat input into the shielding gas $q_o$from the welding process heat input q_T by way of Equation 2.6. This equation was generated by Jin (1992) from experimental measurements from a similar welding process.

$$q_o = q_T \left[-0.1787 + 0.0857 ln(MR_v)\right] \tag{2.6}$$

Where the total heat input $q_T = V_T \times I_T$. From the heat input dissipated into the gas the buoyancy at source $B_o$was then calculated with Equation 2.7.

$$B_o = \frac{g q_o}{\pi c_p \rho T_o} \approx 0.0281 q_o \tag{2.7}$$

Where $c_p$is the specific heat at constant pressure, ρ and $T_o$are the plume density and plume temperature at source respectively. Having obtained the initial buoyancy that

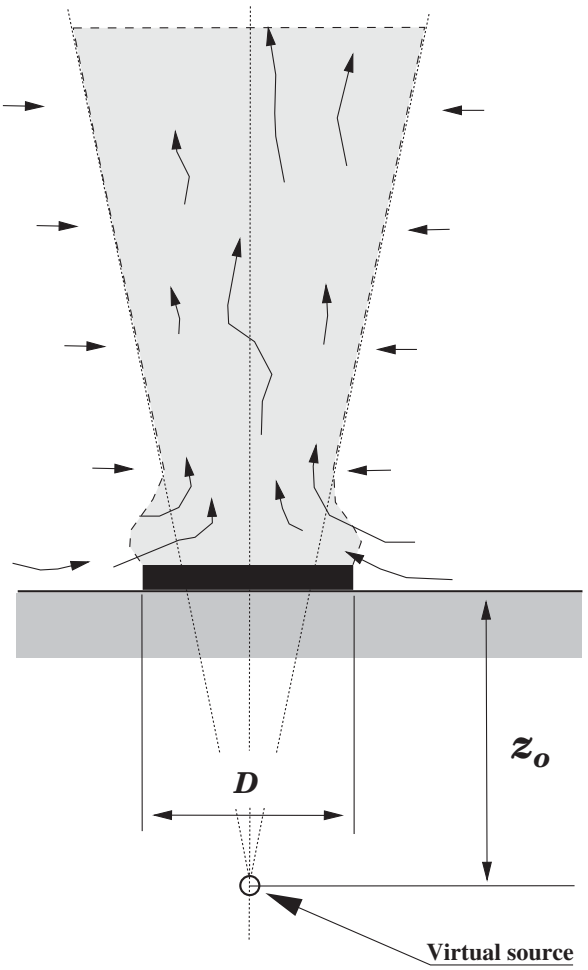

Figure 2.24: Virtual source used to model initial width at plume origin (Goodfellow & Tahti 2001)

propelled the plume Slatter then calculated the volumetric flux Q as a function of the height above the source z. The constant c_1 being derived from the entrainment coefficient $\alpha \approx 0.1$ itself a constant for pure plumes however dependent on the assumed velocity profile across the plume.

$$Q(z) = c_1 B_o^{\frac{1}{3}} z^{\frac{5}{3}} \tag{2.8}$$

$$c_1 = \frac{6}{5}\alpha \left(\frac{9\alpha}{10}\right)^{\frac{1}{3}} \pi^{\frac{2}{3}} = 0.115$$

Slatter then calculated specific momentum flux using Equation 2.9.

$$M(z) = c_2 B_o^{\frac{2}{3}} z^{\frac{4}{3}} \tag{2.9}$$

$$c_2 = \pi \left(\frac{5}{8\alpha\pi}\right)^{\frac{2}{3}} \left(\frac{6\alpha}{5}\right)^{\frac{4}{3}} = 0.294$$

The reduced gravity as a function of height was calculated Equation 2.10.

$$g'(z) = \frac{1}{c_1}\left(B_o^2 z^{-5}\right)^{\frac{1}{3}} \tag{2.10}$$

Mean plume velocity could be determined from the volumetric flow rate and the crossectional area of the plume.

$$u(z) = \frac{Q(z)}{A(z)} = \frac{25 c_1 B_o^{\frac{1}{3}}}{9\pi\alpha^2 z^{\frac{1}{3}}} \tag{2.11}$$

Slatter however experienced difficulty directly observing and measuring the plume dispersion close to the welding source. This difficulty was primarily attributed to the intensity of the light from the arc and the relatively poorly lit fume plume above. Some attempt was made to relate the expected near field plume properties with measurements of the far field plume hight descending as the small enclosure, in which the welding was performed, filled with fume.

2.4.4 Impingement radial spread

The radial spread R_{sp} is the distance that the impinged plume spreads across the work piece before detaching. Cooper & Hunt (2004) used water modelling combined with light induced fluorescence to measure the radial spread from different impinging jets. The non-dimensional separation distance, being the radial spread divided by the source to plate distance, was found to be related to the Archimedes number or the radial jet Ar_{rad} given by Equation 2.12.

$$Ar_{rad} = 2^{\frac{5}{2}}\alpha^2\gamma^{-3}\left(\frac{H}{R_o}\right)^2 Ar_o \tag{2.12}$$

Where α is the entrainment constant for jets for which they used $\alpha = 0.0535$, γ represents the fraction of the vertically down momentum that gets transferred horizontally, H is the source to impingement plate distance and R_o is the source radius. The source Archimedes number Ar_o is given by Equation 2.13.

$$Ar_o = \frac{g'_o R_o}{u^2} \tag{2.13}$$

The relationship between non-dimensional separation distance and radial jet Archimedes number found experimentally by Cooper & Hunt (2004) is displayed in Figure 2.25.

Radial spread was also considered by Slater (2004) by way of Equation 2.14.

NOTE:
This figure is included on page 46
of the print copy of the thesis held in
the University of Adelaide Library.

Figure 2.25: Non-dimensional separation distance Vs Radial jet Archimedes number (Cooper & Hunt 2004)

$$R_{sp} = \psi l_s \left(1 - \frac{c_2 B_o^{\frac{2}{3}} H^{\frac{4}{3}}}{M_o}\right)^{\frac{3}{4}} \tag{2.14}$$

where ψ is a radial spread correction factor that was determined by Slatter to be equal to 2.36 ± 0.5 from salt water models of welding plumes. Further discussion by Slater (2004) mentioned that the model yielded a radial spread 2.7 times that of the experimental but the exact model and experiment used in this comparison is obfuscated.

Radial spread was also used by Slater (2004) to estimate the location of the virtual origin using the rate of entrainment for a pure plume. Substituting values for a particular welding process into Equation 2.14 estimated the radial spread to be 0.355m. From this he then determined using Equation 2.15 the virtual origin was located 2.95m below the actual welding arc.

$$z_o = \frac{5 R_{sp}}{6\alpha} \tag{2.15}$$

2.5 Laser diagnostics

A significant amount of fume research so far has been put into determining the bulk quantity and composition arising from formation process. Indeed fume formation is a significant factor in fume exposure and is also of interest being closely linked to the physics so critical in the welding process. Formation is however the first step in the process, with the fume particles dissipating into, and reacting with, the surrounding atmosphere where it could possibly be inhaled.

Dissipation of fume products takes place by way of the thermally buoyant plume produced by the heat input of the welding process. Several physical and mathematical models of welding fume plumes from the point origin into the work place have been under taken previously (Slater 2004). In the case of GMAW the majority of fume measurements have either been total formation, localised point or far field plume height. However measurement of fume plumes close to the origin of actual welding processes have proven difficult to measure and observe due to the intensity of the light produced by the arc (Slater 2004, Godbole et al. 2007).

Laser techniques have found application in several fields of welding research. Applications where laser diagnostics have been applied to welding include droplet transfer mode measurement (Lin et al. 2001), cold flow modelling of GMAW gas flow (Johnson et al. 2006), and gas shielding of laser beam welding (Dahmen et al. 1993). These applications have relied on the unique properties of light produced by lasers, in particular the narrow wavelength spectrum and coherency. These two properties mean that the light is highly directional, can be sharply focused to form high energy densities and optically filtered from other wavelengths (Halliday et al. 1997). The unique properties of laser light have also been extensively utilised in other areas of research such as combustion. Applications of lasers in combustion include the measurement of gas flow, flame chemistry and carbon nanoparticles know as soot.

The aim of the work presented here was to investigate the application of laser techniques, many of which are used to measure soot, to the measurement of welding fume. In doing so take the logical extension of previous fume plume modelling and collect actual GMAW plume images close to the welding arc. Images collected from this process can then be used to determine the influence that particular welding variables have on fume formation and plume distribution.

2.5.1 Soot

Soot is particulate matter that is formed in carbon rich combustion environments. Particles of soot generally range in size up to about 100nm in diameter and are spherical in shape. Like welding fume, individual soot particles can agglomerate to form clusters or fine chains. Depending on the application the formation of soot in flames can be desirable as the particulate matter acts as a radiant source for heat transfer. However soot in the exhaust gases is undesirable due to environmental and health reasons. Ideally in flames required for industrial radiant heating the soot would nucleate, grow then finally oxidise in the outer fringes of the flame to produce CO_2. In an attempt to optimise this soot formation and oxidation combustion research is interested in the quantity and location of soot within flames. Methods used to measure soot within flames include direct imaging, laser scattering, laser induced incandescence and laser extinction. Due to similarities in the particulates it is proposed that laser techniques

used in combustion research on soot could also prove useful in characterising welding fume plumes.

2.5.2 Laser scattering

Scattering is a term that relates to a number of processes including reflection, refraction and diffraction of the light incident and surrounding an object (Jones 1999). Measurement of scattered light is one of the most basic of all optical diagnostic processes. Indeed general vision and photography is most commonly generated from light scatted from objects rather then directly from a source of light.

Lasers are useful as a source of illumination for scattering measurements due to the high intensity of light that can be obtained. As the light is coherent it can also be accurately focused and shaped to illuminate cross sections. Neglecting Doppler effects the wavelength of scattered light from the object is the same as that which was incident. Resultantly the narrow spectrum of the laser beam results in a scattered signal of the same known narrow wavelength. For this reason it is often possible to differentiate the scattered laser light from other light emanating from the object by way of wavelength.

Several applications of laser scattering to the measurement of fume plumes have already been cited in Section 2.4.1.2 with respect to physical plume measurements. The experiment undertaken by Johnson et al. (2006) introduced oil particles as a tracer to visualise the flow of cold shielding gas from a GMAW torch. Laser light was formed into a sheet with the light scattered from the oil particles imaged by a camera. Dahmen et al. (1993) under took scattering to visualise the gas shielding effect during laser welding. In this case external particles were not artificially introduced, rather the imaging depended on the fume produce by the welding laser plasma to act as a scattering medium. A second laser of a different wavelength was used to illuminate the plume of particles for visualisation. As the laser wavelengths were different an optical filter placed in front of the camera could be used to differentiate the scatter from the imaging laser beam from the significantly more intense welding laser and the plasma emission.

Both of the above examples demonstrate the ability to relatively simply collect images that highlight regions containing scattering sources. However it remains difficult to quantify or even guarantee relative measurements of particulate concentration from the scattered light signal detected. This difficulty is due to the potentially variable optical properties of the fume.

2.5.2.1 Single particle scattering

The total light power scattered by a signal particle P_{sca} is the product of the intensity of irradiating beam I_0 and the scattering cross-section C_{sca}, Equation 2.16.

$$P_{sca} = C_{sca} I_0 \tag{2.16}$$

Scattered power P_{sca} however is not radiated uniformly, being dependent on both the angle to the incident θ and polarisation direction ϕ of the incident beam. The scattering cross-section C_{sca} arises from how the field discontinuity of particle interrupts the path of the light through the surrounding medium. As such it is dependent on a number of optical properties including particle geometry, composition, surrounding environment and wavelength of the incident light. The relative difference between the scattering cross-section and the physical cross-section A of the particle is represented as a scattering efficiency Q_{sca}.

$$Q_{sca} = \frac{C_{sca}}{A} = \frac{P_{sca}}{P_{inc}} \tag{2.17}$$

$$P_{inc} = A I_0 \tag{2.18}$$

The intensity of the scattered light at distance r from the single particle at angles θ and ϕ to the incident can be expressed by way of Equation 2.19.

$$\Im_{sca} = \frac{1}{k^2 r^2} F(\theta, \phi) I_0 \tag{2.19}$$

$$k = \frac{2\pi}{\lambda} \tag{2.20}$$

Where $F(\theta, \phi)$ is a dimensionless scattering function and k is the wave number of the incident beam.

2.5.2.2 Scattering from clouds of particles

Clouds consist of a great number of individual particles. Scattering of light from a cloud however is only proportional to the number of individual particles if particular criteria are met (Jones 1999). These are firstly that the particles are randomly arranged such that the scattered light from individual particles is incoherent and secondly that there is an insignificant level of multiple scattering. That is, once light has been scattered from a single particle it is unlikely to be further scattered by other particles before detection. A third criterion is that particles have sufficient space between them that the field effect of the individual particles do not interact. The upper limit for this third requirement suggested by Jones (1999) is displayed in Table 2.5.

Should the above requirements be met then power scattered by the cloud is the sum of the N individual particles.

Particle radius μm	Concentration m^{-3}
0.1	10^{19}
1.0	10^{16}
10.0	10^{13}
100.0	10^{10}
1000.0	10^{7}

Table 2.5: Maximum concentration of particles to avoid direct interaction effects (Jones 1999)

$$P_{sca,total} = \sum^{N} P_{sca.i}$$

If all the particles exhibit the same scattering cross section then the scattered light is the product of the number of particles.

$$P_{sca,total} = NP_{sca.i}$$

Likewise the intensity of scattered light detected at distance r from the scattering source becomes

$$\Im_{sca,total} = \frac{N}{k^2 r^2} F(\theta, \phi) I_0 \tag{2.21}$$

Resultantly if the optical properties of the scattering particles and the experimental setup remain the same then the intensity of the light detected is proportional to the number of particles from which the light was scattered.

2.5.2.3 Rayleigh approximation

The above explanation of laser scatter hides much of the complexity of the optical technique in variables and functions related to the optical properties of the particles. Practically much of this complexity can often be deliberately overlooked if the particles, and other experimental properties, remain constant. This is likely if the particles are externally introduced from a controlled source and remain unchanged. However if the particles change or are unknown then consideration of how the optical properties change is required. Several different theories and approximations exist for the modelling of scattering. One of the more complete theories is known as Mie theory first suggested by Mie (1908). The completeness of the theory is weighed with mathematical complexity. The mathematical complexity of Mie theory however can be avoided by utilising particular approximations that can be applied to specific cases with generally acceptable levels of correlation.

Where the particles are much smaller then the wavelength of the light Rayleigh approximation can often be applied. Formally this is stated as $x \ll 1$ and $x\,|m-1| \ll 1$ where x is the particle size parameter, Equation 2.22 and m is the complex refractive index of the particle (Jones 1999).

$$x = \frac{\pi \times D}{\lambda} \tag{2.22}$$

Rayleigh approximation is a common consideration for soot measurements in combustion research. That is the soot particle size parameter is small enough that Rayleigh theory is a sufficient approximation on its own or with adjustment for the research application. The particle size parameter limit of Rayleigh approximation for soot suggested by Kent et al. (1981) was $x < 0.3$. Although others have suggested other upper ranges of appropriateness (Jones 1999).

From Rayleigh approximation the scattering cross section for a single spherical particle can be determined with Equation 2.23.

$$C_{sca} = \frac{8\pi}{3} k^4 \left| \frac{3V}{4\pi} \frac{m^2-1}{m^2+2} \right|^2 \tag{2.23}$$

Where V is the volume of the particle. From this it is clear that the scattering cross section and hence the power scattered is proportional to the square of the particle volume. The unfortunate result of this is that doubling the volume of a single particle increases the scattered power by a factor of four, while simply having that same volume split between two particles only results in a factor of two increase. In this way it is difficult to quantify the volume occupied by a cloud of particles of unknown number and variable size based on scattering alone. Indeed this is the case with soot that changes in both size and number during nucleation, growth and oxidation within different areas of the flame. So while simple to perform and good for general visualisation, laser scattering is limited in its quantitative capacity when the particles are changing in volume or other optical properties.

The intensity of scattered light detected from a single spherical particle at distance r from the scattering source from Rayleigh approximation is given by Equation 2.24.

$$\begin{pmatrix} \Im_{\parallel,sca} \\ \Im_{\perp,sca} \end{pmatrix} = \frac{k^4 \left|\gamma\right|^2}{r^2} \begin{pmatrix} I_{\parallel,0} \cos^2\theta \\ I_{\perp,0} \end{pmatrix} \tag{2.24}$$

$$\gamma = \frac{3V}{4\pi} \frac{m^2-1}{m^2+2}$$

Where $\Im_{\parallel,sca}$ and $\Im_{\perp,sca}$ is the intensity of the scatter at the detector in the parallel and perpendicular planes. The incident beam being represented in parallel $I_{\parallel,0}$ and

perpendicular $I_{\perp,0}$ components.

2.5.3 Laser induced incandescence

Scattering measurements can not be used for relative volume concentration measurements when the number and size of the particles are changing. In the case of particles sufficiently small for Rayleigh approximation this is because the intensity of the scattered light is directly proportional to the number but the square of the particle volume. This represents a significant problem in combustion research where the soot size and number is different in different areas of a flame at any instant. As a result other methods have been investigated to provide optical measurement of particulate volume. One method that has attracted interest in combustion research is laser induced incandescence. In this process the incident laser beam is absorbed heating the particles to a temperature where the incandescence is then observable. This is feasible for Rayleigh sized particles as unlike the scattering cross section, Equation 2.23, the absorption cross section is directly proportional to volume, Equation 2.25.

$$C_{abs} = -4\pi k \mathbf{Re}\left(\frac{3V}{4\pi}\frac{m^2-1}{m^2+2}i\right) \tag{2.25}$$

The amount of energy absorbed by a single particle from the incident beam is therefore also directly related to the volume, Equation 2.26.

$$P_{abs} = C_{abs} I_0 \tag{2.26}$$

Within certain limitations the absorption by a cloud of particles is then sum of the absorption of the individual particles on which the incident beam interacts.

$$P_{abs,total} = \sum^{N} P_{abs.i}$$

The total absorption is then proportional to the total volume of the fume particles. A common source of laser illumination for LII is a relatively short duration laser pulse. Due to the small size of particles in the Rayleigh size range and the thermal conduction of the solid particles heating occurs rapidly and fairly uniformly through the volume of the particle in response to the energy absorbed from the laser pulse. Heat dissipation from the particle into the surrounding is much slower.

Figure 2.26 displays calculated temperature and relative energy transfer from a soot particle heated by a laser pulse (Will et al. 1998). Particle heating occurs for the duration of the laser pulse, in this instance approximately the first 10nS. Subsequent to the laser pulse the temperature of the particle decays as heat is dissipated from the

Figure 2.26: Relative magnitudes of various heat loss mechanisms from a laser heated soot particle (Will et al. 1998)

particle into the surrounding environment. Heat transfer from the particle occurs from a number of different mechanisms including vaporisation, conduction and radiation. Thermal radiation being responsible for the particle incandescence detected during LII. While the energy absorbed by particles from the incident beam is proportional to volume, the actual detected signal is not since energy is also dissipated in forms other than thermal radiation. Quantification of LII therefore requires all the different energy transfer mechanisms to be accounted for.

Vaporisation involves the dissipation of latent heat energy as mass from the solid particle is converted into vapour. Reduction in mass and volume of the particle also alters the amount of conduction and radiation. The amount of vaporisation depends on a number of factors including the composition of the particle, the surrounding environment and laser intensity.

Conduction can occur to the surrounding gases or to neighbouring particles in an agglomerate. The amount of heat dissipation by conduction depends on the size of the particle and the surrounding environment.

Thermal radiation is responsible for incandescence signal that is detected. Unlike the scattered signal incandescence is radiated uniformly and is neither polarised or coherent. The spectrum of the incandescence depends on the composition and temperature of the particle, with higher temperatures shifting the emitted spectrum toward the shorter, blue, wave lengths. Since the temperature of the particle decays after laser heating the spectrum of the thermal radiation becomes progressively longer in wavelength. Prompt detection, that is detection of the incandescence for a short period after laser heating, is desirable. The incandescence signal detected promptly is less dependent on on the integrated effects of conduction and vaporisation related cooling therefore more quantifiable. Since the incandescence is strongest

immediately after heating there is also the ability to obtain the best signal to noise ratio. However prompt detection has increased chances of detection of laser excited optical emissions unrelated to the temperature of the particle. Such signals could arise due to direct laser scatter, excitation of the ambient gases or particle vapour, chemiluminescence of recombining vaporised products, particle photoluminescence or particle plasmon resonances (Vander Wal et al. 1999). Spectral filtering of the optical emission can be used to reject some of these emissions along with any other ambient background illumination. Optical filtering however requires the spectrum of the particle incandescence and the undesirable emissions to be known.

In the case of soot significant research effort has been involved in quantifying these different mechanisms to develop applied LII measurements of volume fraction and size (Bladh & Bengtsson 2004). Laser induced incandescence has been used to collect point, line, and 2D images of soot volume fraction. A common source of laser illumination is a pulsed Nd:YAG laser. The type of detector, camera or photodiode, depends on the measurement being performed. Soot volume fraction measurement can utilise a blue optical filter about 420nm with the detector. This filter passes the incandescence of the soot at peak temperatures and blocks identified unrelated emissions including natural soot incandescence from flame heating. The effect of particle vaporisation is usually investigated by changing the laser intensity and recording the incandescence signal. Among other things the shape of the plot is dependent on laser profile, particle size, particle composition, detection spectrum and detection time.

Figure 2.27: Soot LII fluence curve (Vander Wal & Jensen 1998)

Figure 2.27 displays a fluence curve showing a plot of incandescence signal versus excitation laser intensity. The laser intensity is represented by the energy in the laser pulse divided by the cross sectional area of the beam. Initially the LII signal

increases with laser excitation and particle temperatures. Vaporisation increases with temperature and the plot plateaus when latent heat loss accounts for the excess laser heating. At higher laser fluence the mass loss from the particle reduces the amount of incandescence. Undertaking LII measurements with laser fluence in the plateau region is considered desirable providing the strongest incandescence. Also in the plateau region consistency of laser pulse intensity is less critical as changes can occur with minimal change in resulting incandescence signal. Detector sensitivity, and to a lesser extent particle vaporisation, is taken into account by calibrating the recorded incandescence signal. Soot volume fraction calibration could be done by measuring the incandescence from a well studied flame with known properties. Alternatively the incandescence signal could be calibrated with another more easily quantified method for the same flame.

Application of LII to particles other then soot is less developed. Vander Wal et al. (1999) demonstrated LII with pure Iron, Titanium, Molybdenum and Tungsten nanostructures formed with laser ablation in a high pressure Helium chamber. Even in such a controlled environment the results highlighted the necessity of spectral and temporal measurements to identify the LII from other laser excited emissions. Particle vaporisation was also found to be significant particularly in Iron. Further investigations of Iron nanoparticles have been conducted including the application of LII for size determination (Kock et al. 2005).

2.5.4 Laser extinction

Laser beams can interact with clouds of particles in numerous ways. Two general groups of interactions, scattering and absorption, have been discussed briefly in previous sections. Scattering is the deviation of the incident laser energy and absorption is where the energy is taken on by the particle. Both of these processes remove energy from the incident beam. The total energy removed from the incident beam during transmission through the cloud of particles is then the sum of the absorption and the scattering.

$$P_{ext,total} = \sum^{N} (P_{abs.i} + P_{sca.i}) \tag{2.27}$$

The combined effects of scattering and absorption on the reduction of the incident beam is known as extinction. Transmitted laser energy is that which is not removed from the incident beam by cloud extinction. This is useful as the power or intensity of the incident and transmitted beams can be relatively simply measured. The difference between the incident and transmitted beam can be then be used to determine the amount of extinction and integral of the particulate properties along the line of interaction.

The relative difference between the incident and transmitted beam has been used in

combustion research to determine the mean soot volume fraction υ in flames using Equation 2.28 (Kent & Bastin 1984, Kent et al. 1981, Santoro et al. 1983).

$$\upsilon = \frac{-\lambda}{6\pi \times imag\left(\frac{m^2-1}{m^2+2}\right)} \times \frac{ln\left(\frac{I_0}{I_t}\right)}{L} \tag{2.28}$$

Where I_0 is the incident laser beam intensity and I_t is the transmitted beam intensity after passing through the flame, λ is the wavelength of laser, m is the complex refractive index of the soot particles and L is the path length through the flame. Once again this makes the assumption that the the particles are sufficiently small that Rayleigh approximation can be applied with reasonable accurately. The derivation of the equation also uses the simplification that absorption is dominant and scattering is an insignificant component of extinction.

Equation 2.28 provides a quantitative but line of integrated average soot volume fraction. On its own this can be useful for combustion research. Unless the flame is stable and either uniform or radially symmetric this measurement technique can not be used to determine spatial soot concentrations. Extinction measurements however provide something lacking from LII soot measurements. While LII was able to provide relative spatial soot volume fractions without reference the results were not able to be quantified. Extinction measurements can be used to provide the required reference for LII calibration by undertaking both measurements along the same laser path.

2.5.4.1 Refractive index

Quantitative extinction measurements require the complex refractive index m of the particulate matter to be known. In the case of combustion, refractive indexes have been determined for soot in different flames and from different fuels. Metal particles have not had the same level of research interest and resultantly do not have the same quantity of data published. Charalampopoulos & Shu (2003) used laser scattering to determine the optical properties of iron oxide aggregates formed in a $Fe(CO)_5$ seeded flame. Figure 2.28 displays a scanning electron microscope image of Fe_2O_3 Iron oxide aggregates extracted from the flame 55mm above the burner.

The real and complex refractive index found from the laser scattering at different heights in the flame is displayed in Table 2.6, where D_p is the mean primary particle diameter and N_p is the mean number of primary particles in the agglomerate.

2.6 Summary

Gas metal and flux cored arc welding were introduced as widely utilised high productivity metal joining processes. The operation of arc welding is dependent on

Figure 2.28: SEM image of Iron oxide aggregates formed in a flame (Charalampopoulos & Shu 2003)

Table 2.6: Refractive index of Iron oxide aggregates formed in a flame (Charalampopoulos & Shu 2003)

a number of thermal, mechanical and electrical interactions. Interdependent variables result in complex nonlinear behaviour that present a challenge in both industry and research. An unfortunate byproduct of arc welding is gases and particulate emissions collectively known as fume. Inhalation of these fumes potentially cause both acute and chronic medical conditions. For this reason fume exposure reduction is important particularly for career welders. Currently the most effective method of exposure reduction is by intercepting the transfer of fume from the welding arc to the operator breathing zone with ventilation and fume extraction.

Fumes dissipate into the workplace by way of a thermally buoyant plume. Measurement of the fume plume dissipation close to the welding torch has previously proven difficult requiring researchers to use water modelling and computer simulation. Application of lasers in other welding and combustion research situations indicate that similar techniques could be applied to the measurement of particulate welding fume in the region previously requiring simulation. Three different laser techniques are proposed being laser scatter, laser induced incandescence and laser extinction. Laser scattering providing good visualisation of plumes contain particulates. Scattering in some situations however is not proportional to particulate concentration. Combustion research has investigated LII as an alternative measurement of soot concentration. However on its own LII is not quantitative, requiring calibration. In the case of soot, calibration can be done with laser extinction, a relatively simple process. The aim of

the research presented here is to trial these three laser techniques for the measurement of welding plumes and to investigate the fume plume close to the welding torch.

Chapter 3

Experimental methodology

3.1 Introduction

Three different laser diagnostic processes were identified that would provide different types of data on the particulate matter found in welding plumes. The three different laser diagnostic methods were laser scatter, laser induced incandescence and laser extinction. The purpose of these experiments was to investigate the fume plume generated by GMAW and FCAW processes in close proximity to the welding arc. These processes were identified as being able to provide a mixture of results on the shape and particulate density of the fume plume generated from GMAW and FCAW welding processes.

The function of the initial experiments was to investigate the application of laser diagnostics and to study how the laser beams interact with the fume plume. Secondly these laser techniques were applied to investigate the plume and how it dissipates into the surrounding air. The effect of different welding variables were then investigated by adjusting relevant welding parameters.

3.2 Welding rig

The ultimate goal of these experiments was to conduct laser diagnostics to investigate welding processes. For these experiments to prove useful in determining fume control strategies the welding processes studied would optimally be as close as possible to the real world application. The experimental set up was required to emulate a welding process within the confinements defined by laboratory and instrumentation limitations. In addition the experimental set up also needed to be sufficiently flexible to allow for a wide range of welding variables to be studied. One requirement that became clear early in the design of the experimental setup was the necessity of having a welding arc which remained in a stationary position. As the laser and associated optics are fixed it would

have been inconvenient and impractical to have a moving arc and hence moving fume source. It was also determined that the welding process would need to be run for an extended period of time during the setup of the lasers, optics and subsequent number of welding variables investigated. As such, to conduct the welding manually with an operator moving the torch, as would be found in the situations where welding fume is of most concern, would be unsuitable. For this reason an automated welding rig was constructed to undertake the welding. The majority of automated welding processes used in industry move the welding torch with respect to the stationary objects being joined. In this case due to the requirement of needing a stationary arc the metal onto which the weld was deposited needed to move with respect to the welding torch. Several ways of doing this were considered including indexing a flat plate horizontally in the X and Y directions and the use of a rotating flat circular plate below the torch. Due to the space restrictions placed on the welding rig within the laser laboratory and the possible requirement for long weld runs the surface of the material required maximum utilisation. It was determined that the best way to achieve this requirement was with the use of a moving rotating drum. In this configuration the weld could be deposited in a helical pattern around the drum. Doing so utilised three dimensions unlike welding onto a flat plate which only uses two and resultantly more floor space. Using a cylindrical drum also allowed for an increased vertical access angle when passing a laser in the immediate vicinity of the arc. The conceptual design of this welding rig is similar to that used for other fume research including those used by Quimby & Ulrich (1999) and Slater (2004).

Given the geometry of the laboratory it was determined that the floor space available to place the automated welding rig was limited to an area of 1.2m by 1.2m. This ultimately limited the length of the drum which moved within this confinement. For the helical weld to be produced the drum was required to rotate and move linearly along the same axis. These two actions need to be correlated to produce a constant spiral. This was achieved by mounting the drum, onto which the weld would be laid, on rollers mounted to a moving stage. The linear movement of the stage was obtained by using a ballscrew attached to a stepper motor through a 50:1 reduction gearbox. A second stepper motor and 50:1 gearbox was used to turn the rollers that supported the drum. The size of the rollers were designed to obtain the required pitch on the weld spiral when the two stepper motors were run at the same speed. The stepper motors were driven from a controller box built in house. This allowed the weld traverse speed to be set. This control system was calibrated by timing the speed of rotation of the rollers on which the parent material pipe was placed.

The drum onto which the welds were laid, and therefore the weld parent material, was made from 250NB Ultrapipe sourced from Onesteel. This pipe had a nominal outer diameter of 273.1mm and a wall thickness of 6.4mm. This pipe was cut into 450mm lengths by Onesteel so they could be placed directly onto the welding rig. The supplied

surface finish on this pipe was a mixture of superficial rust, millscale and lacquer. These surface contaminants were removed prior to welding with a anglegrinder to expose the clean steel. The composition of this steel used for the drum can be seen in Table 3.1.

$\%C$	$\%Si$	$\%Mn$	$\%S$	$\%P$	$\%Ni$	$\%Cr$
0.135	0.12	0.66	0.006	0.013	0.017	0.018
$\%Mo$	$\%Cu$	$\%Al$	$\%Nb$	$\%Ti$	$\%V$	C_{eq}
0.003	0.017	0.031	<0.003	<0.003	<0.003	0.25

Table 3.1: Typical steel composition for Ultrapipe (Layton 1998)

Where the carbon equivalent C_{eq} is defined by Equation 3.1.

$$C_{eq} = C + \frac{Mn}{6} + \frac{Cr + Mo + V}{5} + \frac{Cu + Ni}{15} \tag{3.1}$$

The welding torch was mounted to the stationary base of the welding rig via an adjustable arm. This arm allowed the height of the torch above the top of the drum to be adjusted thereby setting the standoff distance. The torch itself was mounted vertically normal to the drum surface.

Electrical return from the rotating drum was made via four sintered copper graphite brushes from a truck starter motor. These brushes were spring mounted to provide a smooth running contact against a copper plate bolted onto one end of the rotating pipe, Figure 3.1. Each of these four brushes had a copper tab sintered into them which was bolted to a copper block onto which the earth clamp from the welder was connected. In addition to providing the electrical return the load applied by the brushes on the copper plate held the welding drum in position against a lip on the rollers supporting the opposite end, fixing the drum's axial location.

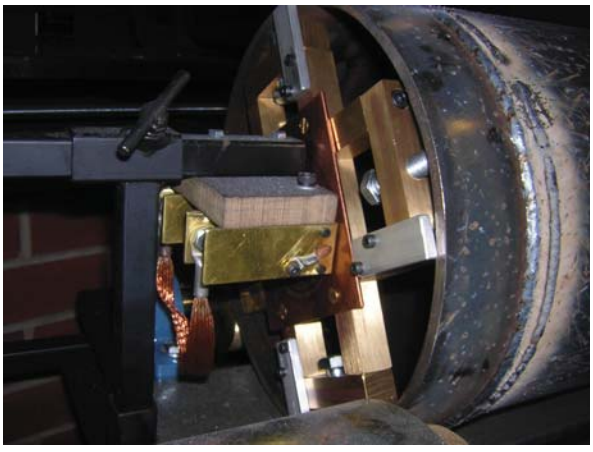

Figure 3.1: Electrical return contact from rotating drum

Some of the weld beads deposited onto one of the drums during the experiments can be seen in Figures 3.2 and 3.3.

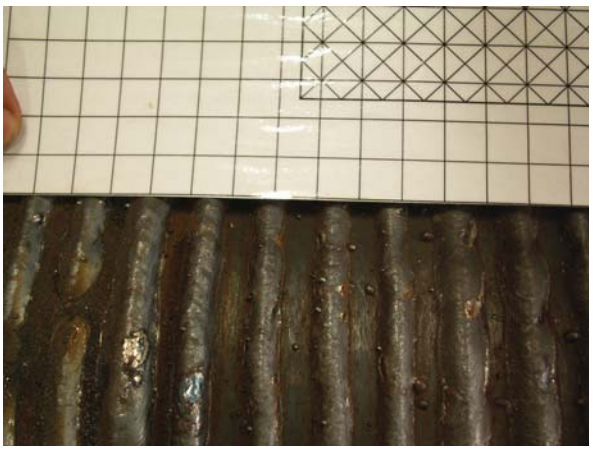

Figure 3.2: Weld beads deposited on drum

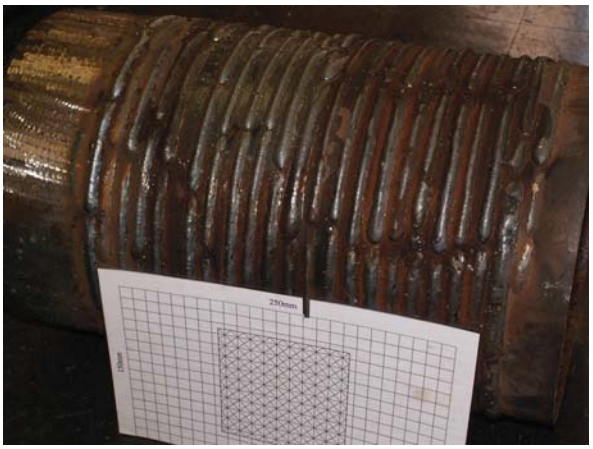

Figure 3.3: Weld beads deposited on drum

3.3 GMAW equipment and variables

One of the most significant difficulties in welding research is the number of variables involved in the welding process. This is particularly true since many of the variables are not independent of each other. The number of welding variables also makes it difficult to evaluate experimental data against published results. In order to make the results from these experiments as relevant as possible a literature review was undertaken to identify similarities between previous fume formation work. In a large number of these publications the full range of welding variables were not presented. One publication that provided a good outline of the variables used was that by Quimby & Ulrich (1999). Where possible the variables used by Quimby & Ulrich (1999) were replicated in the experiments undertaken in this thesis.

Due to the number of welding variables involved in fume formation a number of these were considered constants throughout these experiments. The welding variables considered most important for fume formation and plume distribution were identified as droplet transfer mode, heat input and shielding gas flow rate. To investigate the effect of each of these variables they were adjusted individually while other variables remained constant.

Power supply and wire feed unit The power supply used for these experiments was a Kemppi Pro4000 inverter with a Kemppi ProMIG500 wire feed unit fitted with the optional MX Synergic user interface. The power supply was modified to allow for a remote trigger to operate the process and to be synchronised with the detection equipment. The voltage calibration function of the unit was used to account for the resistance of the torch and the return lead. The process voltage and wire feed were set on the power supply which also displayed the current during the welding process. The power supply and wire feed unit remained constant throughout the laser experiments.

Voltage Voltage is the major component in determining the droplet transfer mode in GMAW welding. It is also one component of the heat input. In line with the work reported by Quimby & Ulrich (1999) voltages between 18 and 32volts DC electrode positive were used to obtain the full range of transfer modes for GMAW.

Current The current used in a GMAW process is generally not set but is rather dependent on the wirefeed speed and to a lesser extent on the voltage used. The currents produced from the voltage and wire feed in these experiments ranged from 150 to 310A.

Traverse rate The typical weld traverse speed used was 360mm/min although higher traverse speeds were used to prevent pipe burn through at several of the higher heat inputs.

Wire feed speed Two wire feed speeds were selected for primary investigation of GMAW. These were 4.6 and 7.6 m/min to correspond with FFR plots presented in Quimby & Ulrich (1999).

Wire type The wire used for GMAW remained constant throughout the experiments. The wire used was 1.2mm diameter copper coated Ultramag S6 made by Lincoln Electric. Literature reviews showed that 1.2mm wire was the standard for both experimental and numerical FFR work. The ER70S6 composition of this wire is a slight departure from that used by Quimby & Ulrich (1999) who used ER70S3 wire, but matches that used by Slater (2004).

Torch and contact tip A Bernard welding torch was used in these experiments and remained constant for the bulk of the GMAW experiments. It has been suggested that the condition of the torch liner and the contact tip are factors in the stability of the arc and consequently the FFR. Considering the low volume of welding undertaken in this research relative to the life of the torch liner, the condition could be considered

constant throughout. The torch lead was positioned so as to avoid tight bends and to reduce the force required for wire feed. The contact tip was replaced periodically so that it remained in a near new condition.

Gas type and flow rate Where gas shielding was utilised Argoshield Universal from BOC gases was used. The composition of this gas is displayed in Table 3.2. The standard gas flow rate used in these experiments was 17l/min. However the effect of gas flow on the plume shape was undertaken by conducting experiments with gas flow rates between 0 and 35l/min.

O_2	CO_2	Ar
2.75%	16%	81.25%

Table 3.2: Composition of argoshield universal (BOC gas code 065)

Standoff As mentioned in the design of the welding rig the welding torch was mounted vertically over the drum. As the torch was normal to the drum surface some difficulty was encountered with the torch becoming clogged with welding splatter. The standoff used in these experiments was 19mm to match that used in Quimby & Ulrich (1999).

3.4 FCAW equipment and variables

Flux cored welding was investigated with the use of 0.9mm Shield-cor 15 wire made by CIGWELD designation E71TG5. This electrode can be operated gassless due to self-shielding properties. The CIGWELD operational guide page on this electrode is included as Appendix H. Much of the welding equipment remained the same as that used for GMAW. Voltage and wire feed were found to be more critical in FCAW than the wide range used in GMAW. As suggested in the CIGWELD manual DC electrode negative polarity was used and a voltage of 16.5volts was found to produce the optimal bead profile. Again Argoshield Universal was used where gas shielding was implemented. The gas flow rate was adjusted between 0 and 30l/min to investigate plume shape and density.

3.5 Environmental conditions

The welding processes used for laser diagnostics were undertaken within a laboratory not normally used for such a purpose. As such a significant amount of work was required to prepare the laboratory for this relatively industrial process. Welding curtains were placed around the welding rig to halt the spread of molten splatter from the immediate

area. An extraction hood above the welding torch extracted some of the fume. However due to its large size and low volumetric flow rate its draft had minimal effect in the area of interest where the velocity of the shielding gas and the buoyancy of the heated fume governed the plume shape. Cross drafts were minimised as much as possible but could not be totally eliminated. Room temperature was typically between 25 and 30 degrees Celsius.

3.6 Laser scatter

3.6.1 Introduction

It has been established that the welder's exposure to welding fume is not directly linked to the bulk fume formation rate found with fume box measurements. This is based on the fact that the welder does not inhale the entire fume formation but rather only the portion that reaches their breathing zone. For this reason the dissipation of the welding fume and the transmission between the source of the fume and the breathing zone is of importance. The dissipation of the fume plume close to the welding torch is also of interest in the formation of gaseous fume components such as ozone and nitrogen oxides which are a result of interactions between UV light emitted from the arc and the atmosphere.

Previous research into welding fume plume dissipation used visual images of the plume and fluid models involving the mixing of salt and fresh water. Direct imaging of the plume needs to contend with the arc emission generated by welding. In addition this direct imaging only considers the extent of the plume and does not allow the investigation of the internal structure of the plume. Similarly salt water modelling of GMAW on its own only displays the extent of the water plume. Salt water modelling has been combined with light induced fluorescence to provide correctional images of the water plume from an emulated GMAW torch. However water models make several assumption in attempting to replicate the real world situation. This is of particular concern since only the external extent of the water plume and actual fume plumes can be compared.

In these experiments light scattered by the particles present in the fume were used to investigate the formation of the welding plume. Obtaining these images in an actual welding plume rather then a water simulation allows for the effect of welding variables to be investigated. These images not only illustrate the plume dissipation but can be used to determine particle density of direct interest in determining welder exposure.

3.6.2 Equipment

The laser system used as a source of illumination for the scattering was a Quantel brilliant BW twins laser. As the name suggest this laser system actually comprises of two individual pulsed Nd:YAG lasers. One of these lasers was used in its normal state for the scattering while the other was reconfigured to provide the laser beam for the LII measurement. The laser beam used for the scattering was a second harmonic of the Nd:YAG being a beam of 532nm wavelength. This laser system produced a 10nS laser pulse at a rate of 10 pulses per second.

A diagram of the optics used for beam forming can be seen in Figure 3.4. The laser beam was directed toward the welding torch with the use of two high powered 532 mirrors. The round laser beam was then turned into a light sheet with the use of two glass cylindrical lenses. The large light sheet used for illumination was formed by using a 750mm cylindrical lens to reduce the width of the beam in a horizontal direction. After passing through this cylindrical lens a second -25mm cylindrical lens was used to increase the height of the sheet in the vertical direction.

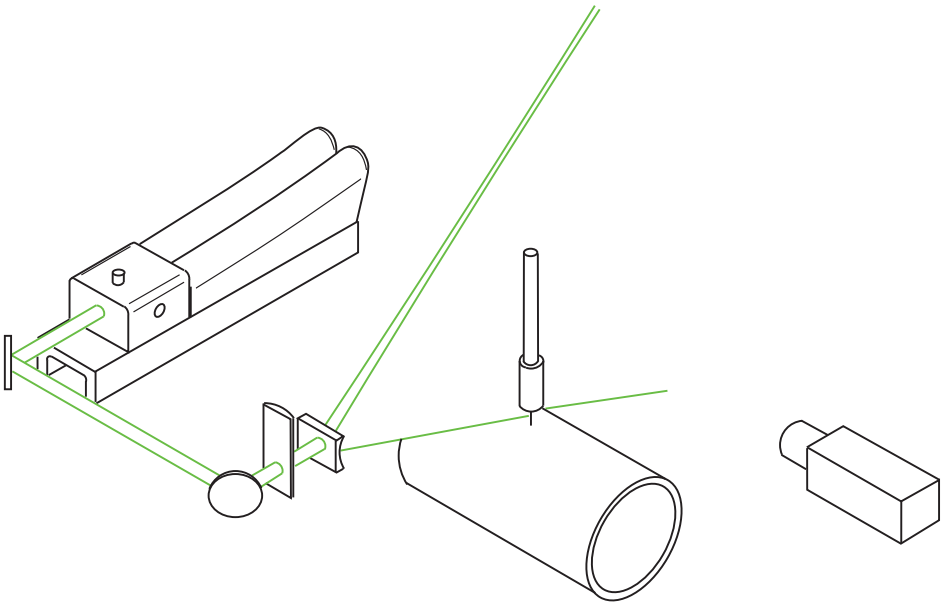

Figure 3.4: Isometric diagram of laser scattering optical layout

With this optical configuration the light sheet was continually increasing in height while the width was reducing up to the focal point of the 750mm lens after which is subsequently expanded. The welding rig was positioned so that the horizontal focal point, and therefore the thinnest part, of the light sheet was adjacent to the welding torch. The light sheet after passing through the welding plume zone was subsequently dumped into a large beam stop to prevent stray laser light. The reflection of the green light sheet off surfaces which it contacts can be seen in Figure 3.5.

A photo of the welding rig taken shortly after the weld had been terminated can be seen in Figure 3.6. The laser scatter from the residual fume can be seen in green to the

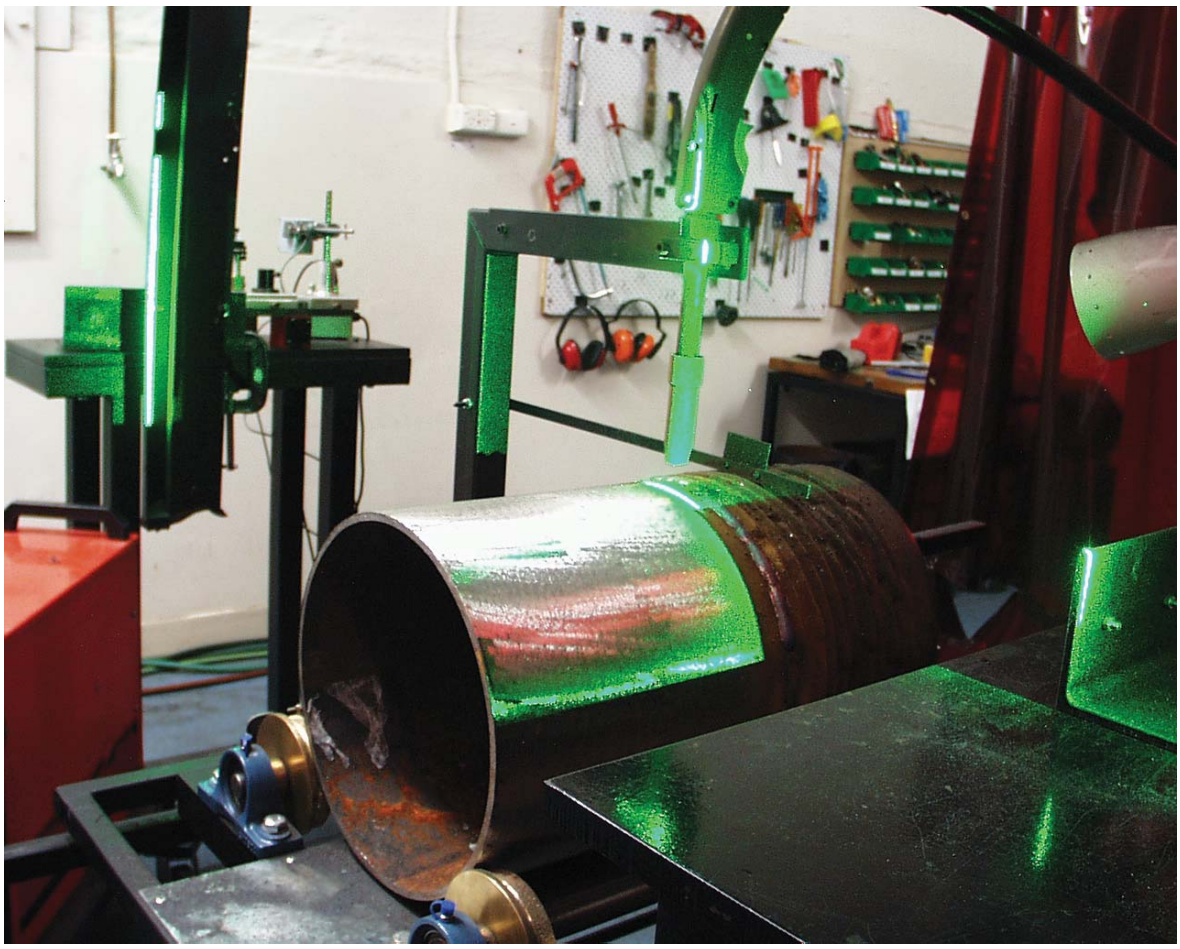

Figure 3.5: Photo of laser sheet reflections

right of the welding torch. Standard digital photos during the welding process were unable to suppress the background light from the arc as seen in Figure 3.7.

Toward the end of the scattering experiments a smaller light sheet was formed to investigate the region immediately beneath the welding torch. This light sheet was formed by expanding the height of the laser beam with a -25mm cylindrical lens and then re-collimated with a 100mm cylindrical lens. The width of the light sheet was reduced with a 1m cylindrical lens placed so that the thinnest part of the sheet was underneath the gas shroud of the torch.

The scattered signal from the laser light sheet passing through the plume was imaged with a megaplus ES1 CCD camera placed normal to the laser light sheet. To reduce the effect of the background light generated by the arc unrelated to the laser scatter a bandpass filter and polariser were fitted to the camera lens. The interference bandpass filter used was made by Andover Corporation having a central wavelength of 532nm band width of 3nm. This limited the spectrum of the light captured to that of the laser and rejected the majority of the intense broad band emission generated by the arc. A Hoya thin film polariser was used so that only vertically polarised light was captured. To reduce the effect of the background light the camera exposure was minimised and synchronised with the laser pulses.

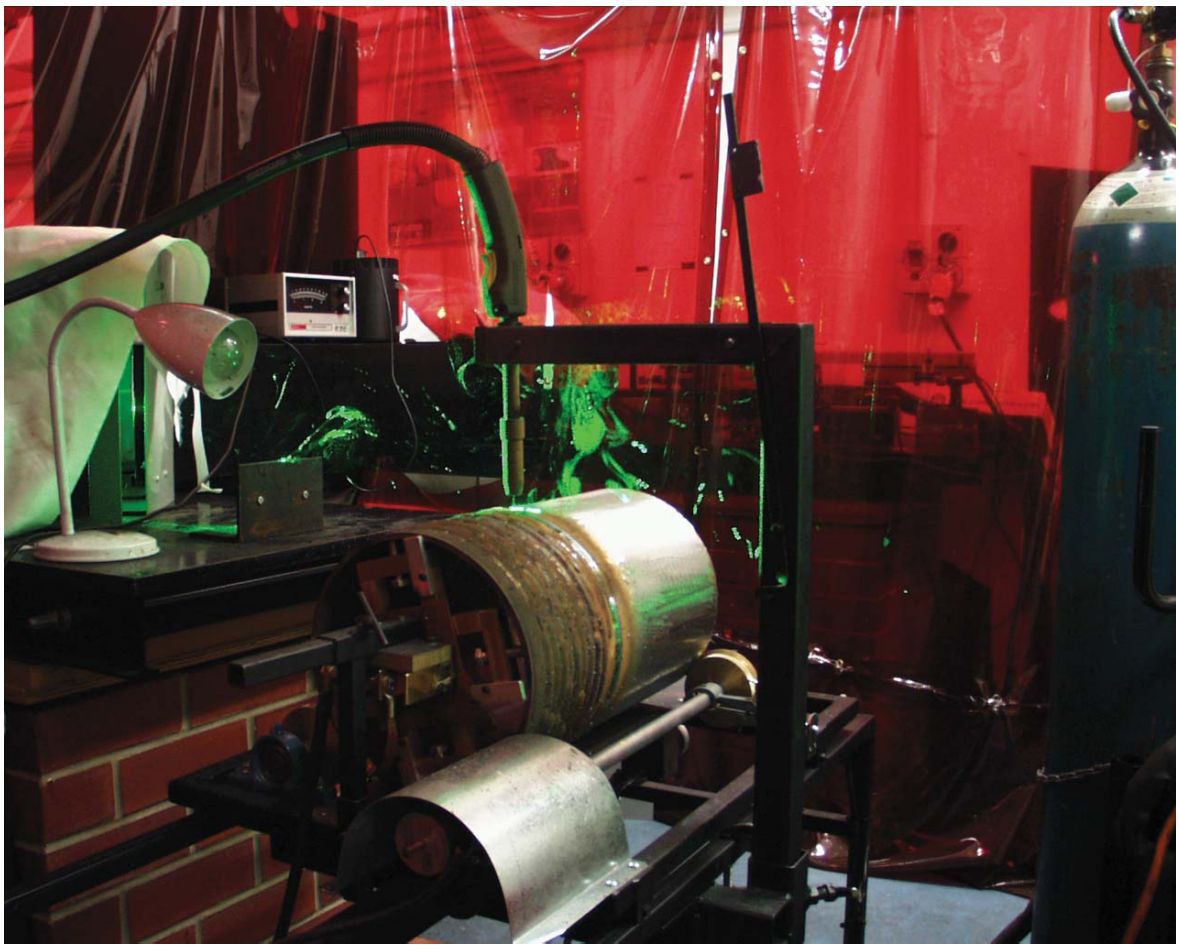

Figure 3.6: Photo of welding rig during the laser scatter experiments

The laser was controlled by externally triggering the flash-lamps and Qswitch to produce laser pulses at a rate of 10Hz. The power of the laser pulse was controlled by adjusting the time between triggering the flash-lamp and the Qswitch. A Standford research systems DG535 pulse generator was used to control these two timing signals. A microprocessor was used to generate a delay from the flash lamp signal to trigger the camera so that the minimum exposure time of 127uS could be used to image the laser pulse. A diagrammatic layout of the experiment control system is displayed in Figure 3.8.

In addition to triggering the camera the microprocessor was programed to control the welding equipment. By doing so the rotation of the welding drum would start rotating shortly before the weld was initiated. Images of the fume cross section were captured from the initiation of the arc at the rate of 10 per second for 20 seconds. The weld was automatically terminated after 15 seconds allowing for the fume dispersion to be imaged post weld for 5 seconds. Initial welding trials indicated that the plume in the area of interest would become fully developed well within this 15 second period. By capturing images in this way the plume shape and density could be studied across the entire welding process.

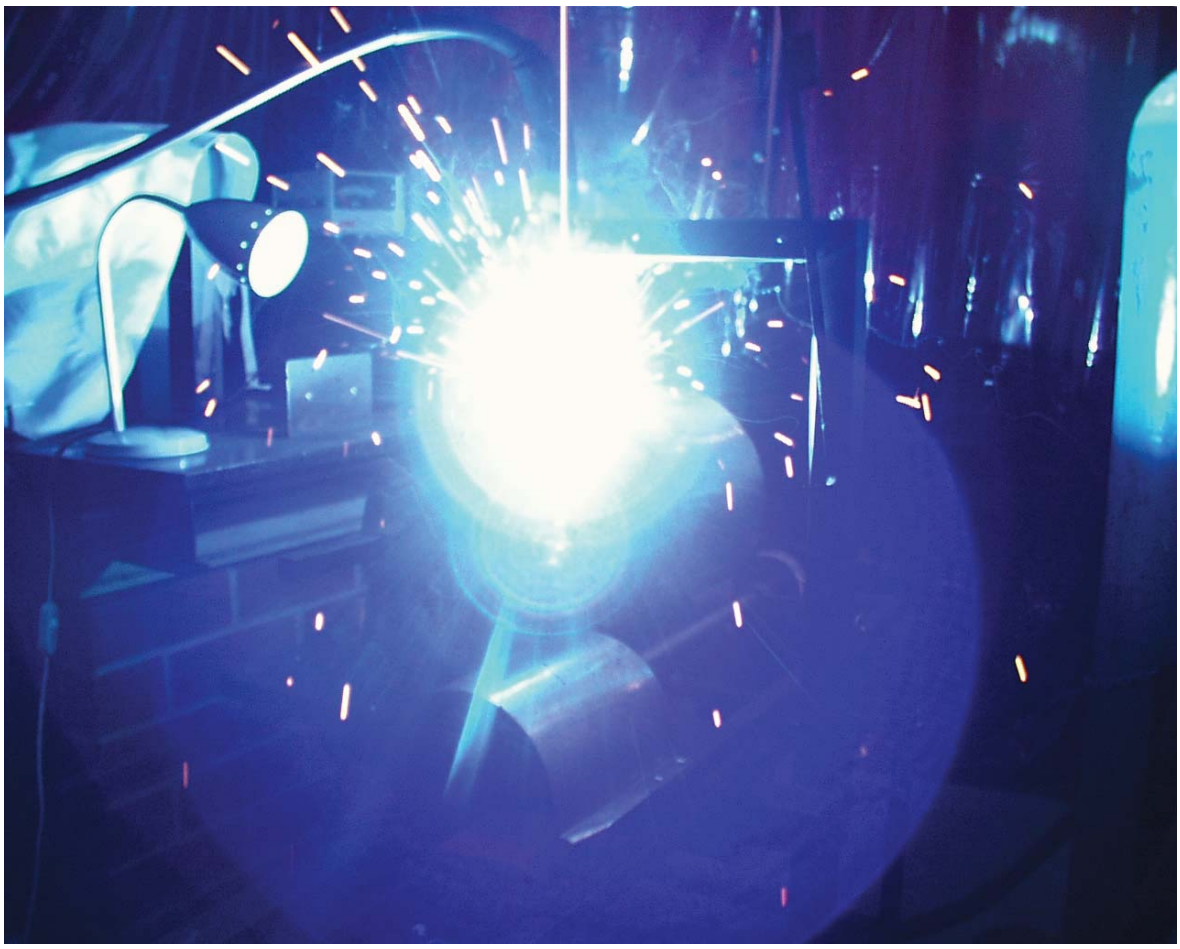

Figure 3.7: Background light from arc

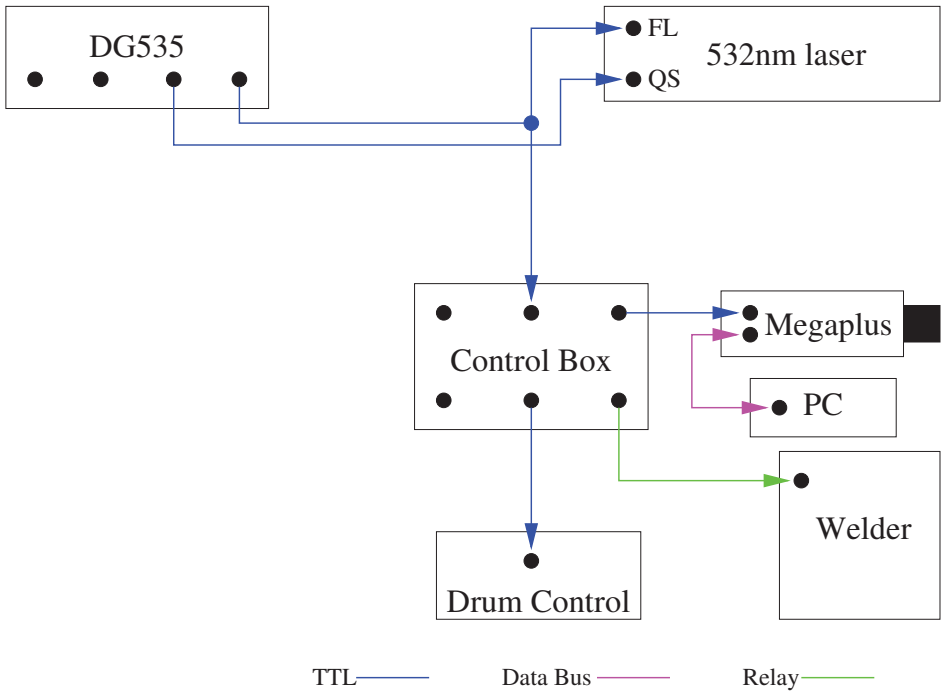

Figure 3.8: Diagrammatic timing layout used for laser scattering measurements

3.6.3 Experimental procedure

Initial experiments conducted investigated the effect of different laser, camera and optical configurations. Having obtained a general understanding of system performance

a large range of different welding variables was investigated.

At the beginning of each day the laser power was measured and the second harmonic crystal angle adjusted as appropriate to obtain the maximum 532nm laser power. Having optimised the laser system the laser power was then adjusted to the appropriate level. The Megaplus camera was then focused on a test target in the same plane as the laser sheet. Several test welds were then conducted to check that all was operational. Experiments were then performed with welding variables defined to outline a particular relationships. Where practical these variables were chosen from the predefined list at random to reduce the effect of time dependent aberrations in system performance. Having set up the welding variables the camera was activated so as to wait for the external timing signals. At this point the central controller was switched on activating the welding rig, the power supply and triggering the camera. Once all the images were collected they were saved to the hard drive of the computer while the variables were being set up for the next weld.

3.7 Laser induced incandescence

3.7.1 Introduction

While scattering provides good visualisation the intensity of scatter is not proportional to fume volume where the size of the particles is changing. As such scattering is considered less than ideal for quantification of soot volume fraction in combustion research. For this reason other methods such as LII have been investigated. The aim here is to investigate LII applied to welding fume.

3.7.2 Equipment

While the first laser in the Quantel BW Twins was used to produce the beam for the scattering the second laser unit was used for the LII. It is unusual to obtain 2 separate laser beams from this laser system as it is designed to collimate the beams into a single output. In its normal configuration the infrared beams from each of 2 lasers are combined then doubled in frequency to produce overlapping 532nm laser pulses. The infrared 1064nm beam from one of these lasers was removed from the combining module by adjusting the location of a mirror and drilling a hole in the case of the laser.

The 1064nm beam was sent directly from the laser to the rear of the optic table and directed toward the welding torch just above the unexpanded 532nm laser beam. This laser beam was then formed into a sheet with the use of three cylindrical lenses. The beam was first expanded vertically with the use of a -25mm cylindrical lens then re-collimated with a 100mm cylindrical lens. This vertically expanded beam then passed

through a 750mm cylindrical lens to reduce the thickness of the laser sheet. In doing so the height of the sheet remained constant while the width of the laser sheet reduced up to the focal point near the welding torch from which point it expanded. This laser sheet was then captured in the beam dump. An isometric sketch of the LII optical layout is presented in Figure 3.9.

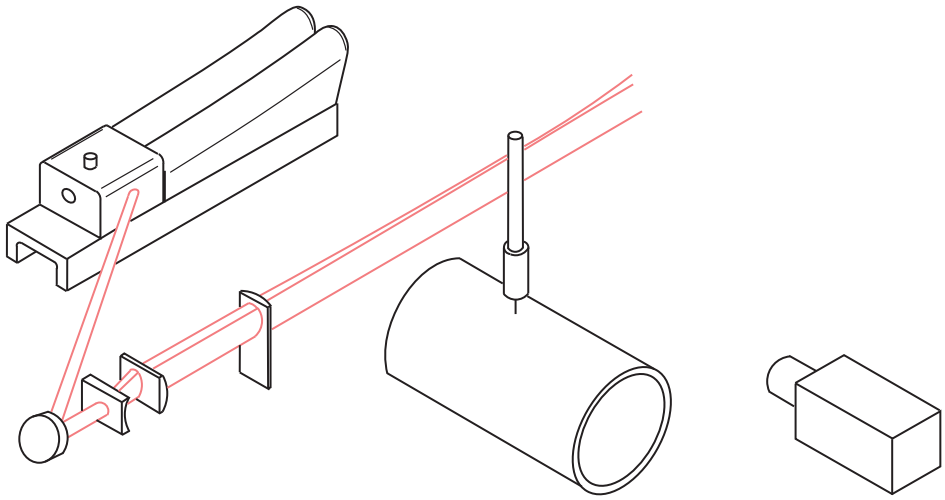

Figure 3.9: Isometric diagram of LII optical layout

The camera used to detect the LII signal was placed with the camera used to detect the laser scatter normal to the light sheet. The camera used to detect the LII signal was a Princeton instruments intensified charge coupled device ICCD with a second generation intensifier. The intensifier on this camera provided increased sensitivity allowing for low light intensity images to be collected. The extra sensitivity provided by the intensifier could be adjusted on a scale between 1 and 10. After having conducted some initial LII measurements in the welding fume the gain of the camera was set to 8. The intensifier was also used to set the duration of exposure with a high voltage gate signal.

The exposure of the camera was controlled by externally triggering the high voltage pulse generator used to drive the ICCD intensifier from the same signal used to trigger the Qswitch input on the laser. Camera exposure was delayed with the high voltage pulse generator to occur some 80nS after the laser pulse to reduce the effect of scattered laser light unrelated to the LII signal. The image transfer rate of this particular camera was slower than the rate at which the laser runs so the busy signal from the camera controller was used to inhibit the output from the high voltage pulse generator. The actual transfer rate of the camera depended on several factors including the amount of electrical interference created from welding arc instability. As in the scattering experiment a microprocessor was used to control the welding equipment and the camera so they commenced operation simultaneously. A diagrammatic layout of the control system used for the LII experiment is displayed in Figure 3.10.

Due to the sensitivity of this camera problems were encountered with the amount of background light unrelated to the LII. The background light could originate as a result

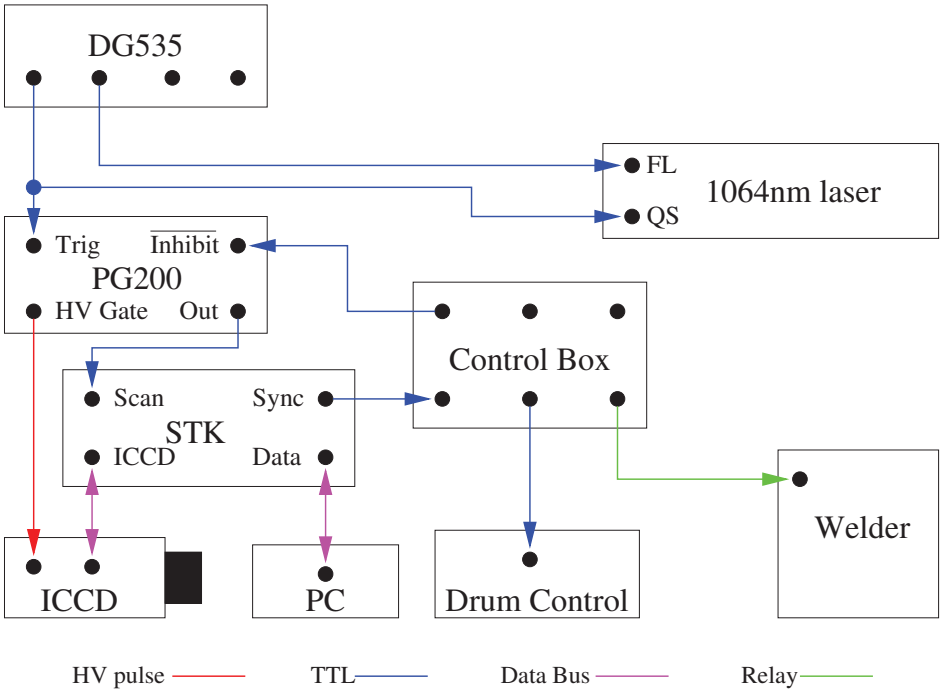

Figure 3.10: Diagrammatic timing layout used for LII

of the intense arc light or as a result of the glowing hot splatter from the weld pool. The camera was shielded from light coming directly from the welding arc with a metal strip attached to the torch support. Without this block internal reflections in the camera lens would interfere with signal collection. The effect of background light from the arc and molten splatter were reduced by limiting the length of exposure. However since the LII signal has a relatively long decay time excessively reducing the exposure time to control background also impacted on signal strength. Typical exposure times were about 800nS. As the LII of the fume particles were more than likely to present a spectrum in the longer lengths of the optical spectrum several optical filters were tried to reduce the background arc light reflected by the fume. Even with this in place the effect of the arc light was noticeable on the detected image. The effect of the molten splatter could be reduced by using welding variable that produced less splatter. However increasing arc voltage to reduce splatter would have also increased arc length and arc background light. Areas closer to the arc had higher background light than further above. For this reason the LII laser sheet was passed through the plume about 140mm above the arc. It should be noted that this is the same height as the line integrated measurement collected with extinction.

3.7.3 Experimental procedure

Since a fundamental laser beam was used for the LII the intensity was more stable and did not require as much adjustment at that used for the scattering experiments. The laser intensity was measured with a power meter. The dimensions of the LII sheet was collected by passing photosensitive paper through the beam path. A resulting burn on

the photosensitive paper is shown in Figure 3.11. Combined the laser power and the dimensions of the burn were used to determine the laser fluence.

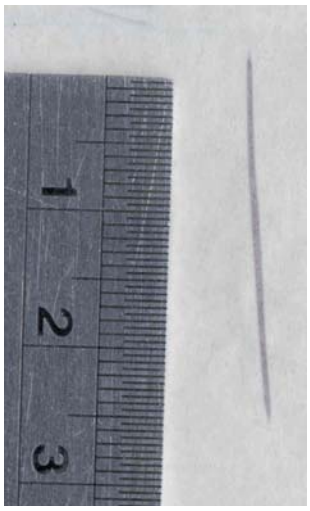

Figure 3.11: Image of IR laser burn on burn paper

Images were collected for a variety of laser fluences and camera timings. Images were also taken for different optical filters in an attempt to minimise the amount of background light relative to the emission.

3.8 Laser extinction

3.8.1 Introduction

Laser extinction was the third laser diagnostic measurement identified of being of some interest. In this process the intensity of a laser beam is measured before and after passing through the particulate matter. While this process is simple and inexpensive relative to other processes investigated it provides baseline information on the interaction between laser beams and the particulate matter. Traditionally laser extinction has been used to measure soot concentrations in flames. This measurement makes a line integrated measurement of the particulate matter through the plume. By making some assumptions on the geometry and optical properties of the particles involved, a particulate volume fraction can be calculated from the laser extinction. Since this measurement is line integrated it does not provide any spatial distribution, but it in the case of soot is used for soot volume fraction calibration of LII images.

3.8.2 Equipment

The laser source used for the laser extinction experiments was a Spectra-Physics Stabilight model 124B Helium Neon laser producing a continuous wave beam of 632.8nm light. This laser beam was then passed through a thin film polariser to ensure

consistent polarisation direction. The continuous wave beam was then modulated with a rotating wheel chopper model SR540 made by Standford research systems. Modulating the laser beam allows for the background light emanating from the welding process to be detected absent of the laser beam and compensated for. Part of the beam was then removed with a beam splitting cube and directed onto a photo diode. The measurement from this photo-diode was used as a reference to compensate for any changes in laser power or sensor temperature drift. The remainder of the beam was then passed adjacent to the welding torch thereby passing through the fume plume. The HeNe beam passed through the plume 170mm above the drum surface. The beam having passed through the plume was then directed onto a second photo-diode which measured the extinguished beam intensity. The amplified photo-diode signals were collected with an analog to digital converter connected to a computer. The capture of the photo-diode signal was synchronised with the beam chopper to allow for phase locked average of the two beam intensities to be collected over a period of time.

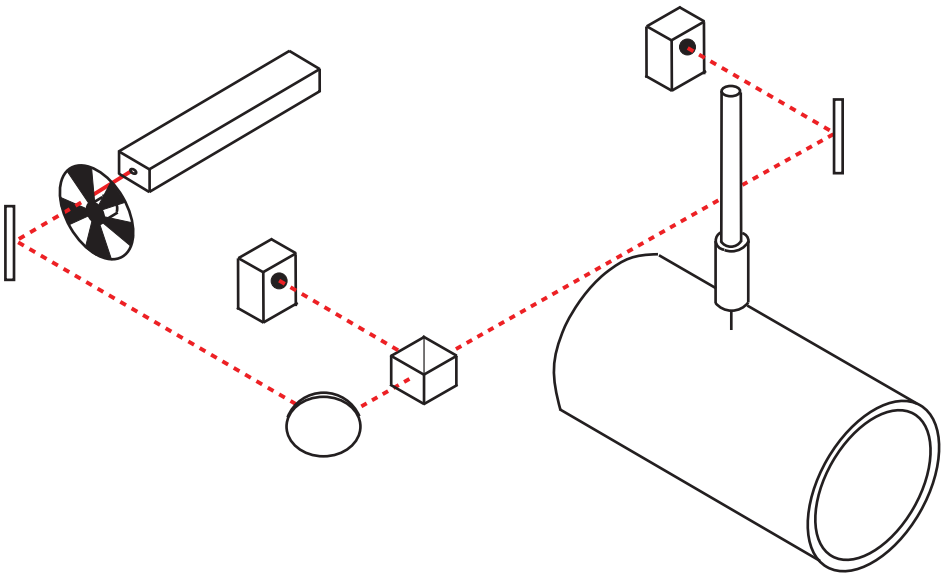

Figure 3.12: Isometric diagram of extinction optical layout

3.8.3 Experimental procedure

Reference and extinguished laser beam intensities were collected once the welding process had started. Extinction data was collected for different shielding gas flow rates in FCAW. Extinction data from GMAW plumes was collected for different voltages in 4.6 and 7.6m/min wire feed rates to investigate the plume density across a number of heat inputs and transfer modes. Relative laser intensities between the photo-diodes was determined by taking measurements without any fume plumes present. This was subsequently used to normalise the photo-diode measurements to have the same intensity when then there was no extinction. From this point the relative extinction could be calculated.

3.9 Simultaneous scattering and LII

3.9.1 Introduction

In principle LII is proportional to the particulate volume whereas laser scatter is proportional to the square. Assuming that this is true then comparing the signals from each of the techniques should give an indication on the consistency of fume particle size across a number of different welding settings.

3.9.2 Equipment

Having set up each process individually it was not particularly complex to combine the two procedures. An isometric diagram of the optical layout is displayed in Figure 3.13. The optics remained the same as in the scattering and LII individual cases outlined in Sections 3.6.2 and 3.7.2 respectively. The combined beam forming optics used are pictured in Figure 3.14. In the simultaneous configuration the LII and scattering laser sheets were aligned to the same plane by adjusting the respective mirrors. Burns marks from the two laser sheets can be seen on the photosensitive paper imaged in Figure 3.15. The thinner lighter burn mark being made by the diverging 532nm beam used for the scattering and the 25mm height darker burn from the collimated 1064nm beam used for LII. Curvature exists in the 532nm burn due to the paper not being flat when it was exposed. A slight curvature did exist in the 1064nm light sheet from optical misalignment required to obtain the two beams parallel and for the most part overlapping.

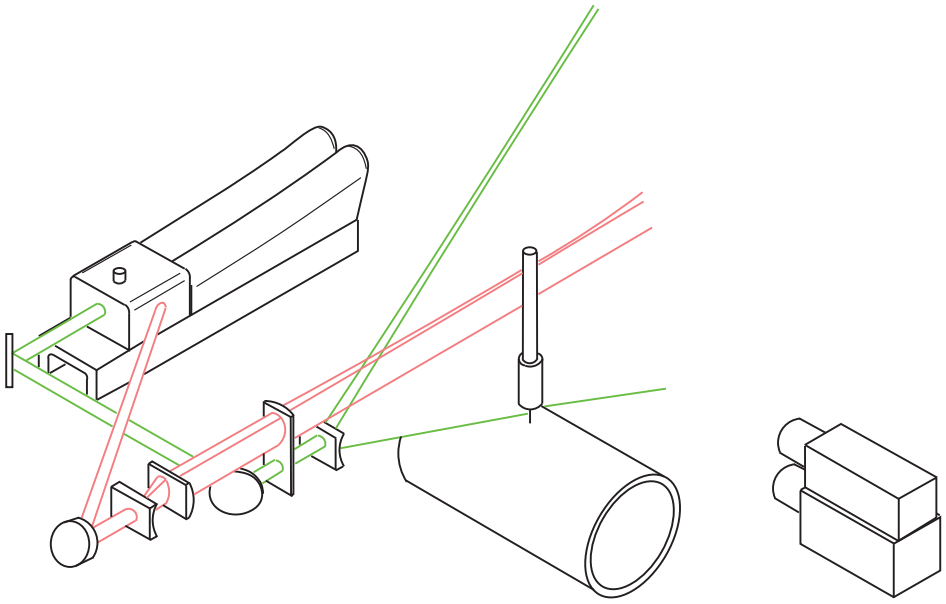

Figure 3.13: Isometric diagram of simultaneous scattering and LII optical layout

The megaplus camera used to collect the laser scatter and the ICCD used to collect the LII were aligned so overlapping images could be collected. An image of these

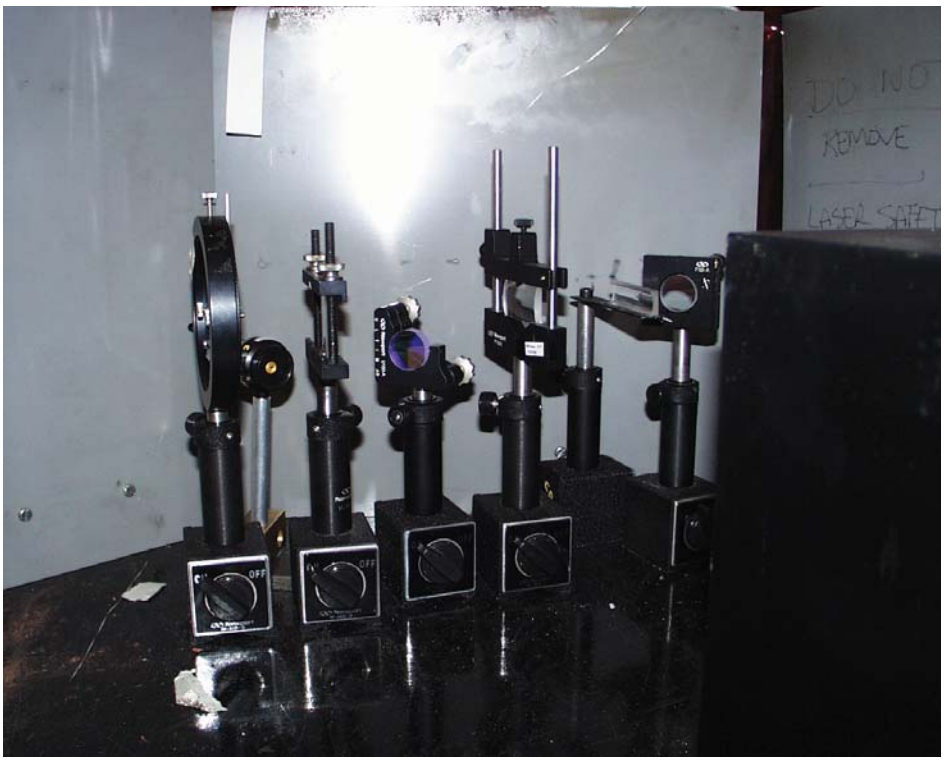

Figure 3.14: Optics used for simultaneous scattering & LII experiment

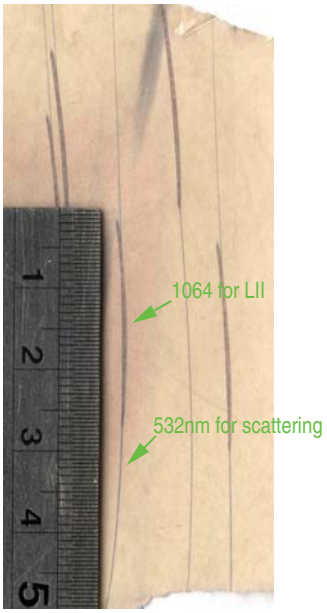

Figure 3.15: Image of 1064nm and 532nm laser burns on burn paper

two cameras bolted together can be seen in Figure 3.17. The camera timing and control, depicted in Figure 3.16, was similar to that of the individual experiments. The microprocessor code used to control the welders and the cameras was adjusted to run both cameras. This code has been included in Appendix D. Combined both cameras collected images at the rate of the slowest, being the ICCD.

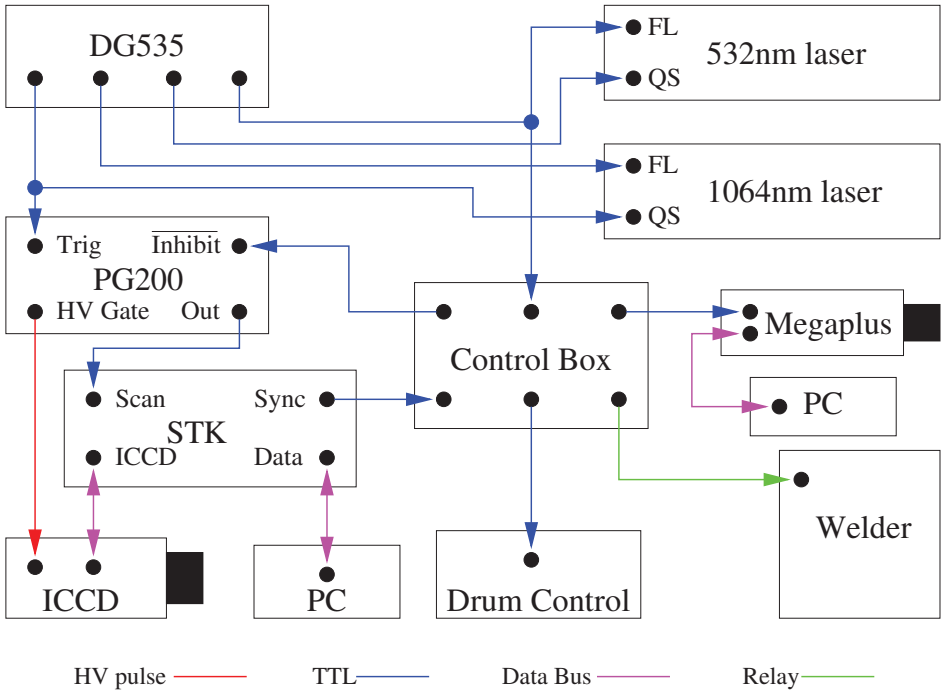

Figure 3.16: Diagrammatic timing layout used for simultaneous scattering and LII

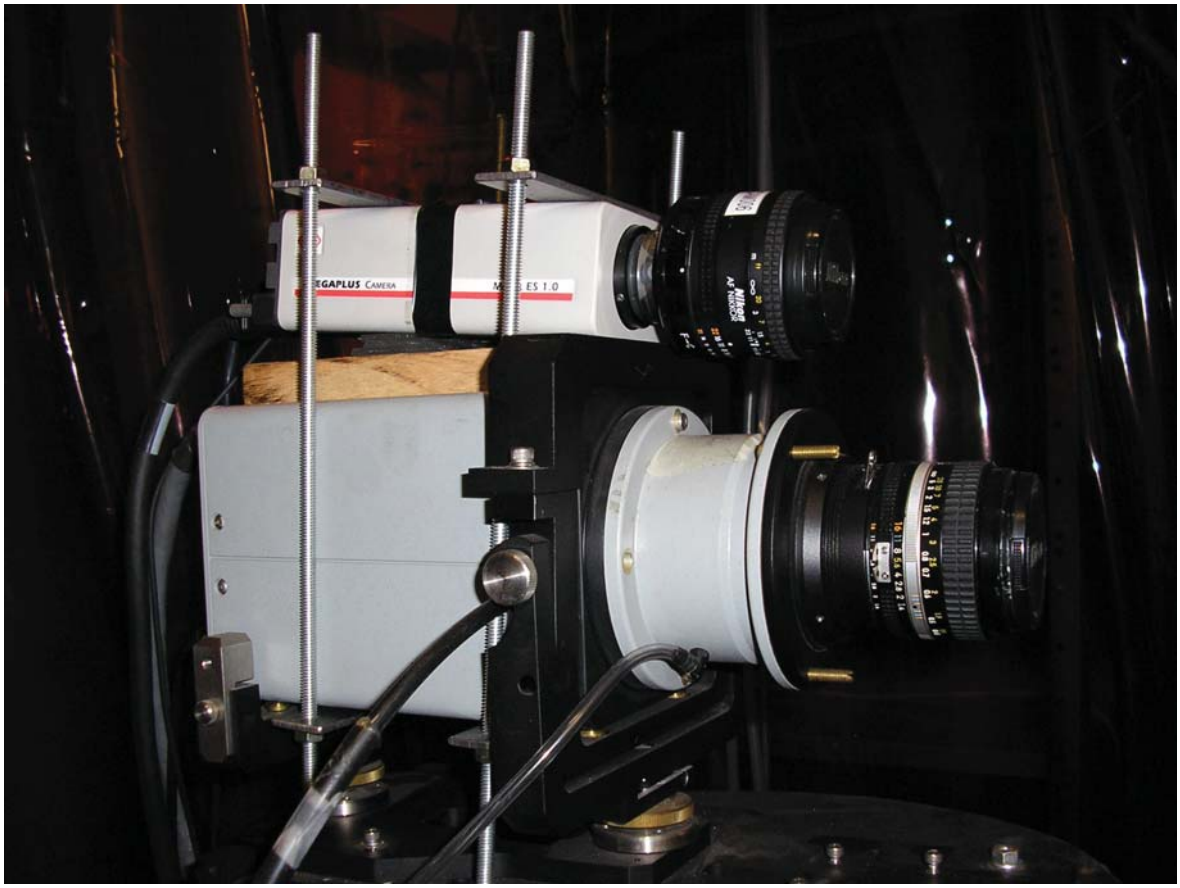

Figure 3.17: Megaplus and ICCD camera setup

3.9.3 Experimental procedure

Once the two laser sheets were collimated the laser power and timing was adjusted. Combined images were taken for a range of different welding voltages to obtain a number of different droplet transfer modes.

3.10 Fume box

3.10.1 Introduction

The traditional method for the measurement of fume formation is with the use of a fume box. Such fume boxes collect the solid particulate fume on a filter substrate for analysis. As outlined previously fume boxes have some limitations but are considered the standard by which fume formation is measured. Subsequent to the laser based measurements an opportunity became available to under take measurements using the fume box at the CSIRO Woodville site. The goal was to undertake measurements of bulk fume with the same welding variables as those used for the laser techniques. Measurements were undertaken for both GMAW and FCAW processes. Since the GMAW welding variables were originally based on those used by Quimby and Ulrich for fume box measurements similar results could be expected.

3.10.2 Equipment

The equipment used for this experiment was already well established by the CSIRO for the measurement of welding fume. The enclosure in which the welding took place can be seen in Figure 3.18. The welding torch was mounted through the access port at the back of the chamber. A linear traverse inside the fume box was used to move the parent material onto which the weld bead was deposited. The substrate material consisted of a 400mm long by 100mm wide by 12mm thick steel strip which was clamped to the top of the traverse. The filter material used to collect the fume was mounted at the top of the chamber and held in place by the suction formed by the exhaust system.

While the fume box measurements were undertaken to replicate the conditions of the laser measurements, due to the complexity and number of welding variables several differences existed. One of the first obvious differences is the reduction in welding traverse rate required due to the geometry and set up of the fume box from 360mm/min to 330mm/min. Impact of this change on FFR was probably very minor given that that doubling traverse rate has been found to produce a 5% change in FFR(Quimby & Ulrich 1999). Another probably more significant difference was in the shielding gas composition from one proprietary gas mixture to an equivalent for different brand. The fume box work at CSIRO Woodville was undertaken with Blueshield23 from their

Figure 3.18: Fume box located at CSIRO Woodville site

supplier Linde gas while Argoshield universal from BOC gas was used during the laser measurements. Both of these gases consist of an argon bulk with oxygen and carbon dioxide additions but in different proportions. Comparison of the two gases is displayed in Table 3.3.

Proprietary gas	O_2	CO_2	Ar
Argoshield universal	2.75%	16%	81.25%
Blueshield23	2.5%	4.5%	93%

Table 3.3: Comparison of shielding gas composition

Due to the time span between the laser and fume box measurements there were a number of variables that may have altered arc properties. Factors such as electrode wire surface finish, torch liner condition and wire feed roller wear may have altered the smoothness of wire feedability.

3.10.3 Experimental procedure

At the start of these experiments the welding equipment was set up in the same way it was for the optical fume measurements. Once again the voltage calibration function was used to correct for resistance in the welding torch and return lead. Due to the limited length of the traverse the 360mm/min speed at which the weld bead was deposited previously could not be obtained. The traverse rate was therefore reduced to match the maximum obtainable on this device being 330mm/min.

Prior to each measurement the parent material was moved and the traverse reset to its initial position. The welding variables were also configured and a new filter placed in the top chamber.

A careful filter handling procedure was undertaken to obtain a continuity in fume measurements. The stock of filter mats were stored in a oven at $90°C$. Before each experiment the filter was removed and cooled for 5 minutes in a container with silicate desiccant. The filter was then weighed using electronic scales and mounted in the top of the fume box and the extraction system activated. Welding was then undertaken for a period of 1 minute. The extraction system was operated for a further minute to collect any residual fume in the chamber. At the end of this time the extraction system was turned off and the filter mat removed and placed over the desiccant in the chamber to cool and dry for a further 5 minutes. The filter was then weighed to get an initial measurement. After this initial measurement the filter mat was placed back into the $90°C$ oven for at least one hour before cooling over desiccant and weighing. This procedure of heating and drying in a controlled environment reduces the effect of moisture variation in the filter mat. This procedure was repeated for each welding variable undertaken.

Chapter 4

Results

4.1 Scope

In this chapter the results of the application of the three different laser techniques to imaging welding fume are presented. The first of these techniques, laser scattering Section 4.3, was undertaken to visualise the development of the fume plume at source. In this section the effect of a number of welding variables on the shape of both FCAW and GMAW plumes was investigated. In addition to plume geometry the intensity of the laser scatter was also of interest in determining a relationship to fume particle density. For GMAW two regions were imaged. The first of these imaged the plume in a region about 150mm either side and above the arc. The second region imaged was immediately adjacent the welding wire under the welding torch gas shroud.

The second experiment laser induced incandescence (LII), Section 4.4, was undertaken to investigate the effectiveness of this technique in the measurement of fume particle density. In combustion research this technique is considered less sensitive to soot particle geometry delivering a signal proportional to the volume of the particulates. While this technique involved imaging a section of the plume, the size of the laser sheet used and the lower resolution of the camera made it less suitable for plume geometry visualisation than the laser scattering presented in Section 4.3. While some FCAW work was undertaken Section 4.4 primarily focuses on GMAW plumes.

The third and final laser technique used, laser extinction Section 4.5, was undertaken in an attempt to develop a quantified optical measurement of the particle density in the plume. Line integrated measurement of beam extinction were taken for both FCAW and GMAW along a path about 140mm above the arc.

In the final set of measurements LII images and laser scattering images were undertaken simultaneously on GMAW plumes. This work was undertaken to determine if there is a relationship between the scattered intensity and the LII. In principle this would indicate if the welding fume particles were changing volume with welding variables.

4.2 Introduction

Due to the potential negative health impacts that welding fume presents efforts have been made to understand the formation of welding fume. One of the common fume research measurement involves the use of a fume box to determine the fume formation rate of a particular welding process. These measurements however are not directly linked to operator exposure based on the fact that welders do not inhale the entire fume formation but rather only the portion that reaches their breathing zone. For this reason the dissipation of the welding fume and the transmission between the source of the fume and the breathing zone is of importance.

In recent years work has been undertaken to investigate and model the dissipation of the fume into the atmosphere (Slater 2004, Godbole et al. 2007). The understanding generated from such work aims at improving the often ad-hoc process of fume extraction and ventilation in the workplace, which is still the primary method of exposure reduction. Previous research however has only been based on direct imaging, salt water models and computational fluid dynamics.

The effectiveness of direct imaging of welding plumes is limited by irregular and disperse lighting of plume by the arc. Such external observation overlooks much of the structure of the plume particularly near the arc. Salt water models, while sufficient for a basic understanding, simplify the true nature of the welding plume and require several analogies to be made in the conversion to salt water equivalents. The effectiveness of these salt water models can only be determined by comparing their external structure with that of direct images of fume plumes. Laser diagnostics of such salt water models have been undertaken to investigate the internal structure and fundamental fluid dynamics involved with impinging buoyant jets.

The work undertaken and presented here takes the next logical step which is to apply laser diagnostics to welding plumes generated from actual welding processes. The primary goal of these experiments is to visualise the plume produced from reasonably typical welding processes. The secondary aim of these experiments is to determine if laser diagnostics techniques can be applied to the measurement of other plume variables such as particulate concentration. Combined together the ability to image the plume dissipation and density would provide useful insight into the transmission of the fume from source to the inhalation of the welder.

While there are a number of arc welding processes the scope of this work is limited to GMAW and FCAW. These welding processes are common in industry due to there high productivity and their semi-automated operation made them suited for application in an experimental configuration. One of the goals of this work was to visualise the plumes generated from a range of different welding variables which is something near impossible to achieve with salt water modelling. The basis for the GMAW welding variables selected for investigation were obtained from Quimby & Ulrich (1999). The

base variables for the FCAW work were determined by optimising the quality of the weld bead obtainable near the wire manufacturer's guidelines for operation.

4.3 Laser scattering

Laser scattering techniques have become a common method for flow visualisation and fluid dynamics research. In many of these cases particles are introduced into the flow as a tracer. In the work presented here the particles are inherently present by way of particulate fume formation. Therefore this particulate fume not only acts as a scattering source for visualisation of the plume but is itself of interest.

The arrangement of the experimental equipment used in this section has previously been outlined in Section 3.6. An image of a calibration target placed in the larger region of interest can be seen in Figure 4.1. When activated, the 532nm light sheet produced by the laser was projected into the same plane as the target imaged. The drum onto which the weld bead was deposited was able to rotate either clockwise or anticlockwise.

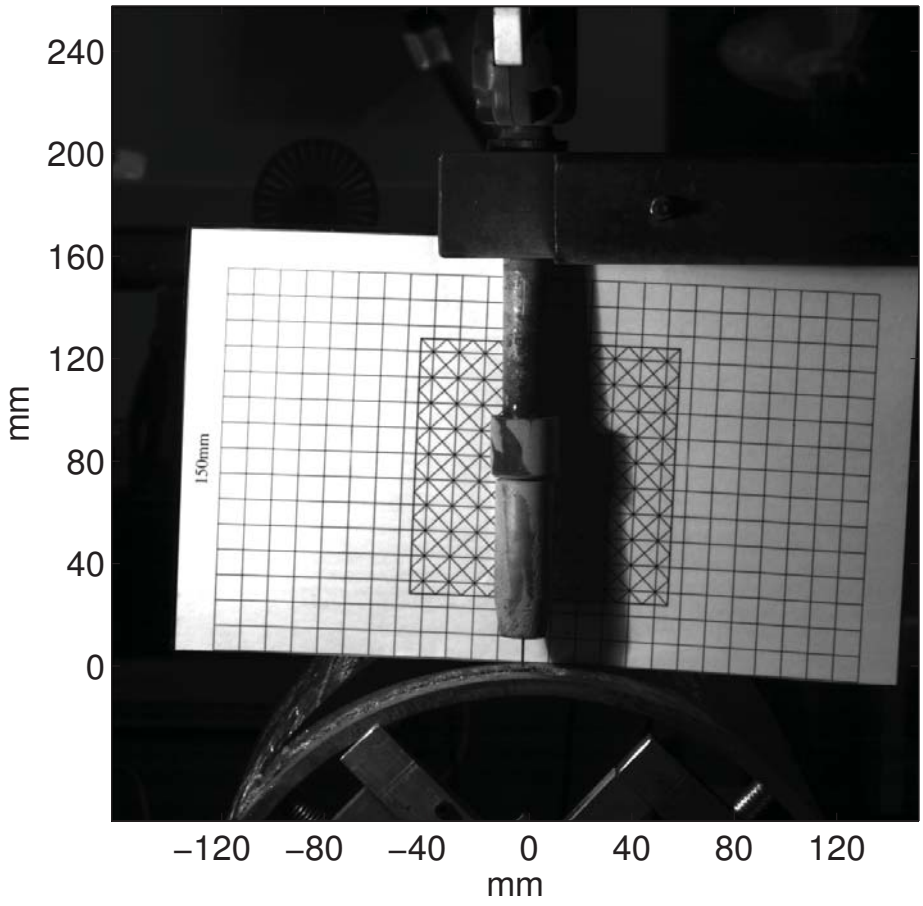

Figure 4.1: Megaplus image of target behind welding torch

For the majority of the results presented here the drum was rotated anticlockwise, depositing the weld bead to the left of the welding torch. For the case when the drum

rotated anticlockwise the drum was slowly indexing toward the camera to produce the helical weld bead pictured in Figures 3.2 and 3.3. As a result of this indexing the weld beads ended up between the welding torch and the camera. It was chosen to operate in this fashion to prevent the weld bead reflecting light from the laser sheet which passed slightly above the drum surface behind the torch.

The laser sheet was directed behind the welding torch to prevent any reflection off the torch or support from entering the camera. As a result the scattering from the fume directly behind the welding torch could not be observed. In early experiments it was found that if the light sheet was passed in front of the torch the reflection of laser scatter and other stray laser light off the torch clouded the image otherwise blocked. As the laser sheet was passed slightly behind the torch the cross-sectional image produced from the scatter is not perfectly radial to the plume as depicted in the schematic top view in Figure 4.2. As a result scatter imaged is actually slightly behind the torch and and actually radially further away then what it may appear.

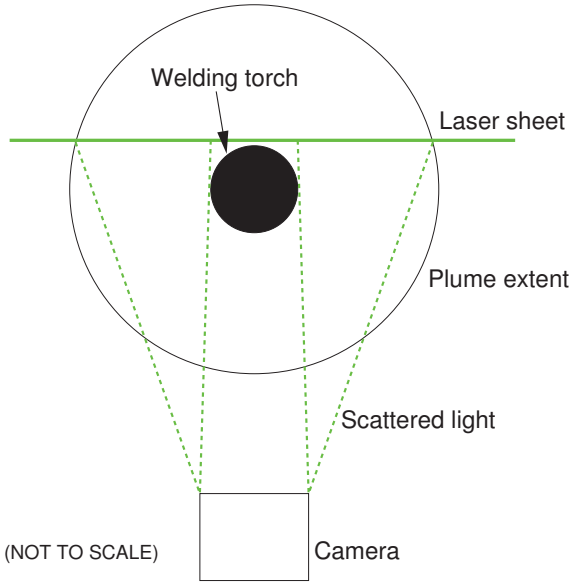

Figure 4.2: Depiction of imaged plane relative to torch

The sheet of laser light diverged vertically from the beam forming optics on the left to the beam stop to the right of the image as depicted in Figure 3.4. Resultantly the laser sheet incident to the particulate fume was shorter and more intense on the left hand side to that on the right side of the images. Due to space constraints the height of the laser sheet was insufficient to cover the entire left hand side of the area imaged. The reduction in laser sheet energy fluence due to the beam divergence was later corrected for during the processing of images. The code used to correct for divergence is included in Appendix E.1.

The intensity of the light sheet incident on the particles also varied from left to right of the images due to the extinction of the beam through the fume plume. Not only is the intensity of the incident light sheet extinguished but also the intensity of the light

scattered from particles in the plane of illumination. This extinction occurred due to the particles between the illuminating light sheet and the detector. In either case the effect of extinction has not been corrected for in the images presented here.

The fluence of the laser sheet also varied along its height due to the beam profile from which the sheet was formed. The bottom part of the light sheet was blocked and the more uniform part near the middle of the sheet height was directed through the region of interest. While it is possible to correct for the sheet profile doing so in a sheet of such size is difficult and was not considered practical for these experiments.

4.3.1 FCAW

4.3.1.1 Gas flow rate

Due to the presence of flux in the electrode of FCAW the fume produced is typically more then that produced by GMAW. FCAW can also be operated with or without gas shielding. One of the first laser scattering experiments undertaken was to look at the difference in plume shape between shielded and unshielded FCAW. For this experiment 0.9mm Shieldcore15 manufactured by CIGWELD was used (CIGWELD 1997) Appendix H. The voltage used in this experiment was 16.5 volts DC electrode negative as specified by the manufacturer. The wire feed speed was set at 4.5 m/min with a traverse rate of 230mm/min. The effect of shielding gas flow rates on the plume from FCAW was investigated by using flow rates of 0, 10, 20 and 30 litres per minute. During the collection of these images welding variables other than gas flow rate remained constant. The addition of shielding gas however lead to a slight increase in current from 93 to about 97 Amps for the same voltage and wire feed. The torch standoff used in the FCAW experiments was 12mm. A summary of the welding variables used is outlined in Table 4.1.

Process	FCAW	Units
Electrode Wire	0.9mm E71TG5	
Voltage	16.5 (DCEN)	Volts
Wire Feed	4.5	m/min
Current	93-97	Amps
Shielding gas	Ar 81.25, CO_2 16, O_2 2.75	%
Gas Flow rate	0, 10, 20, 30	l/min
Weld traverse rate	230	mm/min
Standoff	12	mm

Table 4.1: FCAW variables used to investigate the effect of gas shielding

The laser power used in this experiment was measured to be about 260mJ per pulse. Camera lens aperture was adjusted for each welding variable so that the scattered light intensity was within the dynamic range of the camera. The change in lens aperture

was later accounted for in the post processing of the collected images to obtain the same relative intensity.

During the FCAW experiments the laser light sheet passed the welding torch in the same plane as the calibration target as shown in Figure 4.1 producing plume cross section images longitudinal to the weld direction. Drum rotation during welding was anti-clockwise resulting a weld bead being deposited to the left of the torch.

Images were collected from weld initiation at a rate of 10 images per second for 15 seconds. At that point the arc was extinguished and another 5 seconds of images were collected. This allowed the post weld fume dissipation to be recorded.

Selected images of the fume plume cross section for FCAW can be seen in Figure 4.3 for the four different shielding gas flow rates. These images present a false colour map related to the intensity of the scattered light. Each of these images uses the same colour map which is displayed at the bottom of Figure 4.3.

Figure 4.3 illustrates the application of laser illumination to imaging the structure of the plume for different gas flow rates. Having used a self shielding FCAW wire the no gas flow condition displayed in Sub Figure 4.3a would represent its main usage. Despite being self shielding this wire could be used in conjunction with gas to improve the arc shielding and weld bead profile. For the welding conditions used here a gas flow rate of around 10 l/min would be sufficient to obtain the desired result. Gas flows rates of 20 and 30 l/min are probably somewhat unrealistic compared to what would be practically used.

In the absence of shielding gas the plume produced is primarily driven by thermal convection generated from the arc and weld bead. With the addition of shielding gas comes the influence of the downward gas velocity. Images of the FCAW plume in Figure 4.3 demonstrate that additional shielding gas results in an increased plume diameter as suggested by visual images in Norrish et al. (2005). This increased plume diameter is more than likely the combination of two effects. The first of these is the result of the shielding gas from the torch impinging on the drum surface resulting in horizontal flow (Cooper & Hunt 2004, Norrish et al. 2005). The second effect involved is due to the reduction in plume buoyancy and vertical rise velocity with increasing shielding gas dilution. Indeed for the highest gas flow rate, the dissipation of the plume is primarily horizontal suggesting that it is nearly neutrally buoyant with the atmosphere. In this situation the heat from the arc and the weld bead is barely sufficient to increase the temperature of the shielding gas to a point where its density is less than that of air. Due to thermal cooling and dilution with the atmosphere the other plumes imaged here would more than likely, in an unventilated environment, become neutrally buoyant at some height above the welding arc. In the case of the unshielded arc and the lower gas flow rates this height would be well above the imaged area. The dilution effect of the shielding gas is also highlighted by the reduction in the intensity of the

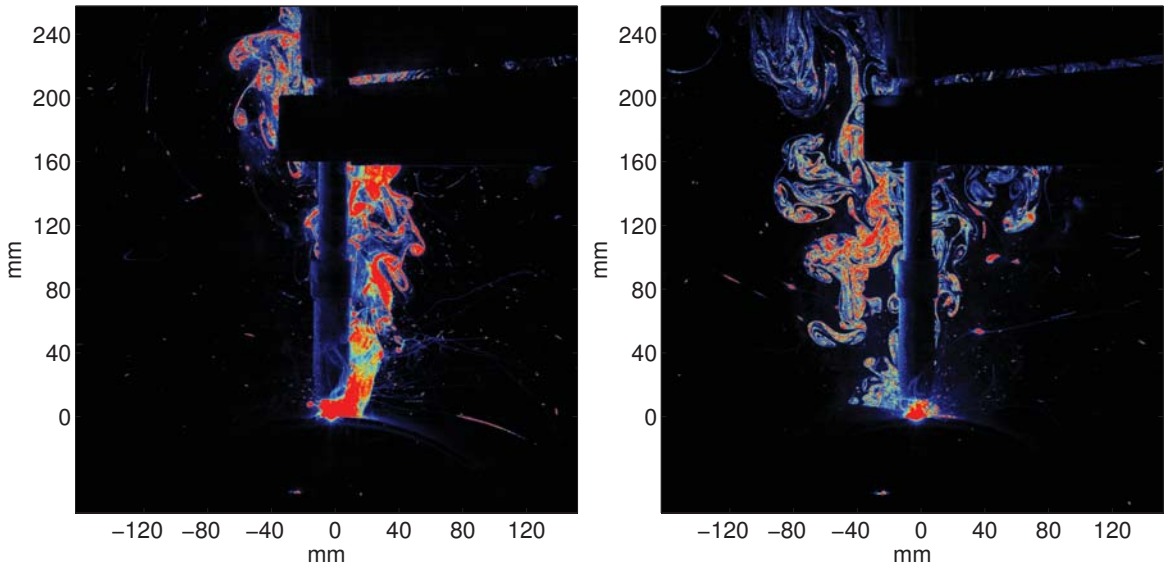

(a) No gas flow

(b) 10 l/min

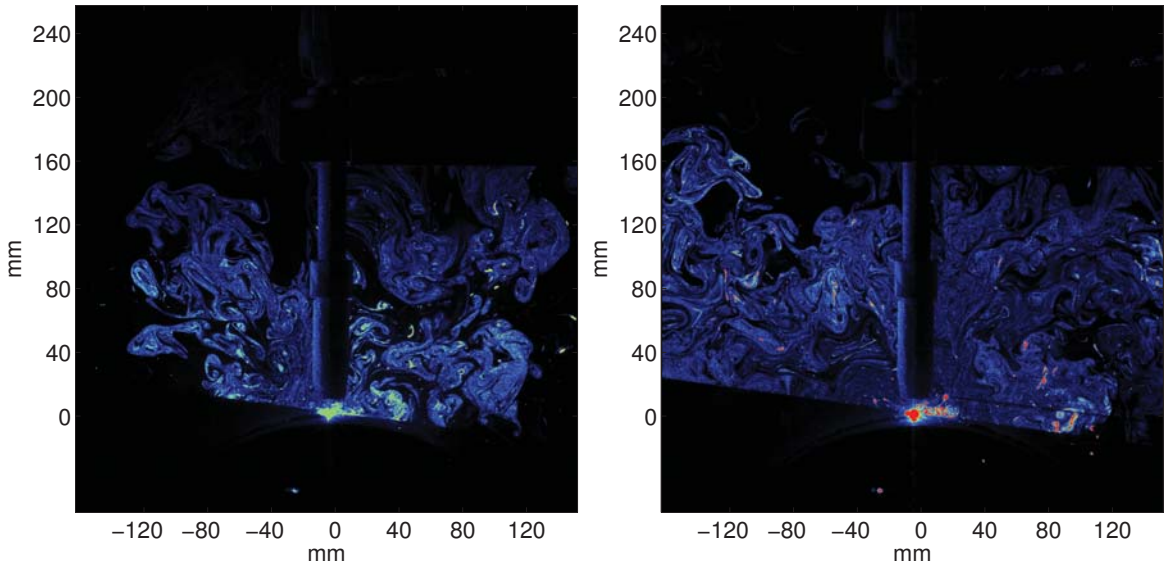

(c) 20l/min

(d) 30l/min

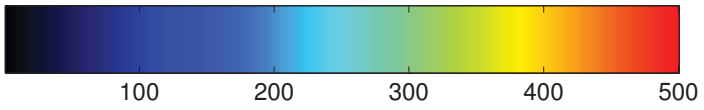

(e) Colour intensity scale

Figure 4.3: Instantaneous images for different shielding gas flows during FCAW

scattered laser light with increasing flow rates. The reduction in the intensity of the scattered light would suggest a reduction in particulate concentration as the plume becomes more dispersed.

4.3.2 GMAW

Gas metal arc welding involved similar welding hardware and optical configuration as that used for FCAW. The consumable electrode wire however was changed from one containing flux to a solid copper coated steel wire. The solid electrode wire allows for a wider range of welding variables to be used than that of FCAW which has restrained operating parameters governed by the flux decomposition. This allowed a wider operating range and effect of several welding variables to be investigated. Solid wire GMAW is also of interest due to the amount of previous research undertaken on the welding fume produced by this process.

4.3.2.1 Weld direction

Early in the experimentation it was noticed that the plume was not symmetrical about the torch particularly at low gas flow rates. Initially this was thought to be due to some external environmental causes or torch geometry. Attempts were made to rectify the asymmetry by further controlling the air flow in the environment and by adjusting the torch. However even with reduced environmental air flow the asymmetry remained. It was therefore determined that plume asymmetry was the result of the welding process. To investigate the effect of the welding process on the plume shape images were collected for a series of 5 welds for both clockwise and counter clockwise drum rotation. The base GMAW welding variables adapted from Quimby & Ulrich (1999) were used as outlined in Table 4.2.

	GMAW	Units
Electrode Wire	1.2mm ER70S6	
Voltage	26 (DCEP)	Volts
Wire Feed	7.6	m/min
Current	230	Amps
Shielding gas	Ar 81.25, CO_2 16, O_2 2.75	%
Gas Flow rate	17	l/min
Weld traverse rate	360	mm/min
Standoff	19	mm

Table 4.2: GMAW variables for welding direction experiments

The mean plume shape obtained by averaging the images from each of the five sets of weld runs is displayed in Figure 4.4. This clearly indicates that the plume had a tendency to be propelled forward of the weld bead. This effect was also noticed in cold flow measurements of gas discharge (Johnson et al. 2006). Since this was observed in cold flow conditions this effect can not be due to bead geometry or thermal buoyancy of the heated air coming off the weld bead but these are likely to have a contribution. This effect is probably further enhanced by the heated section being rotated to a vertical orientation generating increased convection than that obtained from a horizontal plate.

As the two images in Figure 4.4 are not mirrored about the torch it would suggest that environmental air movements were still involved.

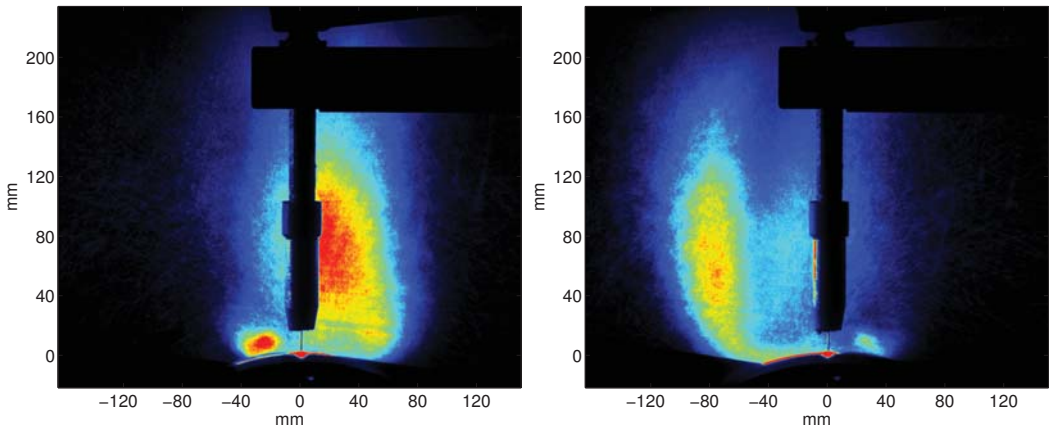

(a) Drum rotated anitclockwise (Weld bead to the left of torch)

(b) Drum rotated clockwise (Weld bead to the right of torch)

Figure 4.4: Effect of drum direction and bead heat on plume shape

The majority of experiments were undertaken with the drum rotating anticlockwise; resultantly the plumes displayed have the tendency to be on the right hand side of the torch.

From a modelling standpoint this asymmetry of the plume source may have some significance. Practically however it would be questionable if this effect would be noticeable given that the torch would be moving while the material would remain stationary. Also in most applications as the gas nozzle is not normal to the drum surface and the momentum of the gas may dominate the plume direction.

The other feature of interest in Figure 4.4 is the tightly wound vortex produced just above the weld bead. This vortex is more clearly visible in Figure 4.4a then 4.4b.

4.3.2.2 Gas flow rate

One of the variables responsible for plume shape is shielding gas flow rate. Laser scattering images were collected for a range of different gas flow rates with other welding settings remaining unaltered. A summary of the variables is displayed in Table 4.3. Needless to say that the unshielded case does not represent a practical application of GMAW but rather the case with no shielding gas flux or momentum involved. Similarly the gas flow rates greater then 20l/min would be unlikely to be used in industry particularly when only using a 0.5 inch diameter shielding gas nozzle.

Figure 4.5 displays laser scatter cross sectional images of the plume for the 8 gas flow rates. The images displayed in Figure 4.5 are averages of the 150 images collected during welding for each experimental condition. As such the general location of the

	GMAW	Units
Electrode Wire	1.2mm ER70S6	
Voltage	26 (DCEP)	Volts
Wire Feed	7.6	m/min
Current	230	Amps
Shielding gas	Ar 81.25, CO_2 16, O_2 2.75	%
Gas Flow rate	0,5,10,15,20,25,30,35	l/min
Weld traverse rate	360	mm/min
Standoff	19	mm

Table 4.3: GMAW variables for gas flow rate experiments

plume is clearly demonstrated but the structure of the plume is lost. Figure 4.6 displays selected individual images from each gas flow rate. These images display the scattered light from a single laser pulse allowing the structure of the plume to be observed.

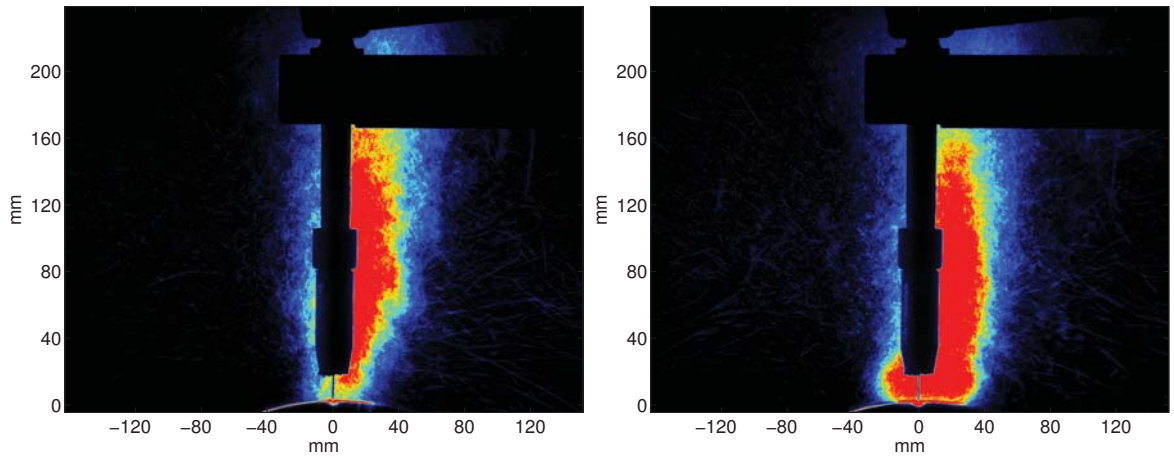

(a) No gas flow

(b) 5 l/min

(c) 10 l/min

(d) 15 l/min

Figure 4.5: Average laser scattering images for different shielding gas flow rates during GMAW

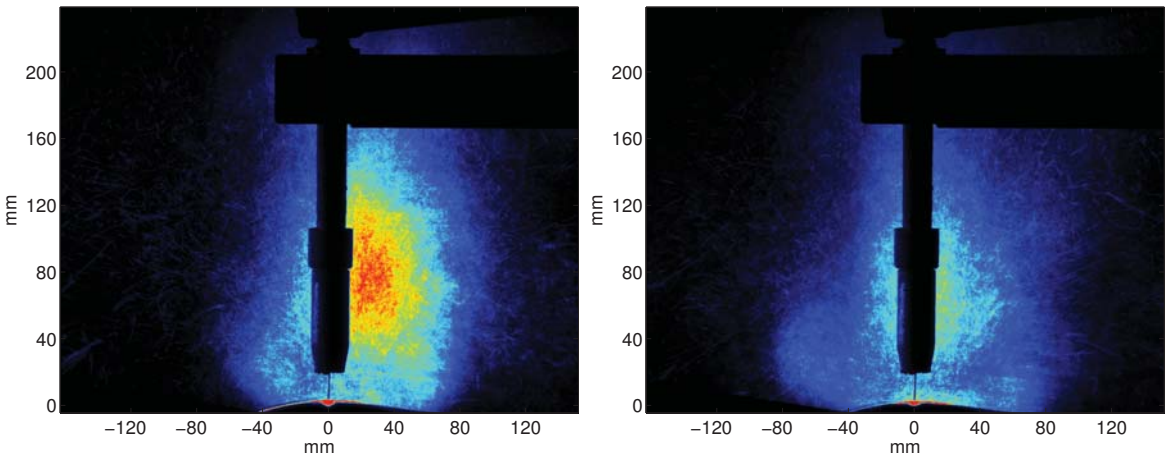

(e) 20 l/min

(f) 25 l/min

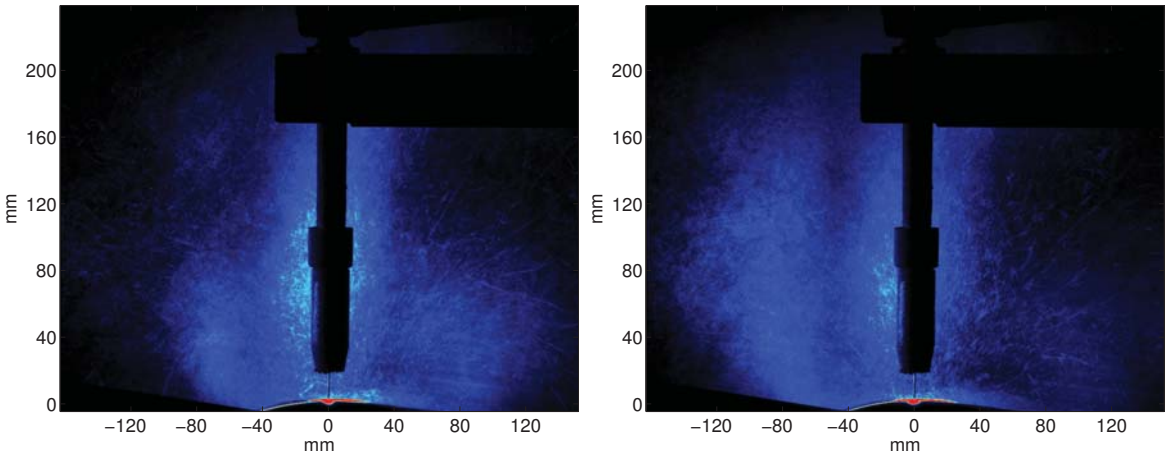

(g) 30 l/min

(h) 35 l/min

Figure 4.5: Average laser scattering images for different shielding gas flow rates during GMAW

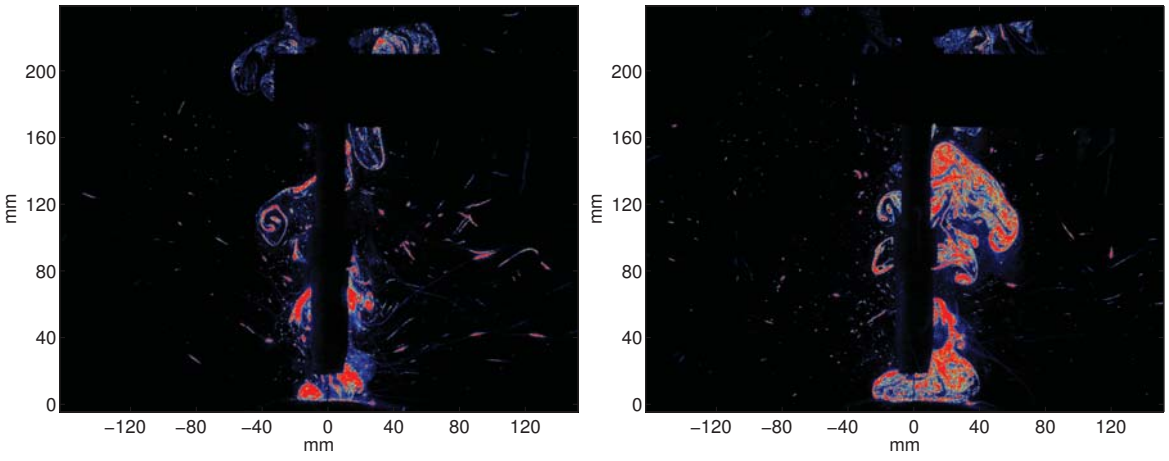

(a) No gas flow

(b) 5 l/min

(c) 10 l/min

(d) 15 l/min

Figure 4.6: Instantaneous laser scattering images for different shielding gas flow rates during GMAW

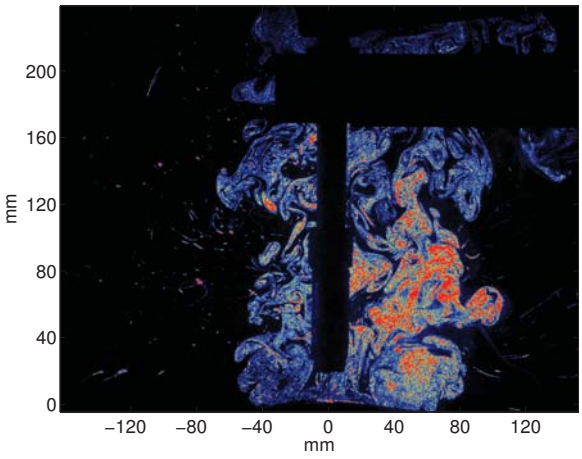

(e) 20 l/min

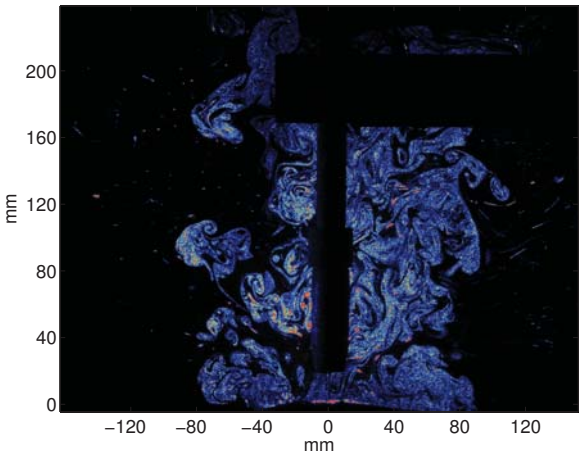

(f) 25 l/min

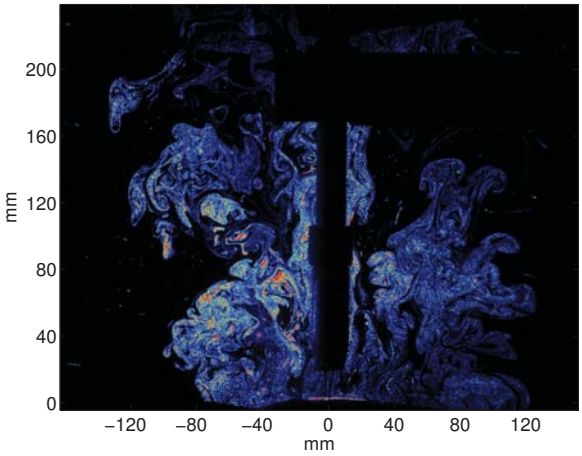

(g) 30 l/min

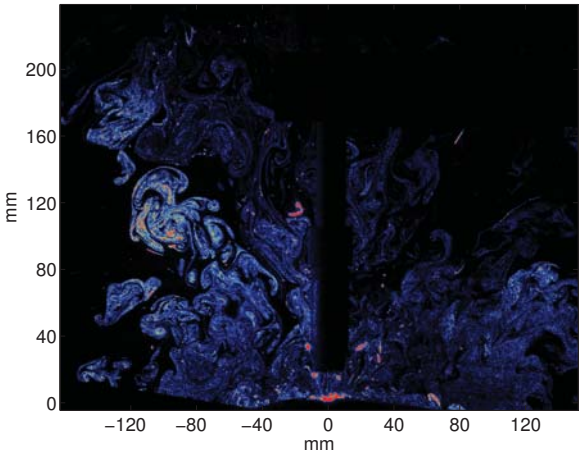

(h) 35 l/min

Figure 4.6: Instantaneous laser scattering images for different shielding gas flow rates during GMAW

As in the case of FCAW the unshielded case represents a thermally driven plume. Shielding gas introduces a downward gas flow and dilutes the particulate fume. Laser scattering images of the GMAW plume in Figures 4.5 and 4.6 also demonstrate that additional shielding gas results in an increased plume diameter.

4.3.2.3 Plume development

Plume development at arc initiation is important in when considering the plume dissipation from short welding operations such as tack welding. This is observable from individual laser scattering images at the start of each experimental set. Figure 4.7 presents images at half second intervals for the base welding condition outlined in Table 4.2. The images show that the plume initially blooms outward at the initiation of the weld before forming a mushroom cloud shape. After about 3 seconds the width of the plume is reasonably uniform. The extra width at weld initiation would suggest that localised fume extraction of the plume may not be as effective during short welds as it is during longer welding periods.

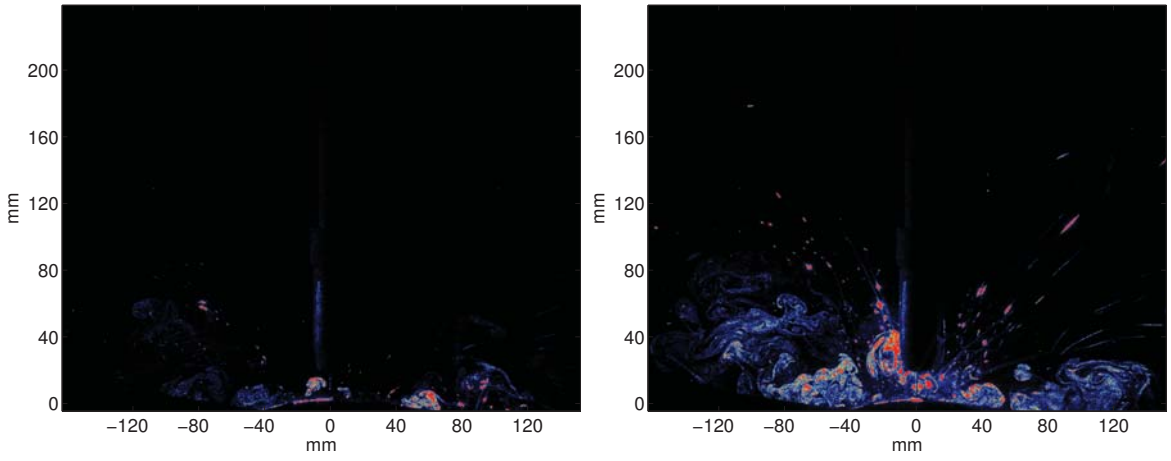

(a) 0.5S

(b) 1.0S

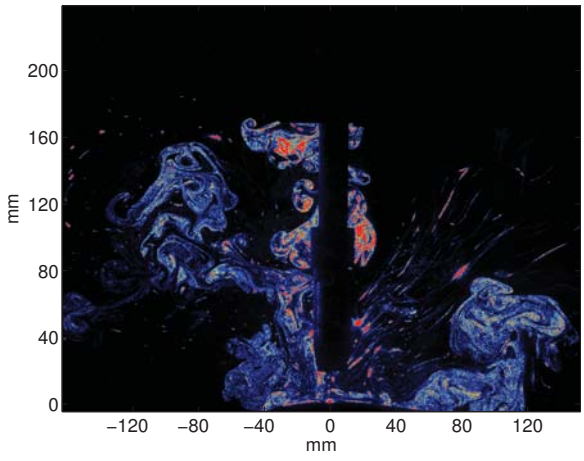

(c) 1.5S

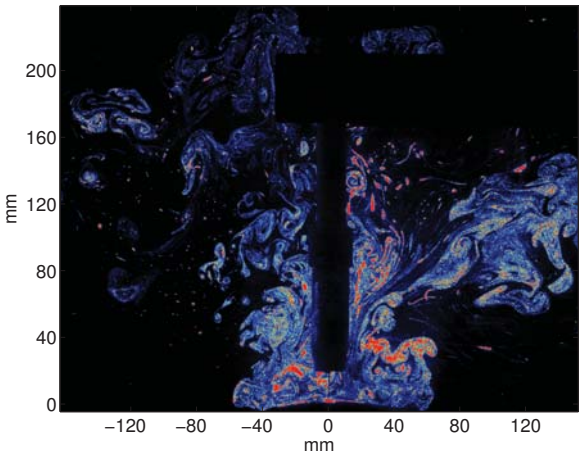

(d) 2.0S

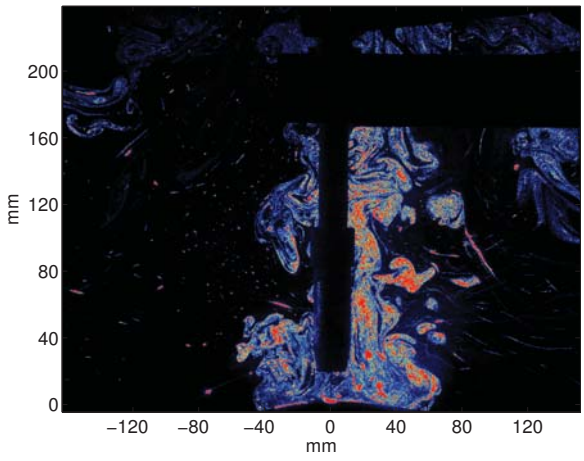

(e) 2.5S

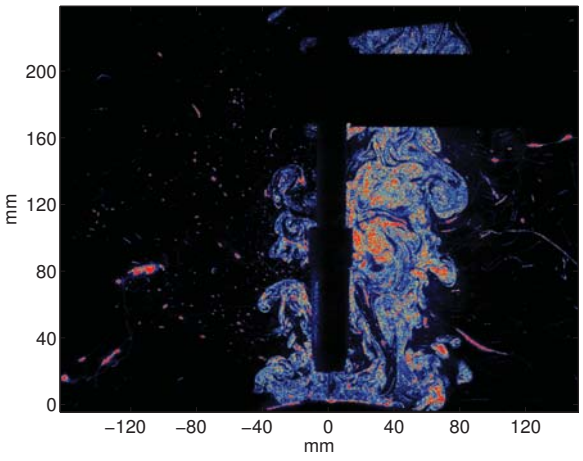

(f) 3.0S

Figure 4.7: Instantaneous laser scattering images of GMAW plume development at half second intervals after initiation

4.3.2.4 Plume movement

Successive laser scatter images collected show the plume cross sections at intervals separated by 0.1 seconds. Figures 4.8 and 4.9 show two sets of successive images.

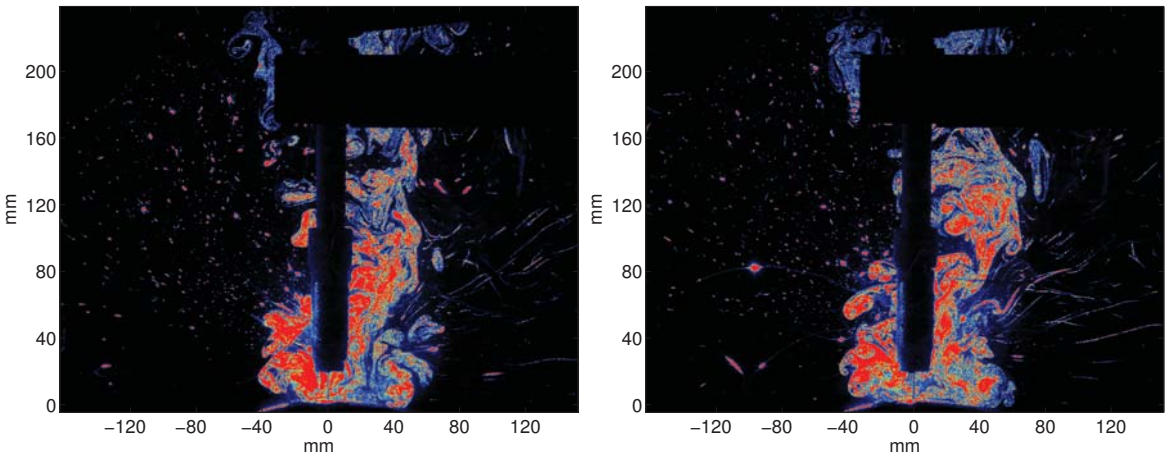

(a) 4.2S (b) 4.3S

Figure 4.8: Successive instantaneous laser scattering images of GMAW plume

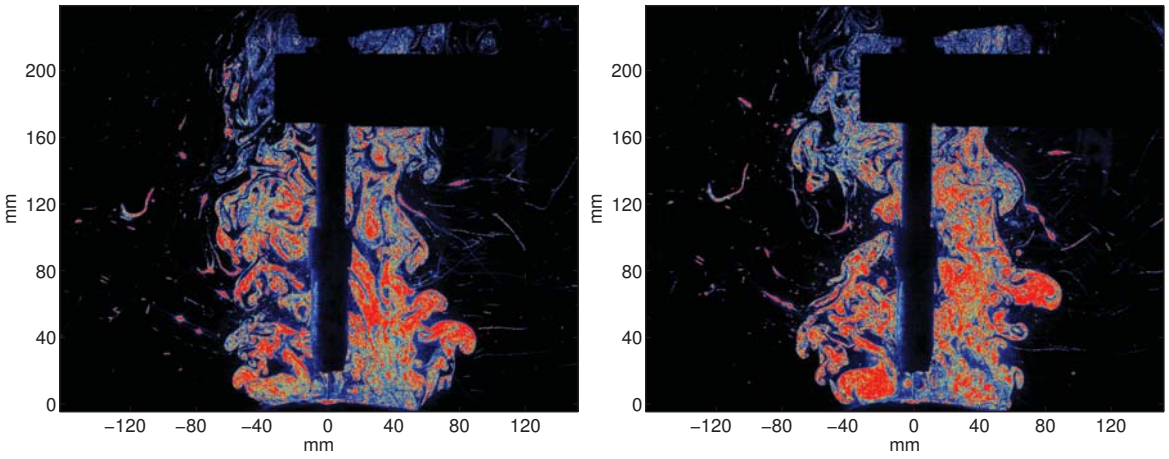

(a) 14.6S (b) 14.7S

Figure 4.9: Successive instantaneous laser scattering images of GMAW plume

4.3.2.5 Plume completion

The welds undertaken were automatically terminated after 15 seconds of welding. Figure 4.10 shows the dissipation of the plume after welding ceased at intervals of 0.2s.

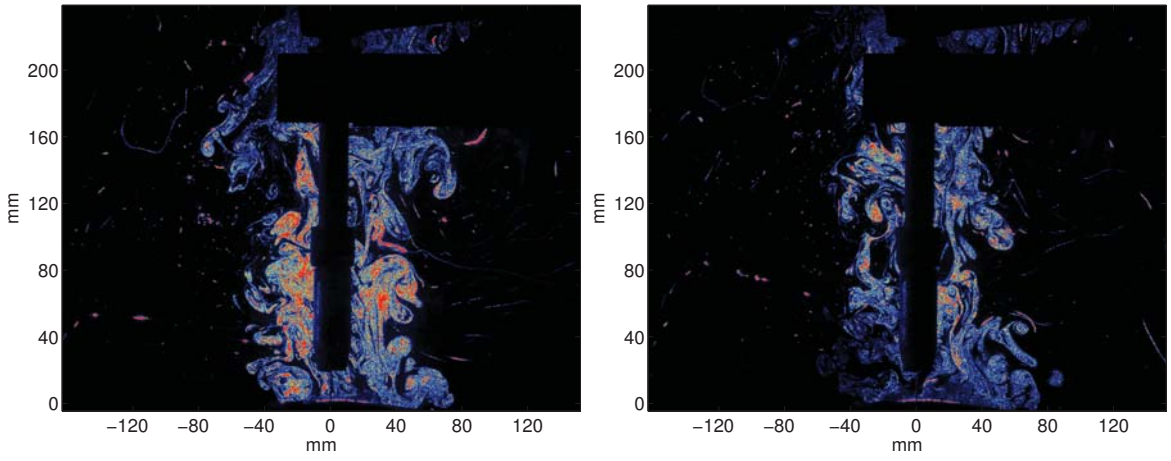

(a) 15.0S

(b) 15.2S

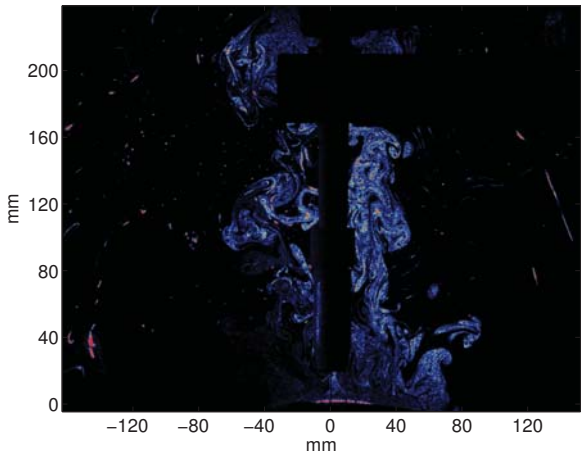

(c) 15.4S

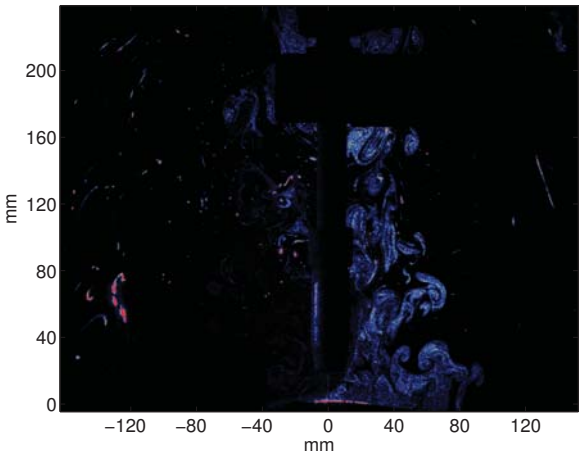

(d) 15.6S

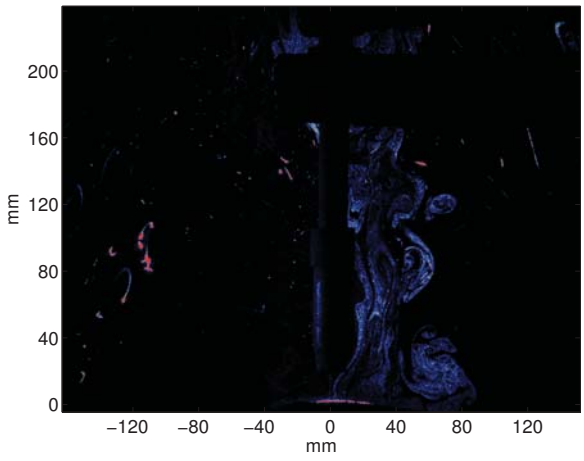

(e) 15.8S

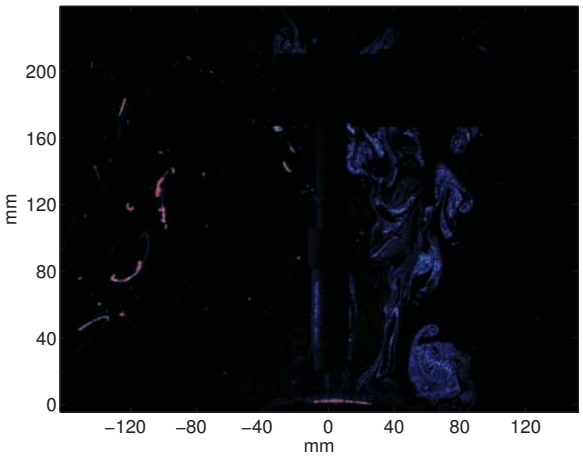

(f) 16.0S

Figure 4.10: Instantaneous laser scattering images of GMAW plume at completion of weld

4.3.2.6 Voltage

To investigate the influence of heat input on plume shape welds were undertaken at a range of different voltages. The wire feed speed was reduced from the 7.6m/min which was used as the base rate to the lower 4.6m/min to obtain a wider voltage and heat input range. Average laser scatter images for four different voltages are displayed in Figure 4.11.

	GMAW	Units
Electrode Wire	1.2mm ER70S6	
Voltage	15-33 (DCEP)	Volts
Wire Feed	4.6	m/min
Current	166-177	Amps
Shielding gas	Ar 81.25, CO_2 16, O_2 2.75	%
Gas Flow rate	17	l/min
Weld traverse rate	360	mm/min
Standoff	19	mm

Table 4.4: GMAW variables for welding voltage experiments

4.3.3 Imaging GMAW fume under the gas shroud

To investigate the particulate fume very close to the welding torch a different arrangement of optics was used to form a smaller, more collimated light sheet that was directed beneath the gas shroud. Figure 4.12 is an images taken of the smaller region imaged with a $2 Australian coin placed behind the welding wire. Once again the laser sheet was projected in the same plane as the target, in this case being the $2 coin. As the light sheet used to investigate this smaller region was not diverging no correction for sheet height was required. As in the case of the larger images no correction for light extinction was made. Once again effort was placed into obtaining a uniform beam profile rather then correcting the subsequent images.

A selected fume cross section image for one of the GMAW variables can be seen in Figure 4.13. In this image the lack of laser scatter to either side of the electrode is a result of a clean cone of shielding gas coming from the gas shroud. Outside of this clean cone the particulate welding fume can be seen. The bright scatter on the left side of the image would appear to be the result of a toroidal vortex as suggested by the water modelling undertaken by Cooper & Hunt (Cooper & Hunt 2004). In the work conducted here this vortex was more noticeable on the post weld side of the torch above the deposited weld bead as observed in the larger images. At this higher resolution the vortex could be seen at times encroaching the clean argon cone up to the wire indicating insufficient gas shielding for this standoff distance.

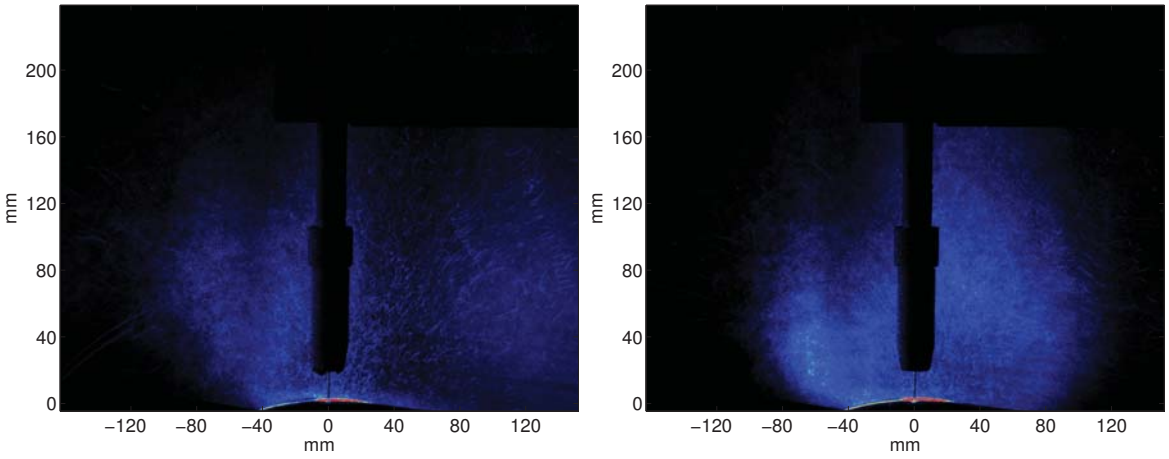

(a) 15Volts 144Amps

(b) 19Volts 159Amps

(c) 25Volts 165Amps

(d) 33Volts 177Amps

Figure 4.11: Instantaneous laser scattering images of GMAW plume at different voltages

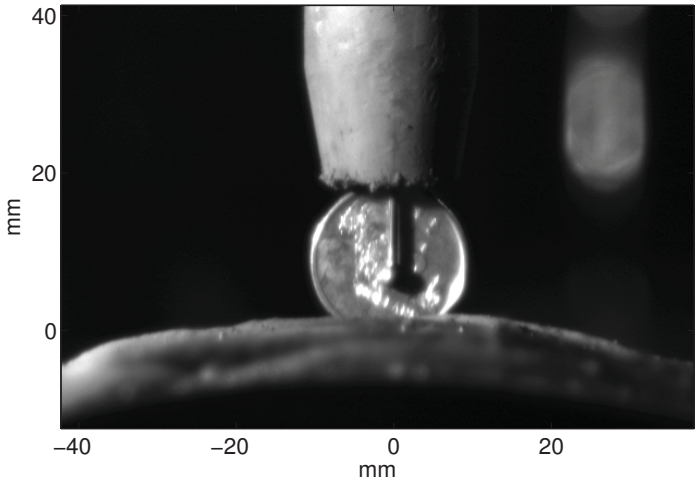

Figure 4.12: Megaplus image of coin in region of interest under welding torch

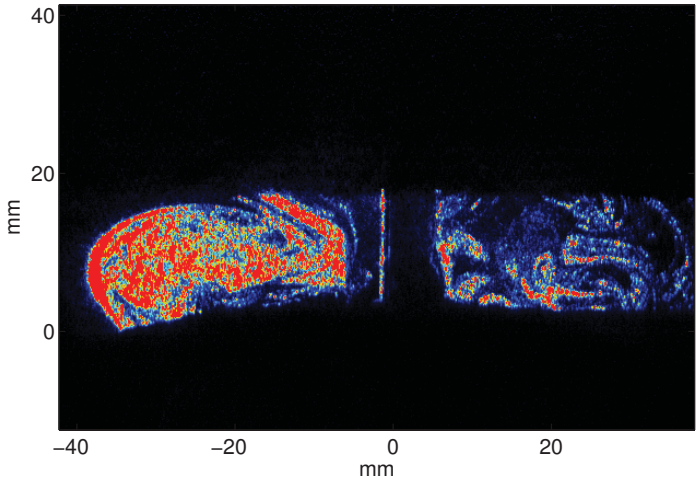

Figure 4.13: Instantaneous laser scattering image of GMAW fume cross-section under gas shroud 17l/min shielding gas

4.3.3.1 Fume formation rate

If the optical properties of the fume particles are assumed to be constant then the amount of scattered light can be equated to the fume concentration present in a particular area. Further, as long as the volumetric movement of the particles through this area are assumed to remain constant, then the amount of scattered light is relative to the amount of fume formation. In this smaller imaged region close to the welding wire the volumetric movement of the particles would appear to be primarily dominated by the flow of shielding gas rather than in the larger area which is governed by buoyancy. It was therefore considered feasible that the amount of scattered light could be related to the fume formation rate for a particular gas flow rate.

To investigate this possibility welding variables similar to those used by Quimby & Ulrich (1999) were used to see if the amount of scattered light was dependent on the droplet transfer mode. The welding variable used for this experiment are displayed in Table 4.5.

	GMAW	Units
Electrode Wire	1.2mm ER70S6	
Voltage	15-33 (DCEP)	Volts
Wire Feed	4.5, 7.6	m/min
Current	160-175,220-241	Amps
Shielding gas	Ar 81.25, CO_2 16, O_2 2.75	%
Gas Flow rate	17	l/min
Weld traverse rate	360	mm/min
Standoff	19	mm

Table 4.5: GMAW variables used for laser scattering measurements of fume concentration near gas shroud

A series of 200 images were collected for a range of voltages between 20 and 33 volts for both 4.5 and 7.6 metres per minute wire feed rate. The intensity of the laser light

scattered was then calculated from accumulating the value of the pixels for the image sets for each welding voltage and wire feed. Pixels in regions of the image where light scatter off the wire electrode or the drum surface was likely were excluded from the accumulation. Boxes depicting the area accumulated are shown in Figure 4.14. The accumulated pixel intensity obtained from this process is displayed in Figure 4.15 at each voltage for both of the wire feed rates.

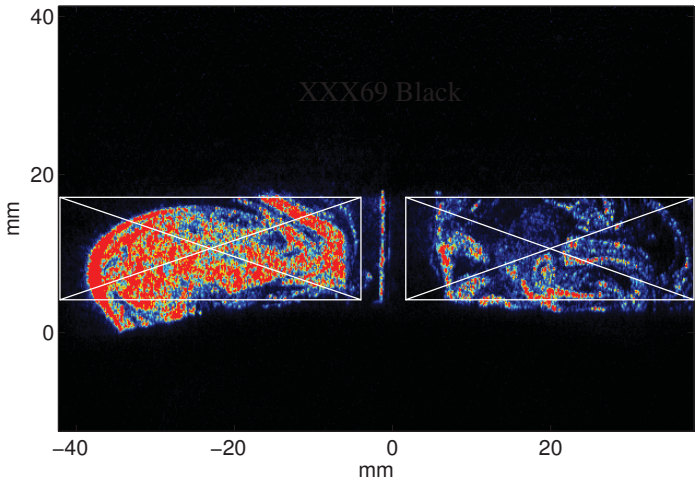

Figure 4.14: Depiction of area accumulated to obtain laser scatter intensity

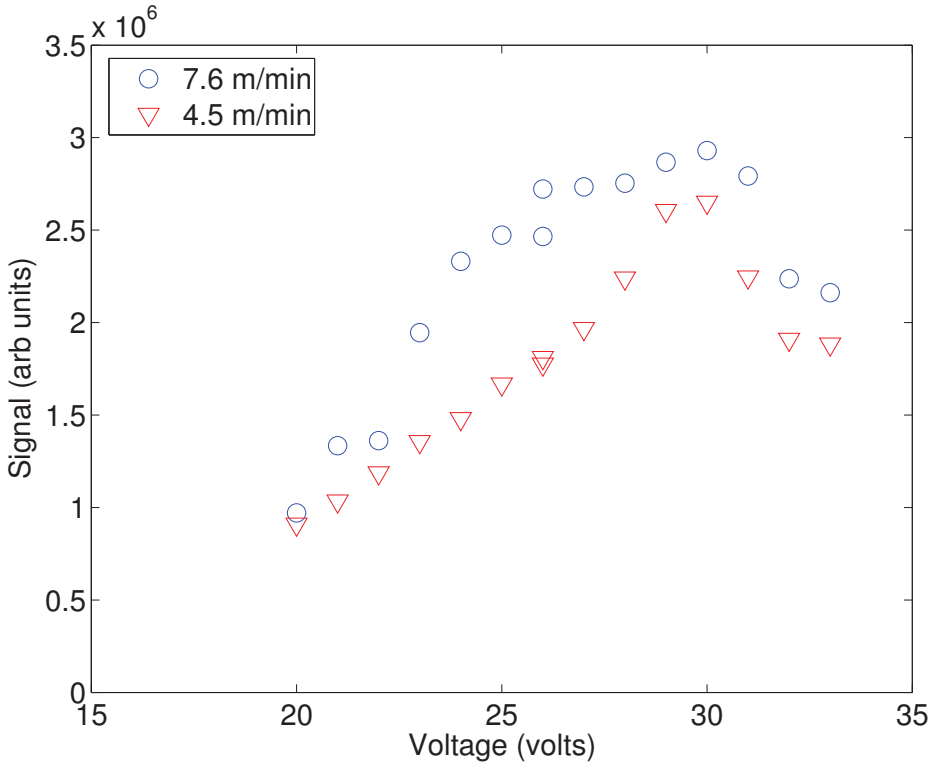

Figure 4.15: Laser scatter intensities for different welding voltages

The intensity of the light scattered from the welding fume exhibits an increase with voltage up to about 28volts. In excess of this voltage the intensity of the scattered light decreases. This plot is similar in shape to the N curve found by Quimby & Ulrich (1999)

for similar welding variables. Figure 4.15 displays similar trends to those displayed in Figure 2.10 suggesting the viability of laser scatter measurements. Probably the most noticeable similarity between the figures is the sharp change in FFR at the onset of the spray transfer mode at 27 Volts in Figure 2.10 and 29.5 Volts in the work presented here. It is more than likely that the variation in this transition voltage is a result of different methods of voltage measurement or power supply characteristics. Variations in FFR may also occur due to the use of a shielding gas with higher percentage of active gas and different welding wire than that used by Quimby & Ulrich (Haidar & Lowke 1997) .

Several problems however are encountered when trying to resolve the actual fume formation rate from the intensity of the laser scatter imaged by the camera. The first of these is that without a reference it is difficult to quantify the relationship between fume concentration and image intensity. This arises because the intensity as captured by the camera is not only a function of particle concentration but also of laser power, laser sheet geometry, camera sensitivity and the optical properties of the particles. The known linear relationship between laser power, sheet geometry, camera sensitivity and the signal means that these variables could be accounted for without too much difficulty. Probably the hardest of the dependent variables to get a handle on is the optical properties of the particles in the plume. This is especially true since the size distribution and shape of the fume particles should have a dependence on many welding variables including transfer mode. The effect of the changing optical properties of welding fume is yet to be fully determined and has been ignored in the above assumption that FFR is proportional to the intensity of the scattered light across a wide range of voltages.

Another problem in determining the FFR from such images is that the volumetric plume flux is not easily determined. To gauge FFR from light scattering techniques would require the measurement to be independent of the plume velocity arising from the thermal buoyancy. This objective can in part be obtained by considering the flow rate close to the shroud to be constant as has been done here. In this area the plume velocity is still dominated by the volumetric flow rate of the shielding gas and not by the buoyancy of the plume. As previously mentioned the FFR in some respects is irrelevant to worker exposure. Considering this and the fact that the welder will inhale a constant volume irrespective of the plume flux means that plume velocity need not be considered when using laser scattering images to gauge fume concentration in the breathing zone.

Collecting scattered laser light close to the welding arc does have its disadvantages when trying to determine FFR. The first of these is that there is no constraints on the size of particle considered. Indeed particles in the size range beyond that which could be inhaled will readily reflect light that could be detected. Should the resolution of the imaging device be sufficient it would be feasible to post process the images in software

to remove the effect of some of the larger particles. The other problem imaging so close to the welding arc is that fine fume formed from condensation vapour off splatter is not considered. This problem however is also encountered in fume box measurements where splatter quenches on the walls of the chamber. In the majority of practical welding processes the amount of splatter and therefore the amount of fume formed via this mechanism would be minimal.

Should the issues above in relating laser light scattering to fume formation rate be resolved or found to be negligible then the use of this technique to measure FFR presents several advantages over fume box measurements. The main one of these is the reduction in time required to obtain a result. While fume box measurements require intricate handling and weighing of filter paper laser measurements could be used to obtain near real time results. Considering that similar trends can be observed between Figure 4.15 and previously published literature, it would suggest that some of the issues involved with optical detection of welding fume particles are not as significant as first thought. Indeed it may eventuate that the uncertainty obtained with light scattering techniques is on a par with that of fume box measurements.

4.3.3.2 Time dependence

With the ability to measure scatter intensity close to the welding arc and assuming that the light intensity is related to fume concentration then there is the ability to investigate fume formation on much finer time scales then that obtainable with fume boxes. While fume boxes require the welding process to be undertaken for sufficient time for the particles collected on the filter paper to reach a weighable quantity, light scattering could be near instantaneous. To demonstrate this possibility the intensity of the scattered light for each image in a series of images is displayed in Figure 4.16.

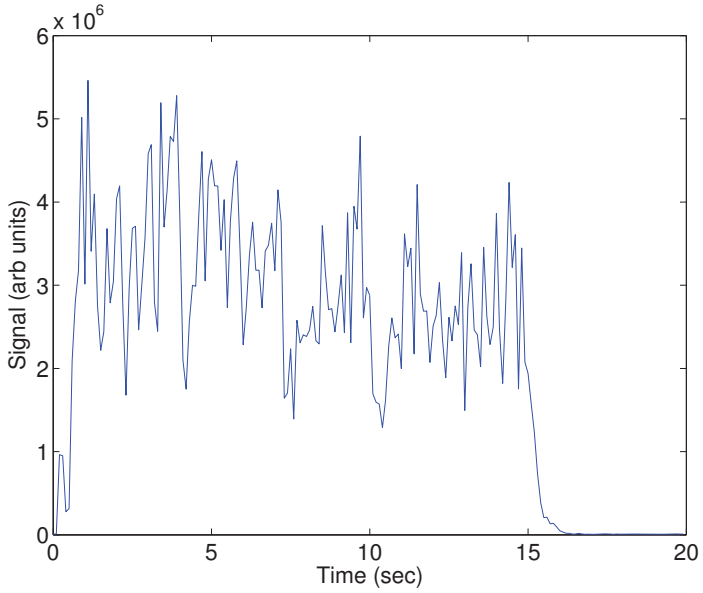

Figure 4.16: Laser scatter intensity versus welding time

In the case of this experiment the time resolution obtainable was limited to 0.1s by the pulsed laser. Much finer time scales could be obtained with continuous laser sources and a high speed camera.

4.3.3.3 Gas flow rate

Laser scattering was used to investigate the flow of shielding and fume distribution immediately adjacent to the arc for different shielding gas flow rates. Figure 4.17 displays the average of 150 sequential images collected with the base welding variables as outlined in Table 4.3 at gas flow rates of 10 and 40l/min. These images demonstrate the cone of clean shielding gas issuing from the shroud. As expected the particulate concentration is more diluted by the shielding gas at higher flow rates. However the size of the internal clean cone of shielding gas from the gas shroud is unchanged.

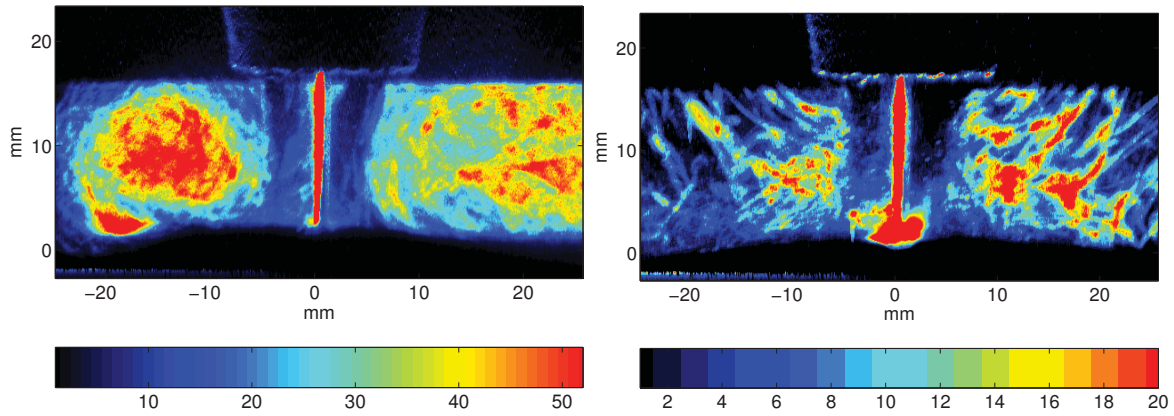

(a) 10 l/min

(b) 40 l/min

Figure 4.17: Average of fume scatter at two different shielding gas flow rates

Figure 4.17 was collected with the base welding parameters with 26volts. To more fully investigate dilution the welding voltage was dropped to 22volts to place the transfer mode well into the dip transfer regime and to obtain a shorter arc. The shorter dip transfer arc should be less affected by the change in the gas flow rate and hopefully produce a more constant fume source. Figure 4.18 displays the relative intensity of the scattered light from the particulate fume from this lower voltage. In principle particulate concentration is equal to the fume formation rate divided by the gas flow rate. Assuming that the fume formation rate remains constant across the gas flow range then the concentration is proportional to one on the gas flow rate. Indeed this inverse gas flow rate trend is found in the signal intensity, plotted as the blue line in Figure 4.18. The correlation between the experimental results and theoretical particulate concentration is significant in the verification of optical scattering as a fume measurement technique. It also demonstrates that in that area imaged the fume plume is very much governed by the momentum flux from the shielding gas flow rather than plume buoyancy.

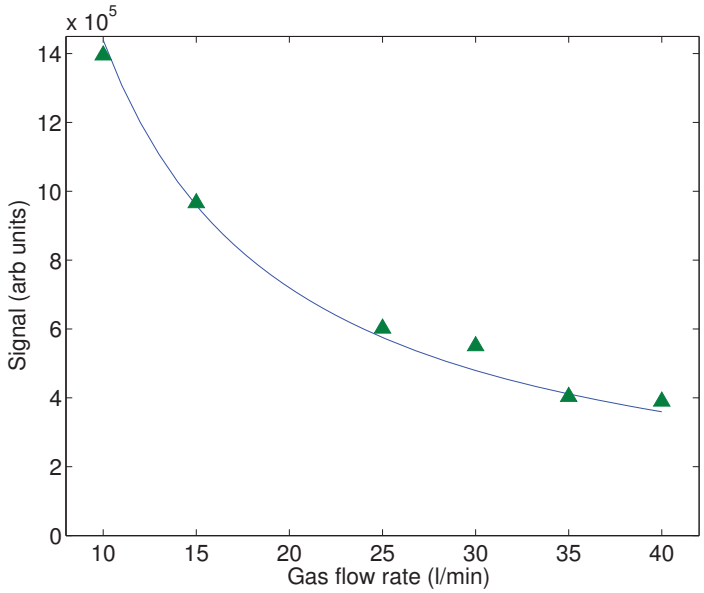

Figure 4.18: Intensity of scattered image relative to gas flow rate

4.3.3.4 Drum speed

Laser scattering images were collected under the welding torch at four different drum speeds. Other than weld traverse rate the base welding variables were as outlined in Table 4.3 and the drum direction remained counter clockwise. Average images for the four different drum speeds are displayed in Figure 4.19. These images possibly show a slight change in fume distribution left and right of the welding torch with traverse rate.

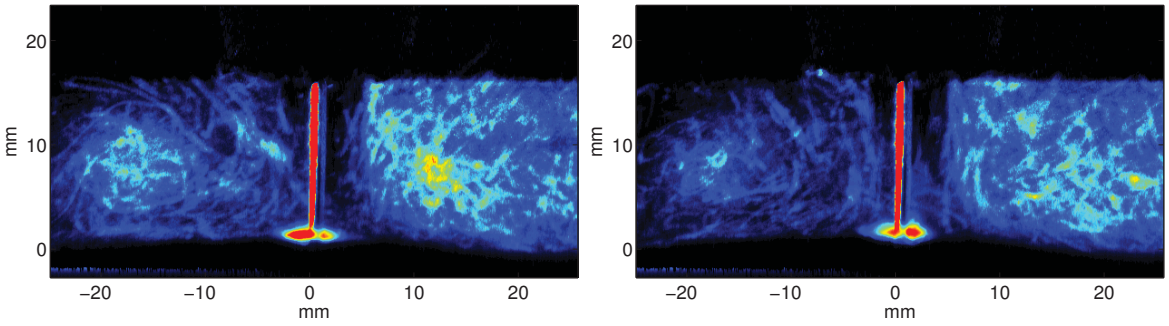

(a) 300 mm/min

(b) 400 mm/min

(c) 500 mm/min

(d) 600 mm/min

Figure 4.19: Average of fume scatter at four different drum speeds

4.4 Laser induced incandescence

Laser induced incandescence measurements were undertaken to investigate the application of this technique to welding fume. Interest in this technique arose from its ability to theoretically produce a signal proportional to the volume of the fume particles present in the medium.

This technique has been extensively developed for the the measurement of soot in flames but as yet has not been widely applied to metal nanoparticles. In flames the advantage of LII is that theoretically it can be used to generate relative particulate concentration measurements for small particles that are changing in size. The goal of the initial experiments presented here was to determine the optical response of the particles to incident laser light.

Figure 4.20 displays an image of a calibration target taken by the ICCD camera. This represents the typical area imaged by the camera during the LII experiments, being approximately 400mm wide and 260mm high. It was required to image this region to obtain the LII image across the entire width of the plume. This allowed for LII comparison against the line integrated extinction measurements across the length of interaction. Figure 4.20 displays the welding torch and the top part of the torch support. The metal arm used to block direct light from the arc entering the camera can be seen just above the drum surface.

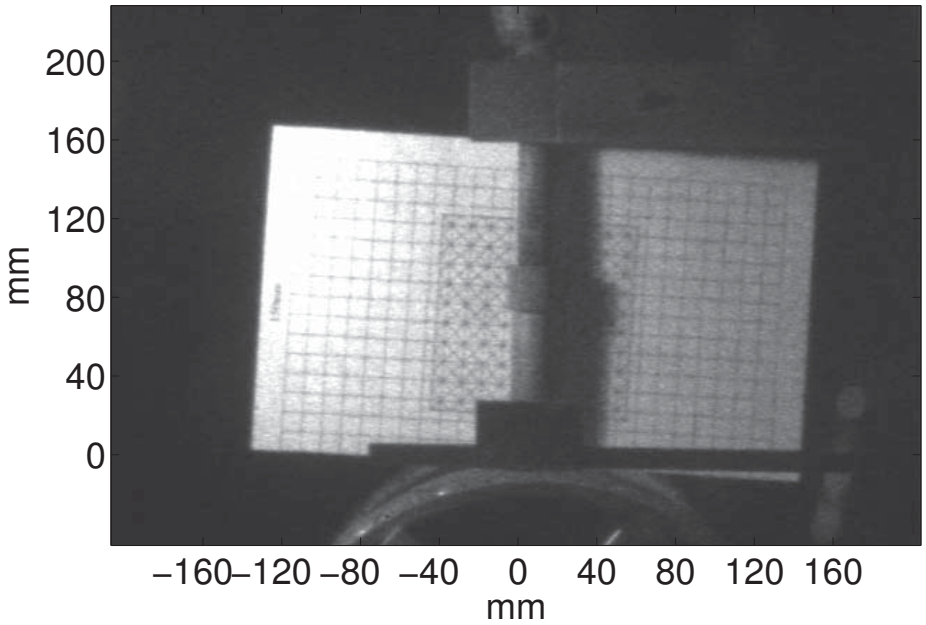

Figure 4.20: Target behind welding torch taken with the ICCD used for the LII experiments

Figure 4.21 displays an image collected by the camera during welding. This image displays a number of features indicative of the effect of background light unrelated to the laser induced incandescence. The area illuminated by the laser used for LII only

represents a small fraction of the image. The region that LII could originate from is therefore limited to the area of the laser sheet which in this case is about 120mm above the arc and having a sheet height of 25mm. The path of this sheet matches that used for the extinction measurements. Background light collected unrelated to the laser induced emission would appear to originate from three sources.

The first of these is from the reflection of arc light off welding particles. This is evident by the strong signal surrounding the arc block. A faint reflection can also be see from the fume higher up in the plume. This problem was more evident at higher welding voltages having longer arc length and emitting more background light. Probably the main problem in relation to this source of the background light was that not only is it related to the arc light intensity, that while unstable could be measured and corrected for, but also the fume concentration which is the variable of interest. The effect of this background light could be reduced with the use of a more appropriate optical filter. The other option that would be available to reducing this effect would be to briefly interrupt the arc during the collection of the image to eliminate the light source. With the equipment configuration used it was considered unfeasible to obtain relevant LII measurements with the laser sheet any closer to the welding arc.

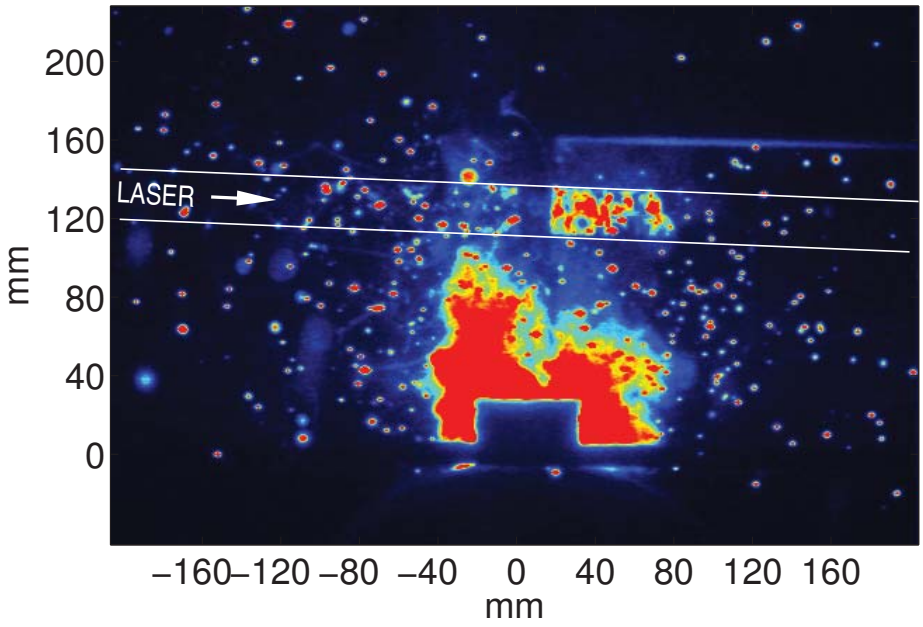

Figure 4.21: ICCD image of LII and background light

The second source of background light originated from the incandescence of large molten globules of metal, called splatter, ejected from the arc. These are evident in Figure 4.21 as dots. The effect of the molten splatter could be reduced by using welding variables that produced less splatter. This can be achieved by generating a stable arc during spray droplet transfer. However increasing arc voltage to obtain spray transfer and subsequently to reduce splatter would also increase arc length and arc background light. As these specks are obvious features it may be possible to remove their effect with post processing of the image.

The third source of background light is from electrical interference recorded by the camera generated by the arc. The extent of this problem was related to the stability of the arc however it was relatively small compared to the effect of arc light and metal splatter.

4.4.1 Fluence curve

Measurements were undertaken to investigate the intensity of the LII emission relative to the power of the infrared laser beam. These plots were undertaken to determine at what point mass loss from the particle, by way of vaporisation, outweighs the increase in optical radiant emission from higher laser powers.

Different laser powers were generated by varying the time delay between the flash lamp and the Q-switch of the relevant laser. A relationship between this delay and the laser power was generated by measuring the laser power with a optical power meter. A plot of this relationship is displayed in Figure 4.22. As the infra-red beam arises from the fundamental wavelength of the laser it was considered repeatable. Intermittent measurement of the laser power verified this assumption.

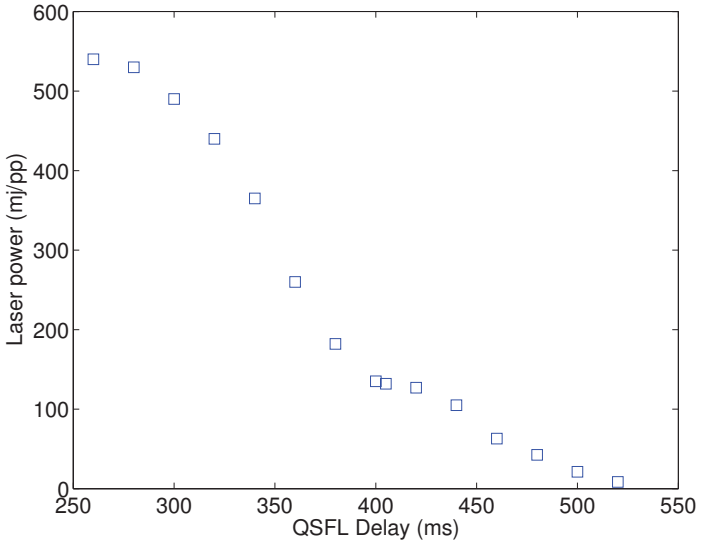

Figure 4.22: Q-switch to flash lamp delay time versus laser power

The intensity of the image was obtained by considering the sum of the ICCD pixels in the region of the laser sheet depicted in Figure 4.23. This was undertake by saving the images from the camera for later analysis in matlab as was done with the laser scattering images collected above. Figure 4.24 displays a fluence curve obtained from the base welding variables displayed in Table 4.2. During this experiment a Hoya red R(25A) filter was fitted to the ICCD. Camera exposure time was 400nS, delayed 125nS after the laser pulse.

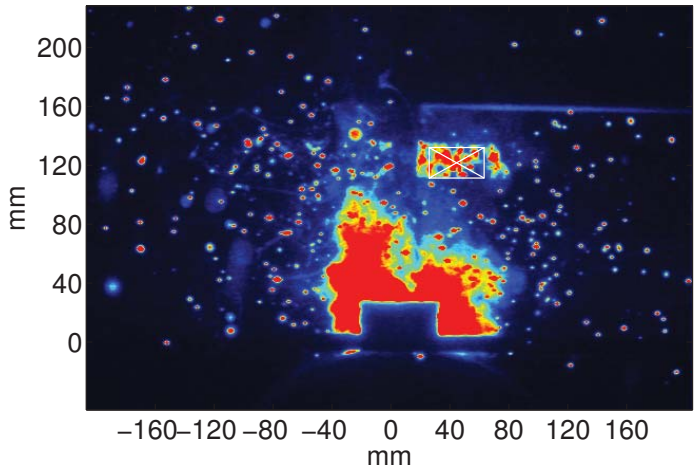

Figure 4.23: White box depicting the area accumulated

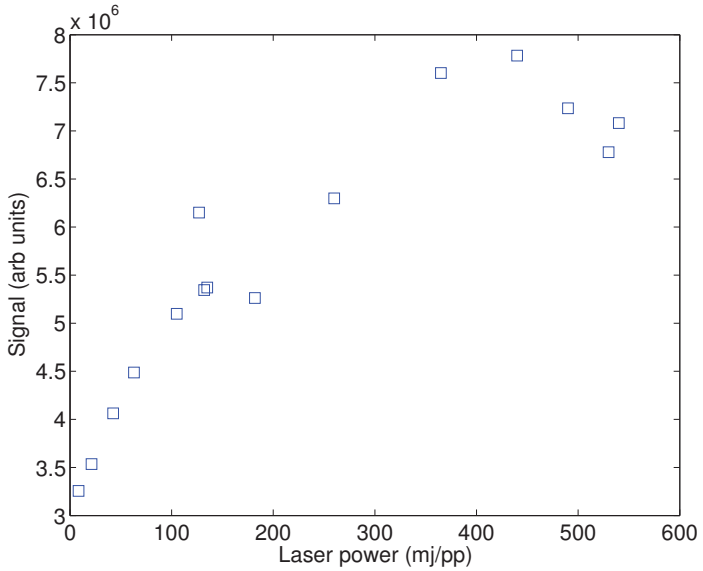

Figure 4.24: LII fluence curve

4.4.2 Optical spectrum

The incandescence emission produced from the laser heated particles is reasonably broad band. The spectrum however is limited by the temperature at which the particles starts to vaporise. To investigate the significance of the spectrum on the LII technique power fluence plots were collected for the 3 different filters pictured in Figure 4.25. The left most of these filters is a UV filter allowing the transmission of visible light only. The middle filter is a Hoya R(25A) optical glass filter and the filter imaged right is a Hoya orange optical glass filter. The actual spectrum collected by the camera is a combination of the transmission spectrum of the filter and the response spectrum of the camera. The relative transmission of background light is displayed in Figure 4.26. This was determined from images collected with the three different filters for the same welding variables with the laser turned off. This demonstrates that as expected the UV blocking filter transmits more background light than the orange and red filters that transmit a smaller portion of the spectrum emitted by the welding process.

Figure 4.25: The three optical filters used during LII

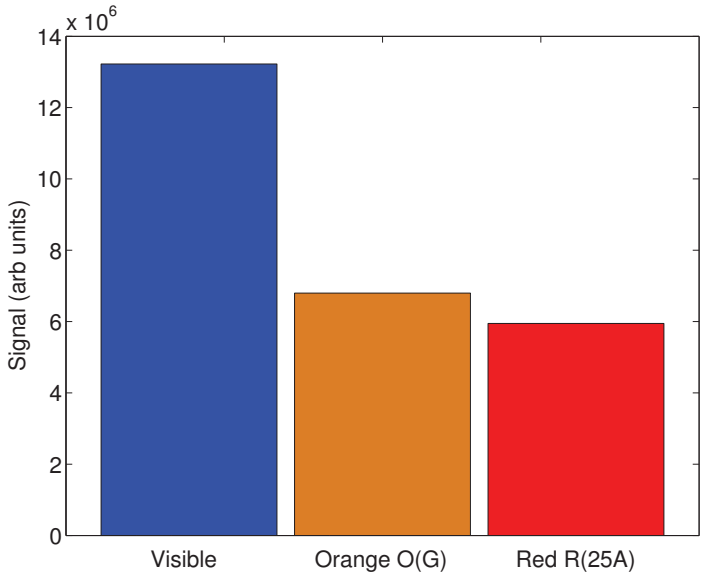

Figure 4.26: Background transmission for the three optical glass filters

The fluence plots obtained from each of the optical filters is displayed in Figure 4.27.

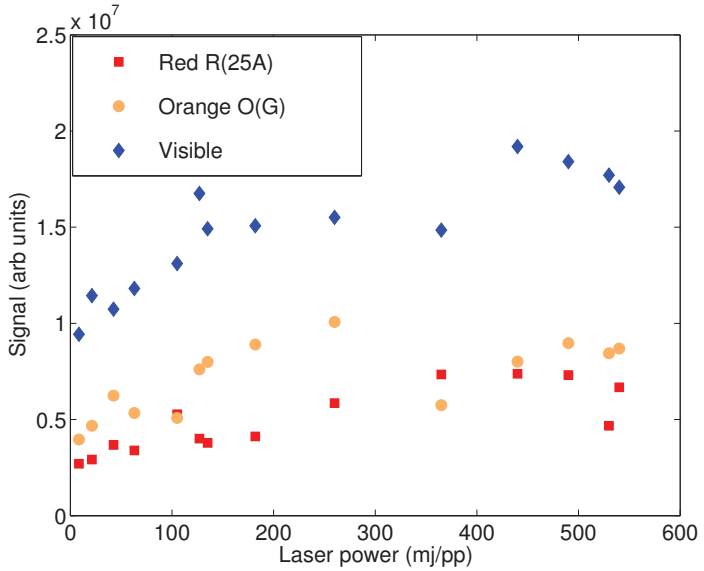

Figure 4.27: LII fluence curves for three optical glass filters

4.4.3 Concentration

To determine if changing particulate concentration from different fume formation rates could be measured LII was collected over a range of welding variables. Similar welding variables as those used for the laser scattering measurements in Subsection 4.3.3.1 were used again for this work. The accumulated pixel intensity from the region containing LII outlined in Figure 4.23 is shown in Figure 4.28 for the different welding voltages and wire feed speeds.

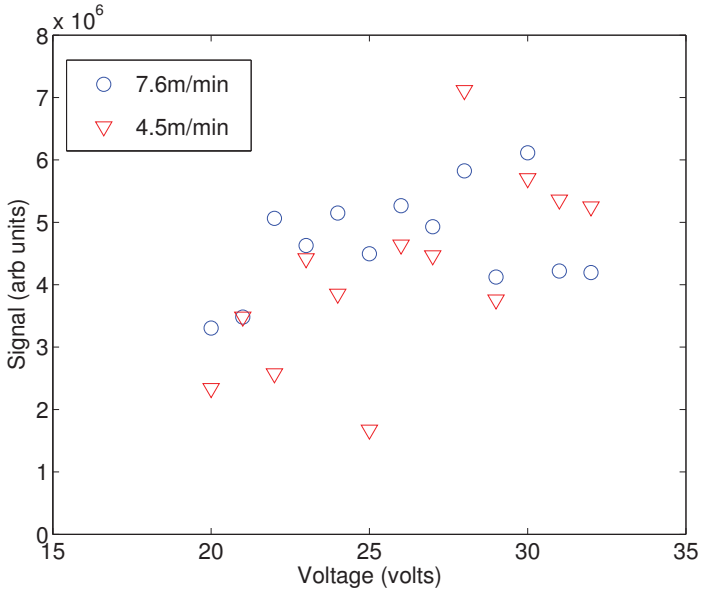

Figure 4.28: LII signal intensity for different voltages and wire feed speeds

4.5 Extinction

Laser extinction provides a line integrated measurement of the light scattered and absorbed by the fume particles. Laser extinction data were collected for FCAW and GMAW welding variables. Extinction data for both the FCAW and GMAW welding processes were collected by recording the modulated laser beam before and after passing through the plume. An example of the recorded modulated laser beam intensity obtained during one of the welding processes can be seen in Figure 4.29. The magnitude of the reference and transmitted signals was calculated for this data by measuring the peak to peak voltage of each of the signals. The peak to peak representing the component of the detected light arising from the modulated laser beam. The base offset voltage arising from the arc background emission detected. As can be seen Figure 4.29 the transmitted beam, that was exposed more directly to the arc light, was raised by the additional background. The arc and room light was negated by only considering the laser component from the modulated beam.

The reference magnitude for each of the measurements was then corrected with a factor

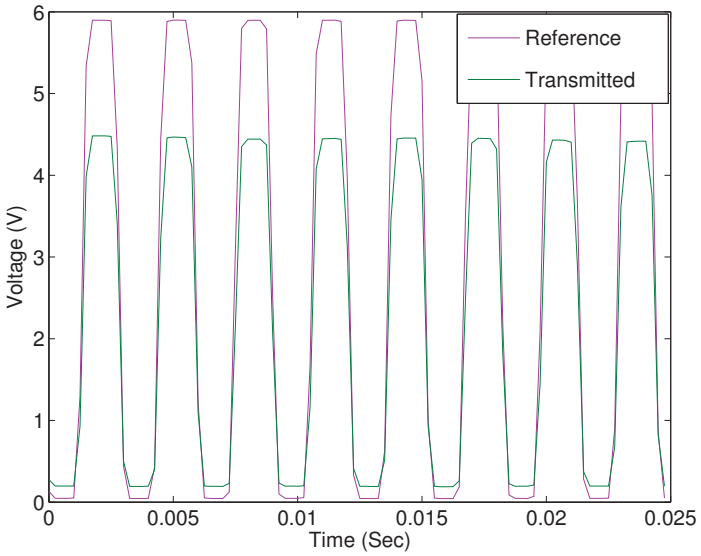

Figure 4.29: Example of recorded extinction and reference beam measurements

to account for the ratio of the beam splitter and differences in photodiode sensitivity. This factor was calculated from a measurement taken with no fume plume present. As such the reference intensity was corrected to be the same as the transmitted intensity when no extinction was present.

4.5.1 FCAW

The results obtained for different shielding gas flow rates in FCAW are displayed in Table 4.7. During this experiment welding variables other then gas flow remained constant. The same welding variables were used as those in Section 4.3.1 repeated here as Table 4.6. The wire used was Shieldcore 15 having the designation E71TG5 with a feed rate of 4.5m/min with a voltage of 16.5V DCEN and a traverse rate of 230mm/min. Extinction measurements were taken for four different shielding gas flow rates being 0, 10, 20 and 30 l/min plus one without any welding used for the optical calibration factor. From the data Table 4.7 a reduction in beam extinction can be seen with increasing shielding gas flow.

Process	FCAW	Units
Electrode Wire	0.9mm E71TG5	
Voltage	16.5 (DCEN)	Volts
Wire Feed	4.5	m/min
Current	93-97	Amps
Shielding gas	Ar 81.25, CO_2 16, O_2 2.75	%
Gas Flow rate	0, 10, 20, 30	l/min
Weld traverse rate	230	mm/min
Standoff	12	mm

Table 4.6: FCAW variables used to investigate the effect of gas shielding

process	Corrected Incident (Volts)	Transmitted (Volts)	% beam extinction
welder off	5.58486	5.58486	0
no gas	5.26045	4.40944	16.177
no gas	5.23538	4.33349	17.226
10 l/min	5.39334	4.87181	9.669
10 l/min	5.36209	4.99181	6.905
20 l/min	5.57034	5.28977	5.036
20 l/min	5.46423	5.26532	3.640
30 l/min	5.33062	5.17512	2.917
30 l/min	5.29459	5.11502	3.391

Table 4.7: Extinction for a FCAW process

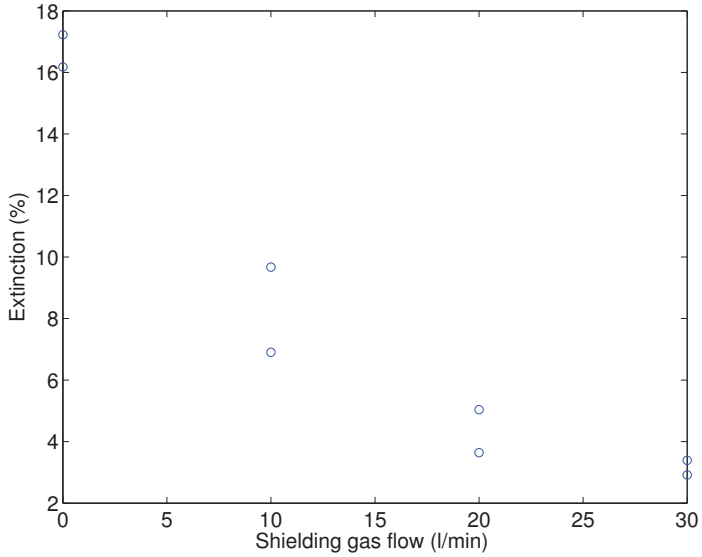

Figure 4.30: Measured FCAW extinction for different shielding gas flow rates

Figure 4.30 demonstrates that the addition of shielding gas reduces the quantity of beam extinction. It would follow that the reduction in extinction is related to a reduction in particulate concentration with increasing shielding gas flow. However this would not necessarily mean that the fume formation rate has been reduced as the plume flux has also changed.

4.5.2 GMAW

Extinction measurements were also recorded for a range of voltages for the 4.5 and 7.6 m/min GMAW wire feed rates. The beam extinction for the two wire feed rates are displayed in Figure 4.31. As outlined in Section 3.3 the wire was 1.2mm ER70S6 with 17l/min Argoshield Universal a standoff of 19mm and a traverse rate of 360mm/min. As a general trend the beam extinction from GMAW increased with the increase in voltage.

	GMAW	Units
Electrode Wire	1.2mm ER70S6	
Voltage	15-33 (DCEP)	Volts
Wire Feed	4.5, 7.6	m/min
Current	160-175,220-241	Amps
Shielding gas	Ar 81.25, CO_2 16, O_2 2.75	%
Gas Flow rate	17	l/min
Weld traverse rate	360	mm/min
Standoff	19	mm

Table 4.8: GMAW variables used for extinction measurements

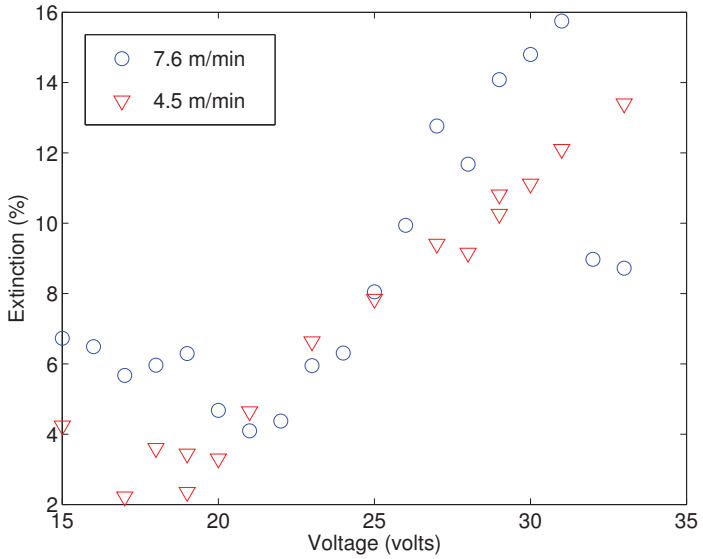

Figure 4.31: Measured GMAW extinction for different voltages and wire feed speeds

4.6 Combined scattering and LII

Images of scattering and LII were collected simultaneously to determine if a relationship between results from the two methods existed. The experimental configuration was similar to the individual methods however in this case the lasers and cameras involved were synchronised together.

Figure 4.32 displays the average scattered image obtained when the 532nm light sheet used for the scattering occurred slightly post the infrared beam used for the LII. In this case the IR beam results in a dark band at 140mm above the arc. The dark band is more pronounced on the left side of the image where the two beams overlapped better. This indicates that the power of the IR beam, in this case 520mJ, was sufficient to cause total evaporation of the particle, something not desirable in the application of LII. Such vaporisation increases the chances that the signal obtained from this region was obtained from a source other then incandescence. Subsequently the laser scattering image was taken slightly prior to the laser activation for the LII.

As the resolution of the cameras were different and were in slightly different positions the images were matched using a transformation routine during post processing.

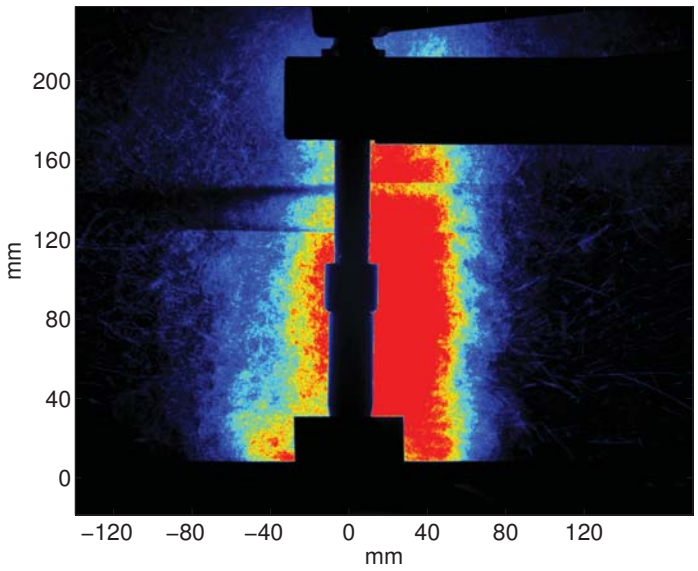

Figure 4.32: Average image from 100 light scattering images with IR beam on

Figure 4.33 displays the ICCD image transformed to match that obtained from the megaplus camera. The transformation can not improve the resolution of the ICCD image which remains significantly less then that of the megaplus camera. Figures 4.34 and 4.35 display matched scattering and LII images of the welding plume.

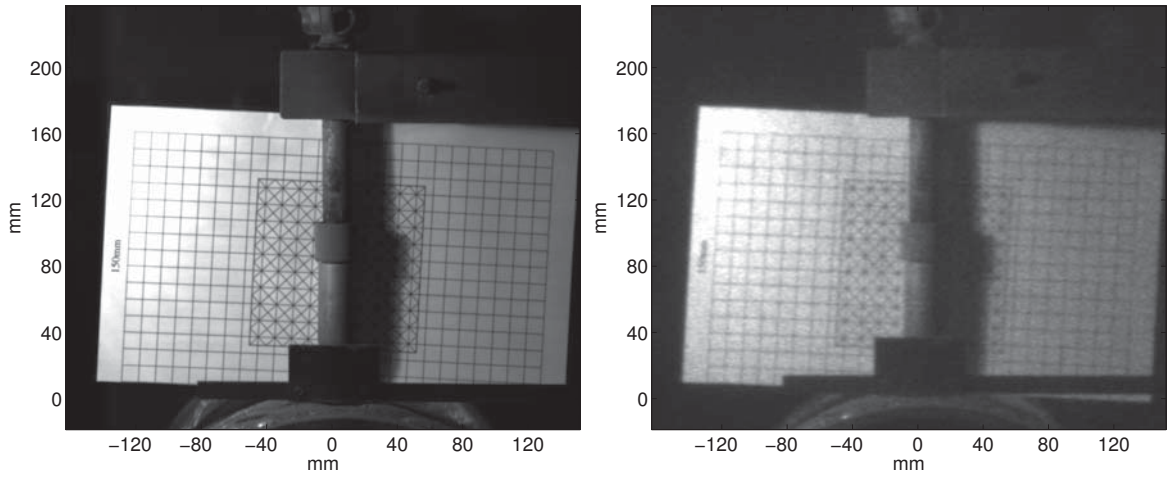

(a) Scattering

(b) ICCD

Figure 4.33: Matched images

To investigate whether a relationship between the two signals existed the intensity of a small region to the left of the welding torch was determined for a series of simultaneous LII and scatter images. This measurement was undertaken at a number of welding voltages to determine if this relationship was related to particle size distribution changes with differing transfer modes. Figure 4.36 displays plots of the relationship between LII and laser scatter intensity for four different welding voltages. Each + mark on the plots represents the LII and scatter intensity from matching images. The red line in each case is a linear best fit of the points on that graph.

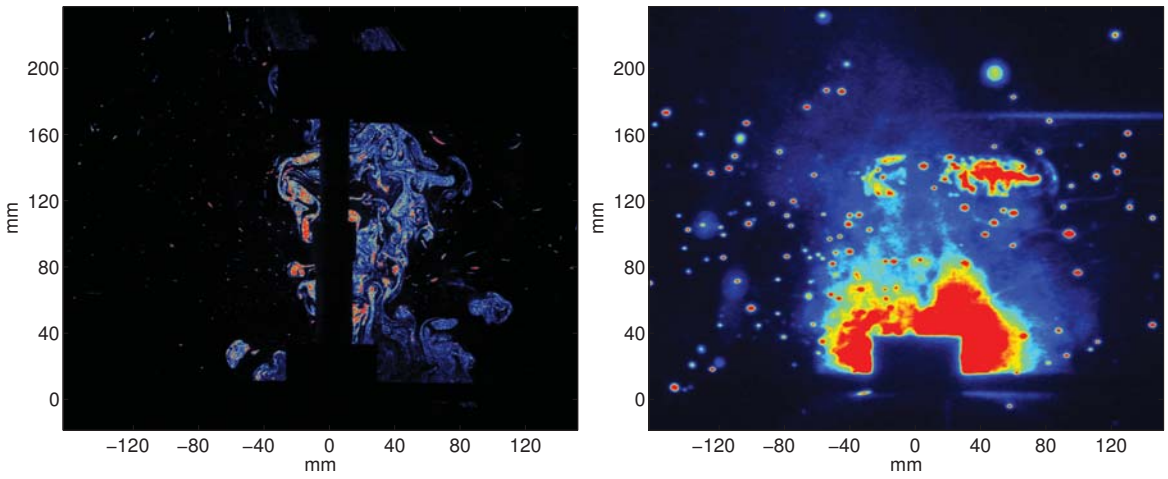

(a) Scattering (b) LII

Figure 4.34: Matched images

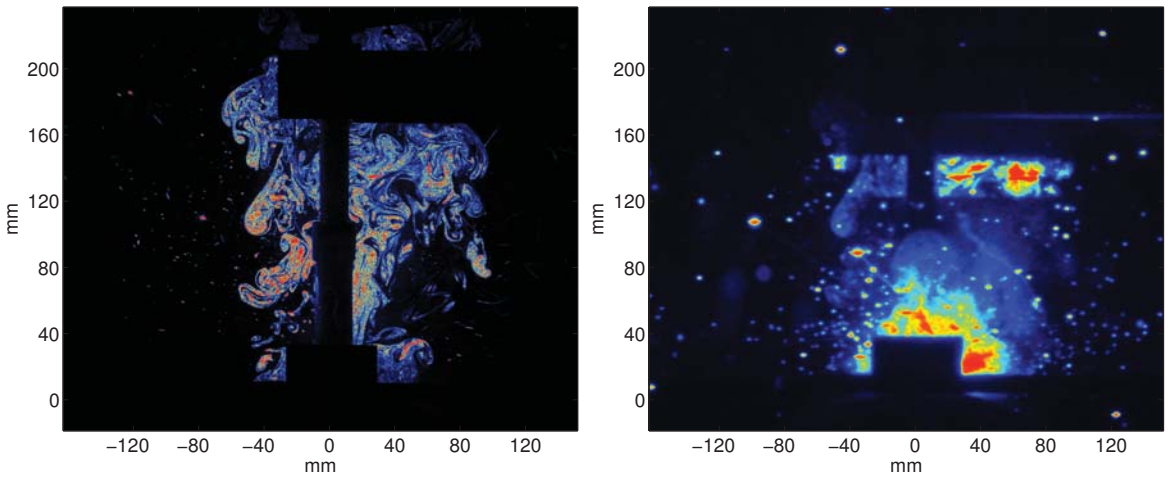

(a) Scatering (b) LII

Figure 4.35: Matched images

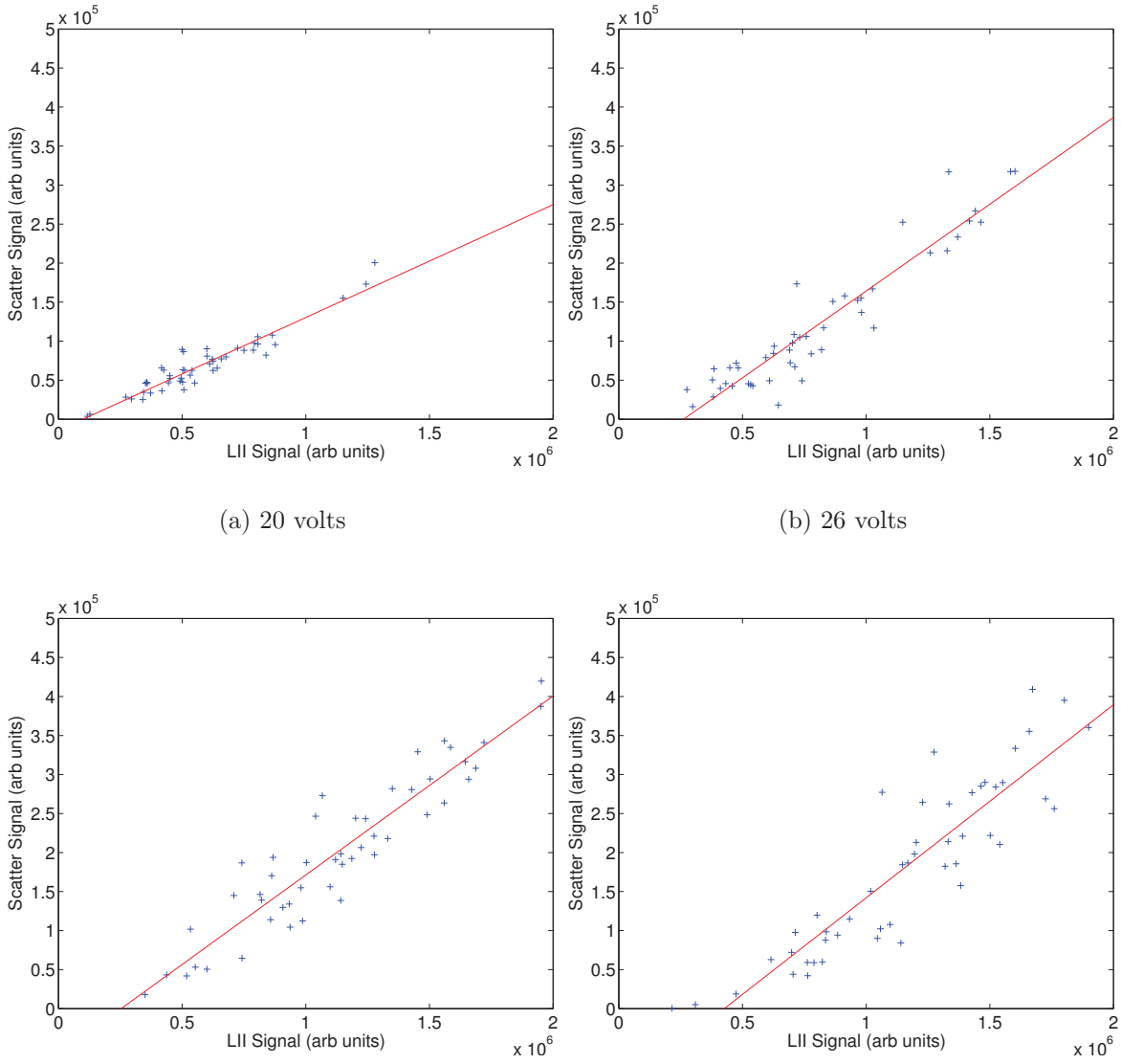

(a) 20 volts

(b) 26 volts

(c) 30 volts

(d) 33 volts

Figure 4.36: Laser scatter intensity versus LII intensity for different welding voltages

4.7 Fume box

Fume box measurements were undertaken at CSIRO Woodville. The aim of these experiments was to gain experience with traditional fume formation measurement and to obtain quantitative fume formation rates.

4.7.1 GMAW

The welding variables used for the fume box measurements are displayed in Figure 4.9. These are similar to those used for the optical measurements from Table 4.5 and therefore also related to those used by Quimby & Ulrich (1999). Unavoidable changes in welding variables from those used in the laser scattering experiments were required. Due to the length of the weld that could be produced in the fume chamber the weld traverse rate was reduced from 360mm/min to 330mm/min. The shielding gas composition was also altered due to a change in supplier. The welding current was found to be higher during the fume box measurements than that for the same voltage and wire feed speed used with the optical measurements. At the time this was attributed to the change in shielding gas composition and weld traverse rate. However later experiments with unshielded FCAW at the same weld traverse rate as used in the FCAW optical scattering measurements exhibited a similar increase in current. This would suggest that gas composition and weld traverse rate was not responsible for the increase in current. The increase may have been due to voltage calibration or numerous other variables such as wire feedability that alter arc stability.

	GMAW	Units
Electrode Wire	1.2mm ER70S6	
Voltage	20-33 (DCEP)	Volts
Wire Feed	4.5, 7.6	m/min
Current	168-192,236-287	Amps
Shielding gas	Ar 93, $CO_2$4.5, O_2 2.5	%
Gas Flow rate	17	l/min
Weld traverse rate	330	mm/min
Standoff	19	mm

Table 4.9: Summary of welding variables used for fume box measurements

Due to the length of time required to handle and weight filter material FFR measurements were taken at less frequent intervals than that used for the optical measurements. The voltages used for the fume box measurements were selected to correspond with different droplet transfer modes mindful of the expected "N" shaped trend. Figure 4.37 displays the increase in filter material weight after welding and drying for a one minute welding time representing the FFR for the two wire feed speeds. The 7.6m/min wire feed speed demonstrates a "N" shaped FFR but far more pronounced than that found by Quimby & Ulrich (1999) or in the laser scattering

experiments conduced as part of this thesis. The FFR for the the 4.5m/min wire feed speed increased linearly for voltages above 24V and no "N" shape was evident.

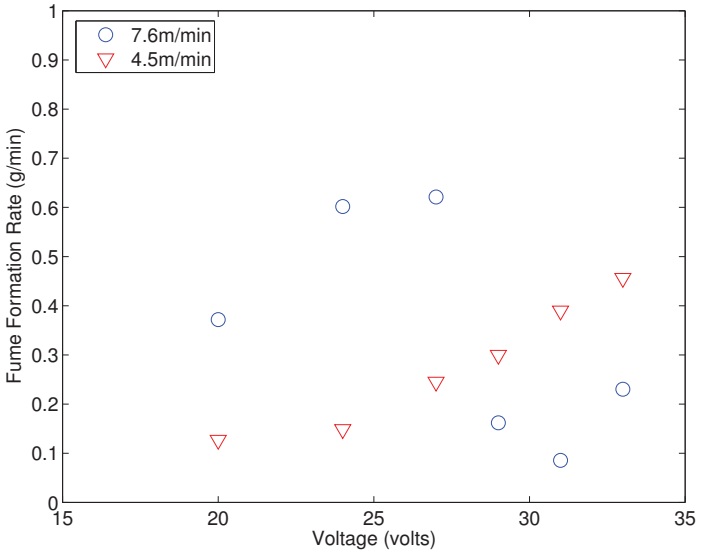

Figure 4.37: Measured FFR of GMAW for different voltages and wire feed speeds

Figures 4.38 and 4.39 display photos of the filter matting from different voltages for the 4.5 and 7.6m/min wire feed speeds respectively showing discolouring of the matting due to fume collection. Visually the discolouring seems to be in reasonably good correlation to the amount of fume collected as displayed in Figure 4.37.

4.7.2 FCAW

Fume box measurements were also undertaken for FCAW at different shielding gas flow rates. With the exception of the shielding gas composition the fume box FFR measurements were undertaken with the same welding variables as those used for laser scattering in Section 4.3.1. While the welding variables were the same the current was higher than that found during the laser scattering experiments.

Process	FCAW	Units
Electrode Wire	0.9mm E71TG5	
Voltage	16.5 (DCEN)	Volts
Wire Feed	4.5	m/min
Current	106-111	Amps
Shielding gas	Ar 93, $CO_2$4.5, O_2 2.5	%
Gas Flow rate	0, 10, 20, 25	l/min
Weld traverse rate	230	mm/min
Standoff	12	mm

Table 4.10: FCAW variables used to investigate the effect of gas shielding

Figure 4.40 displays the FFR for the FCAW at four different gas flow rates. Figure 4.41 displays a photo of the filter mats from each of the four gas flow rates. The unshielded

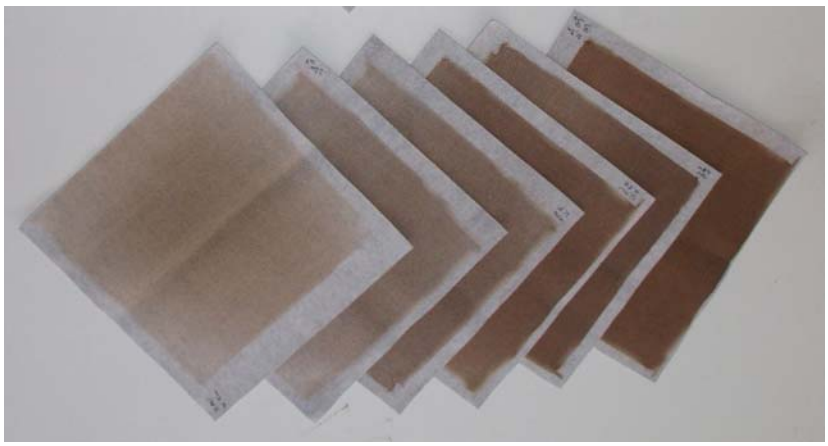

Figure 4.38: Filter mats for 4.5m/s wire feed and left to right 20,24,27,29,31,33V

Figure 4.39: Filter mats for 7.6m/s wire feed and left to right 20,24,27,29,31,33V

FCAW mat on the left being noticeably darker then the other mats despite collecting a similar amount of fume to that for the 20l/min shielding gas flow rate and less fume than the 25l/min shielding gas flow rate. This would infer that the optical properties of the unshielded fume were different to the shielded fume as the discolouration is greater for less fume.

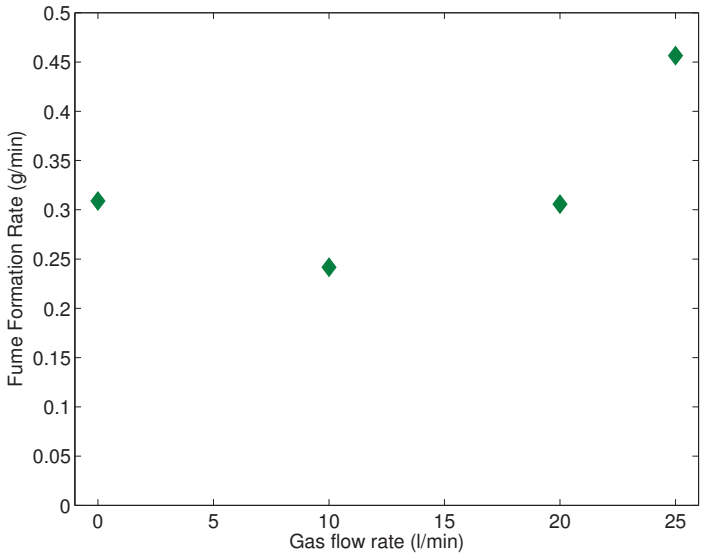

Figure 4.40: Measured FFR of FCAW for different gas flow rates

Figure 4.41: Filter mats for FCAW left to right 0,10,20,25l/min gas flow rate

Chapter 5

Discussion

5.1 Scope

This chapter presents the interpretation of the results detailed in Chapter 4 from the experimental work outlined in Chapter 3. In essence this chapter has been divided in to two sections. The first of these sections focuses on the application of the three laser diagnostic techniques undertaken in the results presented. The second section takes the results obtained and relates them to fume findings.

The first of these two sections discusses the application of the laser scattering, laser induced incandescence and laser extinction. Reference is made to the area of combustion where each of these techniques has been used widely for research into soot formation in flames. Some of the issues found in soot research are addressed along with the implications when applied to welding fume. The composition and particle size distribution of soot however is different to that of welding fume. Considerations are therefore made on the optical properties of welding fume which, unlike soot, is poorly defined in published literature. Resultantly it is determined that assumptions are currently required to determine fume particulate concentrations from the results obtained.

The second section of the discussion considers the findings obtained from the techniques in relation to fume. While assumptions are required in determining fume formation with laser measurements, trends found that match equivalent measurements using fume boxes are discussed. Particular attention is given to the plume shape recorded from laser scattering images. Shortcomings in current welding fume plume formation knowledge are addressed with experimentally obtained cross sections as presented in Sections 4.3.1 and 4.3.2 of the results.

5.2 Laser techniques

Three laser techniques, being laser scattering, laser induced incandescence and laser extinction, were selected to investigate particulate welding fume. These techniques were selected as a result of their traditional application to the measurement of soot in combustion research. The use of these techniques in flames has been to non intrusively measure soot quantity and position. Likewise these techniques were selected to measure particulate fume within the plume of hot gases emanating from the welding process.

The primary reason for undertaking laser scattering was to image the cross section of actual GMAW and FCAW plumes. Practically while easy to conduct due to the strong signal and known spectrum the determination of particle concentration is complicated by the physics behind light scattering off arbitrary shaped and sized particles.

Laser induced incandescence was undertaken as the signal produced from soot particles is proportionl to particle concentration. The application of LII to soot is a relatively new technique in combustion. Similarly the application of LII as a technique to the measurement of metal nanoparticles is still being investigated. In practical terms LII was more equipment intensive and difficult than scattering. The incandescence signal produced is only a small fraction of the intensity of that obtained from laser scatter and is spread over a larger portion of the spectrum. In addition the power of the laser used for irradiation becomes critical. However the physics involved in relating LII signal strength to particle concentration are simple under certain circumstances.

Laser extinction while only providing a line integrated measurement can be used to determine average particle concentration given that the optical properties of the medium are known. In combustion research such measurements are used to calibrate other techniques, such as LII, with the actual soot concentration. Of the three techniques extinction proved to be the simplest to undertake. However uncertainty exists in the results due to assumptions on the average path length and optical properties of the particles.

5.2.1 Laser scattering

The goal of the laser scattering experiments was to obtain cross sectional images of the fume plume close to the welding arc. The expectation of this was to show two things. Firstly the external illumination would allow the internal structure of the plume to be observed. Secondly since the illumination was constant and unrelated to the arc emission then the potential exists for the quantity of scattered light to be related to the amount of fume present.

The experimental configuration of the laser scattering experiment as outlined in Section 3.6 was relatively simple. It involved forming a vertically diverging laser sheet that

passed through the plume adjacent to the welding torch. The resultant scattered light was then detected by a camera normal to the laser sheet.

Three requirements were placed on the illumination source. Firstly the illuminating source needed to produce a known wavelength so that scattered light could be spectrally separated from the welding background with an optical filter. Secondly the light source needed to have sufficient power to produce detectable scatter in the region of interest. Thirdly the light needed to be easily formed into a light sheet to illuminate a two dimensional cross section. All there requirements could be fulfilled with several types of lasers. In this case the laser used for illumination was the 532nm second harmonic of a pulsed Nd:YAG.

5.2.1.1 Background suppression

As can be observed in Figure 3.7, which is a ordinary digital photograph of a welding arc, the light generated by the arc is sufficient to obscure direct imaging of the plume. Suppression of the background light generated by the welding arc and not related to the laser scatter was a prominent consideration in the design of the experiment. This began with the selection of the illumination source which required the laser to produce a high intensity light sheet with known spectrum as outlined above. The camera used to collect the light scattered images was fitted with a band pass filter which transmitted the 532nm wavelength produced by the laser. The band width of the spectrum transmitted by this filter was about 3nm. The use of this wavelength for illumination and matching bandpass filter was particularly effective due to the relatively low arc emission at this wavelength. In addition to spectral filtering a polariser was used to minimise the arc light. Since the illuminating laser was vertically polarised the scattered light normal to the incident beam would also be predominantly vertically polarised. The polariser on the camera was set to pass vertically polarised light and block horizontal components including a portion of the unpolarised arc background. Exposure time of the camera was set to its minimum and synchronised with the pulsed laser to avoid collecting unnecessary arc light while still capturing the laser scatter. The laser power used in the experiments with the larger laser sheet was about 260mJ per pulse. While not the maximum capable power of the laser it provided sufficient contrast to observe the scattered light at a reduced camera lens aperture. Background control mentioned here is similar to that used during laser shadow imaging of droplet formation which also uses a laser and narrow band pass filter.

In addition to the background light emitted from the arc, attention was given to reflected laser light unrelated to the fume scatter. Reflections were the same wavelength and occurred simultaneously with the laser scatter from particles so could not be controlled with the same optical filtering and camera control as outlined above. This was primarily mitigated by careful arrangement of the optics and objects that may

reflect the light. It was for this reason the light sheet was passed on the opposite side of the welding torch to that of the camera. A beam block was also used before the imaged area to clip the light sheet so to pass just above the welding drum. All objects in proximity to the light sheet, other then the drum onto which the weld was laid, were painted mat black to further reduce the amount of light scattered. After passing through the imaged area the laser sheet was collected in a second beam stop to reduce the amount of stray light.

Images displayed in Section 4.3 show that combined the background control measures were successfully even when imaging the plume close to the welding arc. Some reflected laser scatter is still evident off the welding torch and welding wire but can be easily recognised as being unrelated to the plume.

5.2.1.2 Image resolution

Reasonably high resolution images were obtained of the plume structure. The resolution obtainable is a product of the camera resolution and the width of the laser sheet. For the larger imaged region the one pixel represented 0.3mm. The width of the laser sheet varied from left to right being about 2mm at the extremities down to the diffraction limit of the cylindrical lens at the focal point somewhere near the middle of the image. Due to camera problems the smaller images directly under the welding torch were undertaken with only a portion of the full CCD array. For this reason they were not as high a resolution as what could have been obtained should this equipment have been fully functional. For this smaller region the pixel resolution was about 0.13mm.

The actual plane of fume particles illuminated by the laser sheet would have been slightly affected by an amount of beam steering. This arises due to the light sheet not being normally incident on refractive index changes through the plume. The refractive index of the transmitting medium changes due to different compositions and thermal effects in the plume. As these boundaries are continuously changing due to the turbulent nature of the plume the light sheet is deviated slightly differently each time. Changes in beam path were observed on a screen to be several millimetres maximum 2 metres after passing the welding torch. Practically however given the distortion in relation to the image resolution it is considered to have had minimal effect on the images obtained. It is unclear whether such beam distortion is observed during laser shadow imaging of droplet formation which also passes a laser beam through a similar path.

5.2.1.3 Rayleigh approximation

Since the laser scattering is not being used to determine a quantitative particle concentration directly it is not critical that the particles be sufficiently small for

Rayleigh approximation. The base requirement for Rayleigh approximation is both the particle size parameter $x = \frac{\pi D}{\lambda}$ and $x\,|m-1|$ are much less then one. Since the fume particle size range is so large and the optical properties of the fume poorly known it is hard to determine exactly how well Rayleigh approximation would hold. An additional issue is to what extent is agglomeration of primary particles altering the optical properties and the assumption that the particles are spherical. The average particle size, presumably relating to the aggregate, for GMAW obtained by Zimmer & Biswas (2001) was approximately $160nm$. As long as the agglomerate is chain like then the particles have optical properties similar to the primary aggregate. Most of the fine fume primary particles originating from metal vapour have a diameter from a few nanometres up to $\sim 0.1\mu m$ (Jenkins et al. 2005). Using this diameter and the best available data on the refractive index from flame formed Iron oxide particles $m = 1.96i + 0.2$ (Charalampopoulos & Shu 2003) then for the $532nm$ wave length used:

$$x = \frac{\pi 100}{532} = 0.59$$

$$x\,|m-1| = 0.59\,|1.96i + 0.2 - 1| = 1.25$$

The particle size parameter x is less then one but $x\,|m-1|$ is larger. This would indicate that should mathematical modelling be required and the optical properties were available then a more complete Mie solution rather then a Rayleigh approximation would be worth while. These numbers however are based on the upper end of the fine fume primary particle size and an assumed refractive index of unknown applicability.

5.2.1.4 Cloud scattering

A number of considerations are required in determining if the intensity of the scattered light can be related to the density of the plume present. For this to be true a number of assumptions need to hold true. One of these is the requirement that the amount of scatter from a cloud of N particles is a multiple of that scattered from a single particle of equivalent scattering properties. This is not always the case particularly in dense particle clouds. Jones (1999) places three requirements on multiple scattering clouds.

The first requirement is that the particles are randomly orientated and that incoherent superposition can be applied. In the case of welding fume the turbulent nature of the plume, wide size range and particle agglomeration would ensure that the net result would satisfy the the requirement of random orientation.

The second requirement is that there is negligible multiple scattering. This is to say that the light once scattered by a particle is not further scattered by other particles in the

cloud. While there is always the potential for light to be incident on another particle the effective base requirement outlined by Jones (1999) is that the transmission by the plume is at least 60%. Measurements of beam extinction undertaken in Section 4.5 show that extinction is less then 20% at the longer wavelength used in that experiment. When the shorter wavelength used for the scattering imaging relative to that used for extinction is taken into account this maximum extinction equates to about 24%. The transmission of 76% is therefore still higher then the base requirement of 60%.

The third requirement for multiple scattering plumes is that individual particles are not sufficiently close that they affect the scattering potential of each other. To remain as independent scattering sources the volume fraction is required to be less than 3% as a general guide as outlined in Jones (1999). This criteria can be fulfilled through consideration of the extinction data or in the case of GMAW by considering the fume formation rate as determined in Quimby & Ulrich (1999). The latter of these is done by calculating the volume fraction from the fume formation rate from the similar welding case of $1g/min$ being diluted in the shielding gas flow rate of $17l/min$ using the density of iron oxides, the major content of the fume, $5240kg/m^3$. This results in a particle volume fraction of 11 parts per million, significantly less then the 3% guide. This is even further reduced by entrainment and dilution with the ambient enviroment.

Having satisfied these three base requirements it can therefore be assumed that for the most part, the scatter from a cloud of fume particles is a multiple of the scatter from a single particle of mean equivalent scattering potential.

The best experimental evidence of this in the results collected is the correlation between the scattered light intensity from a region near the torch and the particulate dilution from Subsection 4.3.3.3 shown here in Figure 5.1.

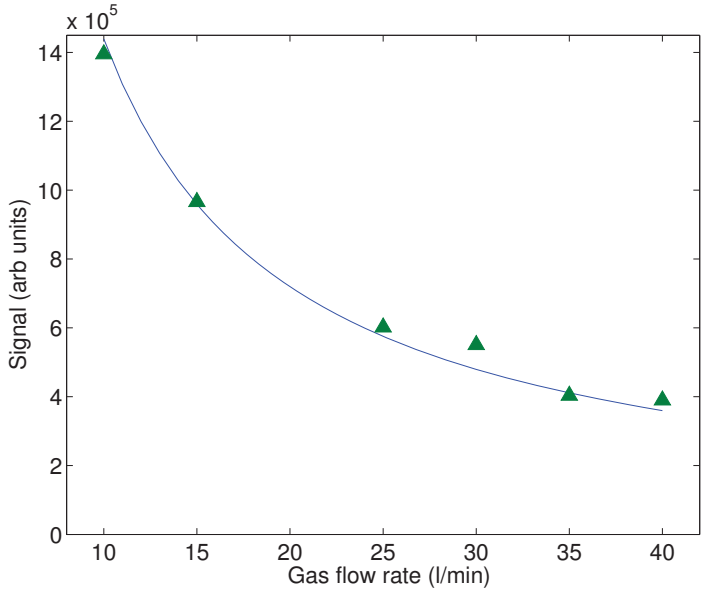

Figure 5.1: Accumulated intensity from scattered image relative to gas flow rate

In this experiment the welding variables were set up to produce a constant fume

formation rate. Gas flow rate can alter arc stability and fume formation. Attempting to minimise this the welding voltage was set up to produce dip transfer which has a short arc length and arcing time. The primary fume mechanism is from droplet neck rupture which should not be altered by shielding gas flow. An additional benefit is dip transfer has relatively low heat input. Neglecting any thermally driven effects the fume concentration immediately adjacent the welding arc is then the amount of fume divided by the dilution from the shielding gas. Indeed this is what is found in Figure 5.1 where the experimental signal is in good correlation with a fitted inverse relationship, Equation 5.1.

$$SignalAU = \frac{14.4 \times 10^6}{GFR} \tag{5.1}$$

The 14.4×10^6 in this case being a constant resulting the signal detected at the camera rather then a meaningful fume quantity. This correlation between experimental results and dilution would suggest that the signal is proportional to the particulate concentration even very close to the welding arc where the particulate density is highest. Therefore both theoretical and experimental evidence supports that the intensity of scatter light from a cloud of fume particles is a multiple of that from a single particle of mean equivalent scattering potential.

5.2.1.5 Particulate concentration

Since there is both theoretical and experimental evidence that the total scattered light is a multiple of that from a single particle then actual intensity of light $\Im_{sca,total}$ at the detector scattered by N particles can be described by the equation.

$$\Im_{sca,total} = \frac{N}{k^2 r^2} F(\theta, \phi) I_0 \tag{5.2}$$

Where $k = \frac{2\pi}{\lambda}$, r is the distance between the scattering source and the detector, $F(\theta, \phi)$ is the mean scattering function of the particles and I_0 is the illumination intensity. Alternatively the number of particles illuminated N could be expressed as the particulate concentration per unit volume φ multiplied by the volume illuminated V. In the case of images V is the volume illuminated by the laser or a subset thereof. In these experiments the volume illuminated changes in thickness across the image as the laser sheet converges up to the focal point then diverges. However the volume illuminated is counteracted by laser intensity as the laser sheet thickness changes. Equation 5.3 could then be rewritten for the intensity at the detector for a single square $l \times l$ imaged area where $l \ll r$:

$$\Im_{sca,area} = \frac{\varphi l}{k^2 r^2} F(\theta, \phi) P_{0,area} \tag{5.3}$$

Where $P_{0,area}$ is the laser power illuminating the $l \times l$ imaged area. Equation 5.3 could be thought of as the intensity of scattered light at the camera lens that would subsequently fall on a single pixel imaging a $l \times l$ area of illuminated plume. For comparable experimental setups many of these variables become constants. All the scattering experiments were undertaken with the same wavelength as such the wavenumber k is constant for all experiments. Distance between the scattering source and the camera remained constant for comparable experiments. Since the distance was fixed then for a fixed lens focal length the illuminated area detected per pixel is constant. Both laser and detector polarisation were fixed vertical. The camera was always normal to the area illuminated by the light sheet. In these experiments the duration of the pulsed laser was approximately constant and much shorter then the camera exposure time so the mean laser power is proportional to the laser pulse energy. Given a fixed pixel sensitivity then all these constants can be compacted in to one experimental setup constant κ. The pixel signal χ_{pix} in arbitrary units could be expressed by Equation 5.4.

$$\chi_{pix} = \kappa \varphi F() E_{0,area} \tag{5.4}$$

Where φ remains the particulate concentration, $E_{0,area}$ is the light energy illuminating the area imaged by the pixel. Since for a particular experimental setup κ is a constant then the relationship between the signal detected by a camera pixel χ_{pix} and the particulate concentration φ depends on the consistency of illumination energy $E_{0,area}$ and mean particle scattering potential $F()$.

Due to the process by which the laser is formed some variation in individual pulse energy exists. The standard deviation in laser pulse intensity in the experiments was measured to be about 2% of the mean. The energy illuminating the area imaged changed due to mean divergence, profile and extinction. In the case of the larger scattering images divergence was resolved by later correcting for beam height across the image. In the case of the smaller images under the welding torch the sheet height was collimated with the use of a second cylindrical lens negating the need for correction. The sheet varied somewhat in intensity across its height due to the profile of the laser beam from which it was formed. The experiment was constructed so the most uniform part of the sheet passed through the region of interest and the outer portions where power varies significantly were clipped before passing through the plume. It is possible to measure and correct for beam profile but this was not considered feasible with the equipment and experimental time limitations. The intensity of the sheet would have been reduced as it passed through the plume due to beam extinction. As the extinction experiment undertaken in Section 4.5 demonstrated this could result in an intensity reduction in the order of 20%. By assuming that the amount of extinction is relative to the amount of scatter it is possible to undertake further experiments and correction (Abu-Gharbieh et al. 2000). The effect of extinction however is not readily observable on the images

collected. There are obvious occasions where the beam is incident on a large molten spatter particle which fully blocks the beam but these occurrences were a rarity.

Where appropriate if the illumination energy is considered constant then the ability to equate the detected signal to particle concentration depends on how constant the particle scattering function remains. The average scattering potential of the plume is dependent on such things as particle size distribution, composition and agglomeration. At this time there appears to be no published literature on the consistency of the optical properties or even geometry of the fume particles over a range of welding variables. As the fume formation mechanisms change due to droplet transfer mode so should the contribution of each fume mechanism (Albert 1996). However Jenkins et al. (2005) has shown that for GMAW the proportion of fine fume to microsplatter does not change greatly with GMAW parameters. But the process by which this data was obtained was unable to determine size distributions in the fine particle range which makes up the majority of the fume. There is suggestion however that the extent of particle agglomeration is effected by the FFR and welding variables (Jenkins et al. 2005).

It has already been determined with the dilution experiment that the intensity of scatter light from a cloud of fume particles is a multiple of that from a single particle of mean equivalent scattering potential. That is the fume concentration was changed with dilution and the signal trended as predicted. Alternatively this could be thought of as showing that the signal is proportional to concentration for a single welding variable. This is significant as it follows that if the detected signal is proportional to concentration for a single welding variable then, accounting for laser energy, relative fume plume images could be collated. Should an appropriate method be made to calibrate the detected signal then quantitative images of fume plume dispersion should be possible for a single welding variable. But welding is a complex process and the variables are often changed.

With the equipment and time available the only experimental way to investigate if the optical properties of the fume particles changed significantly was to undertake scattering experiments with different welding variables and compare the results to what would be expected from other fume measurements. Due to the lack of fume concentration measurements across a range welding variable the best comparable data was determined to be the FFR from Quimby & Ulrich (1999). However the intensity of scattered laser light results from the particulate concentration in a particular region rather then the actual formation rate. To equate the laser scattering signal to the FFR from Quimby & Ulrich (1999) the assumption needs to be made that the plume flux through the imaged area is unchanged. That is the volumetric flow rate of the plume remains constant and that the increased FFR relates directly to the increase of particulate concentration. Close to the welding torch where the plume is dominated by shielding gas momentum this seems to be a reasonable assumption. From the laser scattering images dilution from the ambient air would appear negligible in the

boundary layer on the drum up to the point of radial jet detachment. Also being momentum dominated the plume buoyancy has minimal effect on plume flux. Plume flux could be slightly altered by thermal expansion of the gas due to different welding heat inputs. But the increase in plume flux is cancelled by the increase in dilution from gas expansion caused by the same thermal mechanism. For these reasons, for a fixed gas flow rate, there is a strong link between FFR and particulate concentration in the radial impinging jet and the two measurements can be compared.

Figure 5.2 displays the FFR results by Quimby & Ulrich (1999) and the intensity of scattered laser light close to the welding torch as detailed in Section 4.3.3.1. Due to unavoidable differences in welding variables and method of voltage measurement the laser scatter intensity results have been shifted horizontally so that the peak expected due to globular droplet transfer matches that found in the FFR measurements. The laser scatter results possess arbitrary units but have been scaled vertically so that the peak value of the 4.5m/min wire feed rate due to globular transfer is similar to that of the quantified FFR measurement by Quimby and Ulrich.

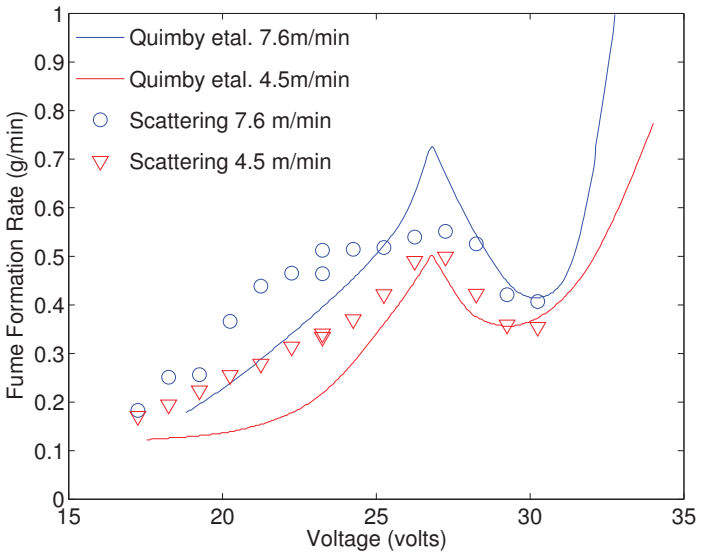

Figure 5.2: Scattering results scaled to trend found by Quimby & Ulrich (1999)

Given the complexity of the welding process and unavoidable differences in experimental set up, the plot shows surprisingly good correlation between the methods. Indeed the consistency of trend in the scatter intensity is better than that of the raw FFR measurements from which the lines displayed in Figure 5.2 were created by Quimby & Ulrich (1999). There is no obvious variation in scattering trend that could be related to any change in particulate optical properties from the different transfer modes. That is that the trend in the concentration does not depart significantly from the FFR as may occur if a large change in the bulk particle optical properties for different transfer modes existed. This would suggest that the optical properties of the fume particles remain reasonably constant across droplet transfer modes for a particular process. Further evidence that the optical properties of GMAW fume remain

reasonably constant can also be inferred from the filter matting collected during the fume box measurements. The discolouration of the filter matting visually appears to correlate with the mass increase of the filter. This would suggest that discolouration, an optical effect, was related to the amount of fume but the optical properties of the fume did not significantly alter.

Absent of any actual measurements of the optical properties of welding fume, given the above experimental evidence, the assumption that optical properties remained constant across droplet transfer modes would appear valid. If the optical properties of the fume can be considered constant then the intensity of scattered light can be used as a relative measurement of particulate concentration.

Equation 5.4 can be rewritten in form of Equation 5.5.

$$\varphi = \frac{\chi_{pix}}{\kappa F() E_{0,area}} \tag{5.5}$$

Given the consistency of illumination $E_{0,area}$, the sensitivity of the camera κ for a particular experimental set up and the mean particle scattering potential $F()$, these factors could be combined into a single constant. Therefor the particulate concentration φ is equal to the pixel intensity χ_{pix} by way of a single calibration factor Υ.

$$\varphi = \Upsilon \chi_{pix} \tag{5.6}$$

5.2.1.6 Application

The images obtained demonstrate the usefulness of laser scattering for visualisation of plume distribution. The intensity and the narrow spectrum of the laser scatter allow for very good back ground suppression and plume visualisation even near the arc. Laser illumination in this case was used to image the plume directly beneath the welding torch along with a larger region above it. However given the space and correct optics, larger or smaller regions could be imaged. In this case a pulsed laser was used limiting the imaging rate to 10 frames per second. However a continuous wavelength laser and high speed camera could be used to collect images at a much higher speed. Laser scattering is therefore a relatively simple and flexible method for obtaining plume images from actual welding processes.

In addition to imaging the extent of the plume, evidence suggests that the intensity of the detected laser scatter is proportional to the particulate fume concentration in certain situations. This technique therefore can be used to generate relative particulate fume concentration images. This is significant as the fume concentration in the operators breathing zone is what would be inhaled. Concentration at the breathing zone is therefore more closely linked to welder exposure than FFR determined by more traditional methods such as fume collection with fume boxes.

The intensity of laser scatter is proportional to particulate fume concentration. However in regions where volumetric flow rate of the plume is constant laser scattering could be used to gauge relative FFR, as demonstrated above. While this would not provide quantified FFR, like a fume box would, laser scattering provides a number of potential advantages. The primary advantage would be the speed at which measurements could be made without the need to weld for a sufficient period of time to collect a weighable amount of fume on the filter material. Laser scattering also does not require the time consuming handling and weighing of filter material.

Measuring the laser scatter from fume close to the welding arc minimises the time between formation and detection allowing for relatively high temporal resolution.

In the experiments undertaken here a sheet of light was used to obtain cross sectional images. If the primary intent was for use to determine relative FFR a wider sheet or beam could be considered desirable as it would illuminate a larger proportion of the entire particulate formation.

5.2.2 LII

Laser induced incandescence has become increasingly popular for the measurement of soot in flames. This is primarily since for particles in the Rayleigh regime the signal obtained can be proportional to the volume fraction of the soot. It is particularly popular as both point measurements soot concentration images can be measured.

The principle behind LII is that the particle is heated by the energy absorbed from the incident laser beam. The heated particle then radiates energy to return to thermal equilibrium. The ability for the LII to be proportional to soot volume fraction arises since the laser absorption and within reason the resulting incandescence emission occurs volumetrically for particles in the Rayleigh regime. This is critical in soot measurement as the soot nucleates, grows, agglomerates and typically burns off. Resultantly the diameter of the soot particle is not constant and dependent on location in the flame.

5.2.2.1 Rayleigh approximation

For incident light to be absorbed volumetrically by the particle it needs to be sufficiently small relative to the laser wavelength that Rayleigh approximation is adequate. The infrared $1064nm$ fundamental beam from the Nd:YAG laser was used to improve the approximation. As in the case of Rayleigh consideration for scattering primary particle diameter will be said to be $\sim 0.1\mu m$ with minimal or chain like agglomeration. The refractive index will once again be that obtained from (Charalampopoulos & Shu 2003) for flame formed Iron oxide particles $m = 1.96i+0.2$. Then for the $1064nm$ wave length used:

$$x = \frac{\pi 100}{1064} = 0.3$$

$$x\,|m-1| = 0.3\,|1.96i + 0.2 - 1| = 0.63$$

The wavelength used for the LII is double that used for the scattering and results in half the particle parameter x for the same particle. Consequently $x\,|m-1|$ is also halved and now less than 1. Conditional on the assumptions about particle size and refractive index the use of a longer wavelength has improved the appropriateness of Rayleigh approximation to a point where it could at least be considered.

5.2.2.2 Laser induced emission

The success of LII depends on several different factors. One of these factors being that the signal detected is particle incandescence and not originating from numerous other sources of laser induced emission (LIE) that are unrelated to particle volume. These include direct laser scattering, emission from ambient gases, electronically excited vaporisation products and chemiluminescence from recombining vaporised products (Vander Wal et al. 1999). It is stated by Vander Wal et al. (1999) that to distinguish these LIE processes from each other and from particle incandescence requires spectral and temporal characterisation. Neither a monochromator or temporal sampling equipment was available for the work presented here. Even if such equipment was available, such fundamental research of incandescence would most likely require a more constant fume source then that offered by the welding setup used.

Vander Wal et al. (1999) found a complex spectrum of LIE from a laboratory setup producing relatively fine pure metal particles in a high pressure inert Helium environment. In the case of the welding plume environment there are a large number of elements and molecules originating from the weld metal, shielding gas and atmosphere. The likely result is a LIE spectrum several orders of magnitude more complex then that for the pure metal particles. This being the case even with a full complement of equipment it may not be possible to separate LII from other LIE in an experiment upon welding fume.

The measurements performed as part of this work were taken to reduce obvious likely sources of LIE not related to LII where possible. The detection of the signal was delayed from the laser pulse to avoid detecting laser scatter. But delaying detection of the emission means that particle heat loss from vaporisation and conduction becomes more significant and the incandescence signal less related to the volumetric energy absorbed by the particle (Bladh & Bengtsson 2004, Will et al. 1998). The likelihood

of detecting laser scatter should have also been minimised by the low sensitivity of the camera to infrared light.

In the delayed spectra by Vander Wal et al. (1999) the Iron particles present a reasonably constant emission indicative of LII in the visible wavelengths above 400nm. As a result orange and red filters were used here for spectral filtering. With these in place it is still not possible to guarantee that the signal is LII as the spectrum for all the other elements and molecules in the welding plume is unknown. Resultantly signal detected in the red or orange could still be long lived emission from any number of reactions. Further discussion of LII must be made in the knowledge that other LIE can not be discounted.

5.2.2.3 Background suppression

Figure 5.3 displays an image captured by the ICCD camera. In addition to the strip 30mm high strip of LIE 130mm above the welding arc it also displays that other optical emissions completely unrelated to the laser were detected. Direct light from the arc was blocked from entering the camera with a metal guard running on the drum surface close to the arc. However arc light was still detected being reflected by particles in the fume plume. Light was also detected from the natural incandescence of splatter ejected from the arc.

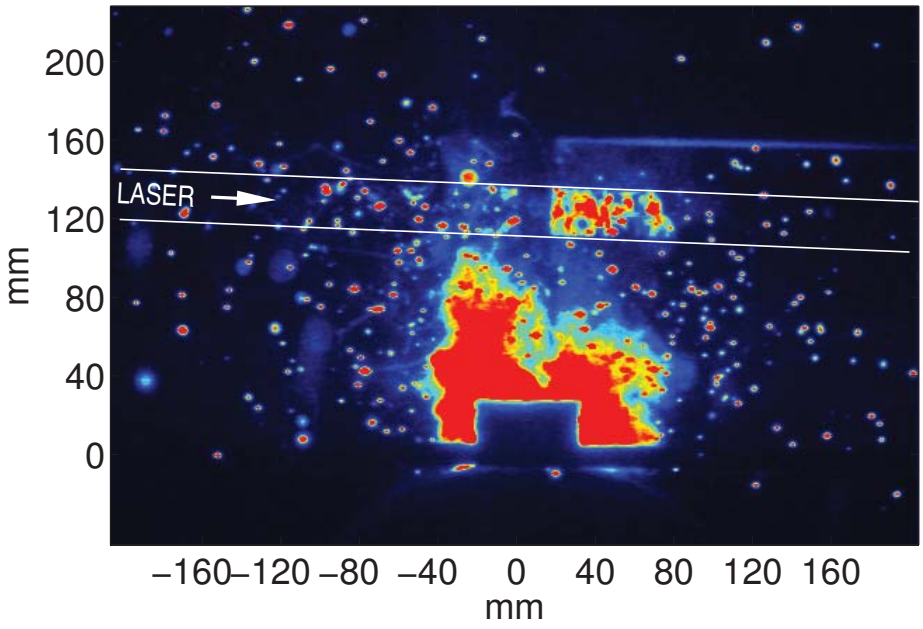

Figure 5.3: ICCD image of LIE and background light

Optical emissions are also encountered in flames primarily arising from soot incandescence due to natural flame temperatures. Laser induced heating of soot however increases particles to temperatures in excess of that naturally found. Resultantly the radiant heat spectrum is blue shifted compared to the natural incandescence of the flame which can then be removed with optical filters. In the

welding case the emission from the arc has a very wide emission spectrum. For this reason it is hard to filter the arc emission from the LII which has an unknown but probably reasonably wide spectrum. Indeed the LIE and background intensity detected from three different optical filters presented in Figure 4.27 is for the most part relative to the transmission of the background Figure 4.26. This suggests that in the welding case where the background optical emission is very wide spectral filtering is less effective than in the case of soot in flames. This is contrary to scattering where the spectrum is known, narrow and, in the case of the 532nm illumination, in part of the spectrum with low arc emission.

Unlike in the case of laser scattering laser power can not simply be increased to improve LII signal strength. This is because LII is non linear with power and indeed increases in laser power may increase vaporisation to such a point the radiant emission from the particles is reduced.

Background incandescence from the welding splatter could be reduced by altering welding variables. But the experiments undertaken here found that variables with less splatter usually involved hight voltages and longer arc lengths. This in turn increased optical emissions from the arc and the background from light reflected off particles.

In this case the background was reduced by sampling higher up in the fume plume where arc illumination of the plume was lower. Reductions in background illumination were traded off with reduced particulate concentration and LIE signal in determining the height at which to sample.

5.2.2.4 Fluence

Another critical factor in the application of LII is laser fluence. This laser radiance heats the particles to induce the incandescence. However particle heat loss is done not only via incandescence but also via conduction and vaporisation. Increased heat input increases particle vaporisation and mass loss. The particles can only be heated so far until the laser incandescence is reduced by the mass loss caused by vaporisation. So excessive vaporisation decreases LII and increases the potential for emission from recombining vaporised products. This problem is more significant in metal particles which have lower boiling temperatures then soot. The problem is further exacerbated in atmospheres containing oxygen where oxygen assisted vaporisation occurs.

To determine the laser fluence at which increased vaporisation outweighs any increase in incandescence the LII signal strength is plotted relative to laser intensity. Such a plot is displayed in Figure 5.4 obtained from separate weld runs at different laser intensities. The maximum signal occurred at about 400mJ per pulse. Above this energy the amount of light detected by the camera decreased with increasing energy.

The effect of particle vaporisation is evident in laser scattering images taken shortly after the IR laser pulse used for LII such as displayed in Figure 4.32. This demonstrates

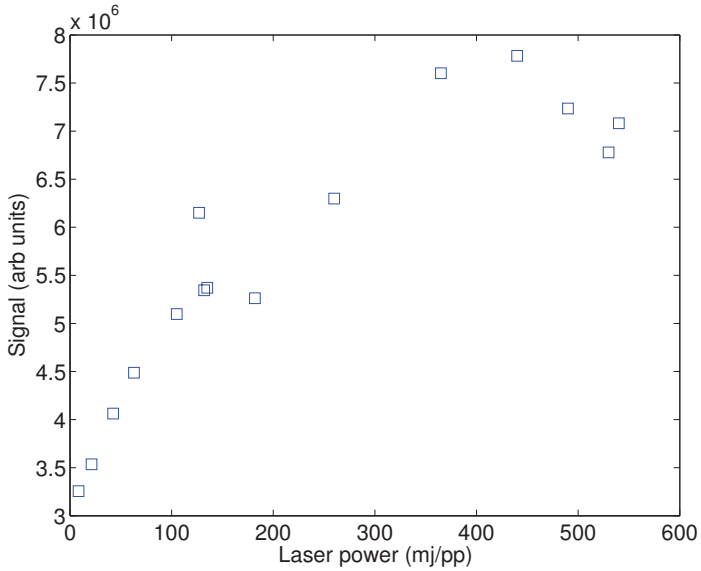

Figure 5.4: LII fluence curve

that the IR laser pulse of 520mJ was capable of vaporising the particles to the extent they can not be detected with laser scattering. This vaporisation effect is also evident at lower laser powers. Curiously while the scattered image shows that the vaporisation induced mass loss is very significant the fluence curve in Figure 5.4 shows that LII is still evident at this IR laser power.

Three different optical filters were used to investigate the spectrum of the signal being detected by the camera. These three filters passed red, orange and all visible light as shown in Figure 4.25. It is clearly the case that the visible filter transmits more background light than that of the red and the orange filters. This is due to the wider spectrum transmitted by this filter and the high arc emission in the blue. This visible filter is intended to block UV light to which this camera system is particularly sensitive. The red and orange filters should block both the shorter portions of the spectrum and only transmit the longer portions where the LII is meant to be most evident. Figure 4.27 displays fluence curves recorded for each of the three filters. Each filter has a similar trend separated by the arc background transmitted by each filter.

5.2.2.5 Concentration

In the case of laser scattering a comparison was made between the detected signal and the FFR measurements by Quimby & Ulrich (1999), Figure 5.2. In the case of LII this is not possible as the sampling can not be taken in the radial jet region near the welding arc due to the intensity of the background. The LII could only be collected in the thermally buoyant plume. Since the plume flux in this region is not constant a link between particulate concentration and FFR can not be made. Regardless LII was undertaken for the same welding variables as used previously for the laser scattering.

Figure 5.5 displays the LII from a region in the plume for two different wire feed speeds

and welding voltages. Each point on the plot represents the average intensity from 50 LII images collected at each welding variable. Unlike the equivalent scattering plot, Figure 5.2, no distinctive trend can be identified and variation between data points is significant. Its not possible to determine if this is due to the LII technique or the fact the laser is only interacting with a very small portion of the plume in an area where the plume flux is constantly changing. That said laser extinction along the same path of the same welding variables did demonstrate a generally more consistent trend with that expected from the FFR, Figure 4.31.

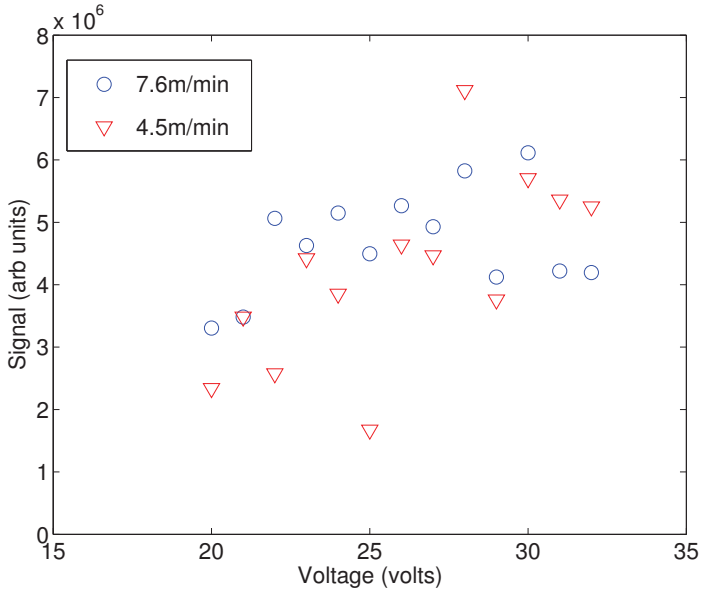

Figure 5.5: LII signal intensity for different voltages and wire feed speeds

5.2.2.6 Application

Given the success of laser scattering as an applied welding fume measurement technique LII is not particularly attractive. Combustion research considers LII potentially useful for generating relative concentration images of soot as the particulate size changes within the flame. That is different areas of a flame may have different sized particles and different concentrations at any particular instant. But welding fume particles entrained in the plume are well mixed, not changing in size and therefore probably have a uniform size distribution at any particular point in the plume. This being the case then fume plumes do not have the same requirement for LII to obtain relative particulate concentration images as exists for soot images in flames. As the optical properties of the fume particles are uniform in all regions of the plume then laser scattering is a valid method for obtaining relative concentration images.

Background light suppression is less effective for welding than it is in flames. In flames LII signal from soot is blue shifted relative to the natural emission. In the case of welding the intense light emitted from the arc has a very wide spectrum making it difficult to spectrally separate from the LII. In the experiments undertaken here the

background light from the arc was minimised by sampling well above the arc. Arc light however could be eliminated by extinguishing the welding arc during the LII sampling period. Given the short duration of the LII sampling this could be achieved with negligible impact on the welding process but would require a special or modified welding power supply. Temporarily extinguishing the arc however will not reduce the background light emitted from the natural incandescence of ejected welding splatter.

The application of LII to soot is more appropriate as the composition of the soot, primarily carbon, remains constant. In the case of welding fume the composition, including level of oxidisation, potentially could change with welding variables. This may result in a changed spectrum, power dependence and other optical properties. To quantify the LII signal for a particular welding variable, given that particle size is constant across the imaged area, quantification of laser scatter would be just, if not more, viable.

Given the complex composition of the welding plume without continuous spectral analysis it is difficult to attribute the detected light to LII and not to other long lived LIE. Delaying the LII detection may reduce the chances that LIE is detected but it also results in a less intense LII signal which is dependent on vaporisation and conduction heat loss. Due to the lower boiling point of the fume particles compared to soot the effect of vaporisation induced mass loss becomes more significant. In addition to this oxygen assisted vaporisation of the fume particle makes the quantity of vaporisation and therefore LII signal dependent on particle oxidisation and surrounding atmosphere composition important. Both of these factors in turn make laser power more critical and analysis of the LII more difficult.

Detection and analysis of LII from welding fume is more difficult than that performed on soot. Also since the welding fume particle size distribution would appear constant the benefits of LII over laser scattering is less than that for soot. As a technique LII is more difficult than laser scattering primarily due to the dependence on laser power, particle vaporisation, thermal conduction and the potential of LIE. Resultantly given the increased complexity, cost and lack of requirement, it would be hard to justify LII over laser scattering for plume imaging.

In addition to particulate concentration, LII can theoretically be used for other measurements such as particle sizing. Given that fume particles in the plume are relatively stable it would be hard to justify the complexity of LII over traditional methods of sampling and sizing.

5.2.3 Extinction

The aim of the extinction experiments was to investigate how the laser beam would interact with the fume plume and determine the mean concentration of particulate

matter. In combustion this technique is combined with the optical properties of soot to quantify the average soot volume fraction along the path of the laser beam.

The extinction experiment, as outlined in Section 3.8, utilised less expensive equipment then LII and scattering as it did not require a high power laser or imaging equipment. The laser used in this experiment was a Helium Neon producing a continuous beam of light at 632.8nm. The laser intensity pre and post passing through the plume was detected with photodiodes and the resulting voltage signal recorded on a computer.

5.2.3.1 Rayleigh approximation

The determination of mean particulate concentration from extinction measurements with a simplified equation requires the application of Rayleigh approximation. This means that the particles need to be sufficiently small relative to the laser wavelength that Rayleigh approximation is adequate. As has been done previously the upper primary particle diameter of the fine fume will be assume as $\sim 0.1\mu m$ with a refractive index obtained from (Charalampopoulos & Shu 2003) for flame formed Iron oxide particles $m = 1.96i + 0.2$. Then for the $632.8nm$ wave length from the HeNe:

$$x = \frac{\pi 100}{632.8} = 0.496$$

$$x\,|m-1| = 0.496\,|1.96i + 0.2 - 1| = 1.051$$

The wavelength and therefore the resulting particle parameter x is between that found for the laser scattering and LII. Ideally for Rayleigh approximation both the particle parameter x and $x\,|m-1|$would be much less then one for good correlation. In this case $x\,|m-1|$ is in the order of 1 for the assumed optical properties and particle geometry. For the traditional application to soot in the size parameter x approaches 1 in some flames. In these cases a correction factor is used based on the calculated departure of the Rayleigh approximation from the expected Mie solution to obtain a more accurate quantified particulate concentration (Kent & Bastin 1984). In the case of welding fumes such correction factors do not exist so concentration can only be determined with base accuracy.

5.2.3.2 Back light suppression

As with the other laser techniques arc light countermeasures were required. Being the measurement of a direct laser beam the extinction optical signal is relatively strong in comparison to the LII and laser scatter signals. This makes the effect of the background light less significant particularly since it was possible to direct the laser beams so that

the detectors were located away from direct arc light. The effect of the background light from the arc was further accounted for by modulating the beam at the exit of the laser. In this way the modulated signal could be differentiated from the arc light. While the arc light is to some extent modulated by droplet transfer through the arc as it was not synchronised with the acquisition of the data the average result over the the collection period would have been near constant. Examination of the recorded data such as Figure 4.29 show that modulating the beam was sufficient to differentiate the laser from the background light. Indeed it was noted that the offset of the signal increased with increasing arc light. However the peak to peak remained constant when the beam was not passed through the plume. These background countermeasures are the same as those used when this technique is used to measure soot in flames.

5.2.3.3 Concentration

The results displayed in Section 4.5 showed that up to 20% of the beam was extinguished along its path through the plume. This has significant relevance to the application of laser techniques as outlined in the application of laser scattering. Such measurements also have some direct applications in determining the attenuation of light generated by the arc. This would be of some interest when investigating the penetration of UV light, responsible for ozone formation, into the welding environment. However these extinction percentages alone proved little information about the fume plume concentration. Applications of this technique in combustion considers a derivation from Rayleigh theory to determine mean soot volume fraction υ (Kent & Bastin 1984, Kent et al. 1981, Santoro et al. 1983).

$$\upsilon = \frac{-\lambda}{6\pi \times imag\left(\frac{m^2-1}{m^2+2}\right)} \times \frac{ln\left(\frac{I_0}{I_t}\right)}{L} \tag{5.7}$$

Where I_0 is the corrected reference beam intensity and I_t is the transmitted beam intensity after passing through the flame, $\lambda$is the wavelength of laser, m is the complex refractive index of the soot particles and L is the path length through the flame. The same equation will be used here to determine mean fume concentration through the plume.

In the welding situation the intensities I_0 and I_t were obtained from corrected photodiode measurements before and after the beam passed through the plume respectively. The wave length of the laser used in the experiments here was constant 632.8nm. The refractive index m of the particles will be assumed to be $m = 1.96i + 0.2$ (Charalampopoulos & Shu 2003). Determining beam path length L through the plume however is difficult. The average path length through the fume plume can be approximated from the laser scattering images. This measurement is quite subjective due to the non homogeneous structure of the fume plume. However if the mean

particulate concentration obtained from extinction is to be used as calibration then the length imaged can be used. In this case as long as the entire intersection length through the plume is imaged then the the path length of the extinction can be set as the length of the imaged area. The average particle volume fraction obtained with this path length then can be equated to the average imaged signal along the same path to quantify the image.

The main application of extinction would be to measure the volumetric fume concentration. To assess the capability of laser extinction, as in the case of the laser scattering, due to the lack of fume concentration measurements across a range of welding variables the best comparable data was determined to be the FFR from Quimby & Ulrich (1999). But to make a comparison the volumetric fume concentration in the plume needs to be converted to a rate of formation. This was undertaken by determining the mean particulate fume volume fraction υ from extinction measurements with Equation 5.7. The fume volume fraction was then multiplied by the volumetric plume flux to obtain the total volume of particulates which was then multiplied by the density of iron oxide ρ to obtain a mass formation rate.

$$FFR = \upsilon u \frac{\pi L^2}{4} \rho \tag{5.8}$$

The plume flux was determined from the approximate velocity u and path length L of the extinction. Approximate vertical fume rise was determined to be 60mm in one tenth of a second from sequential images such as those in Subsection 4.3.2.4 giving a plume velocity of 0.6m/s. The extinction path length and plume diameter was determined to be about to be 80mm at the height of the extinction measurement.

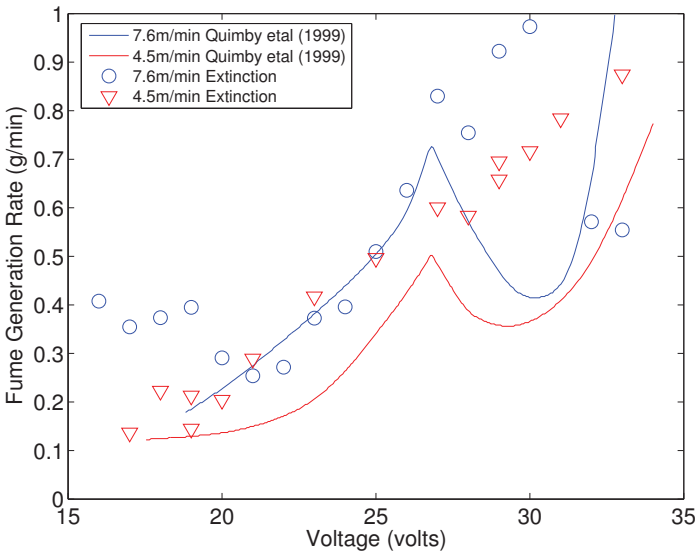

Figure 5.6: Calculated GMAW FFR from extinction versus that found by Quimby & Ulrich (1999)

Figure 5.6 displays the FFR calculated from the extinction and that measured by Quimby & Ulrich (1999) for a similar GMAW process. Given the approximate cross section and velocity no account has been made for the change in the plume properties with welding variables. The welding variables with higher heat input would likely have higher volumetric plume flux resulting from increased heating and buoyancy. The difference in buoyancy between the two wire feed rates in Figure 5.6 if taken into account would probably cause the 7.6m/min FFR to be slightly higher then the 4.5m/min FFR. Figure 5.6 demonstrates a characteristic change in FFR with droplet transfer mode for the 7.6m/min electrode feed speed which is not evident in the for the 4.5m/min. This is similar to the fume box measurements undertaken for this welding process displayed in Figure 4.37. Once again considering all the variables involved the correlation between the experimental results obtained here and those of Quimby and Ulrich is surprising. This gives further confidence that the optical properties of the plume particles are not changing significantly. Also since this result is comparing actual FFR with calculated FFR from extinction, rather then just a normalised signal value, the assumed refractive index m obtained from Iron oxide in a flame is fairly reasonable for welding fume.

5.2.3.4 Application

The primary application of laser extinction in this case would be for the calibration of other techniques such as laser scattering. In isolation laser extinction provides little information on the shape or the structure of the plume. However laser extinction would be useful for monitoring of background particulates in a workplace where the distribution is uniform. It would also have applications for monitoring the particulate concentration in ductwork such as those used in fume extraction systems. Laser extinction would also play an important part in experimentally determining the optical properties of fume plumes.

5.2.4 Scattering and LII

Combined measurements were undertaken to investigate the signal relationship between laser scattering and LII for different welding variables. A series of both laser scattering and laser extinction images were collected. The laser scattering image was collected several nanoseconds before the laser beam used to induce incandescence which caused particle mass loss through evaporation. Images were collated and the intensity detected by the cameras for the same plume region plotted. Figure 5.7 displays the signal intensities for four different welding voltages. Each point on each plot representing the the intensity for the region from the cameras collecting the laser scatter and the LII.

In Figure 5.7 the crossing point of the trend lines on the LII signal axis shift right with increasing voltage. This would be due to increasing background light with welding voltage, detected along with the LII.

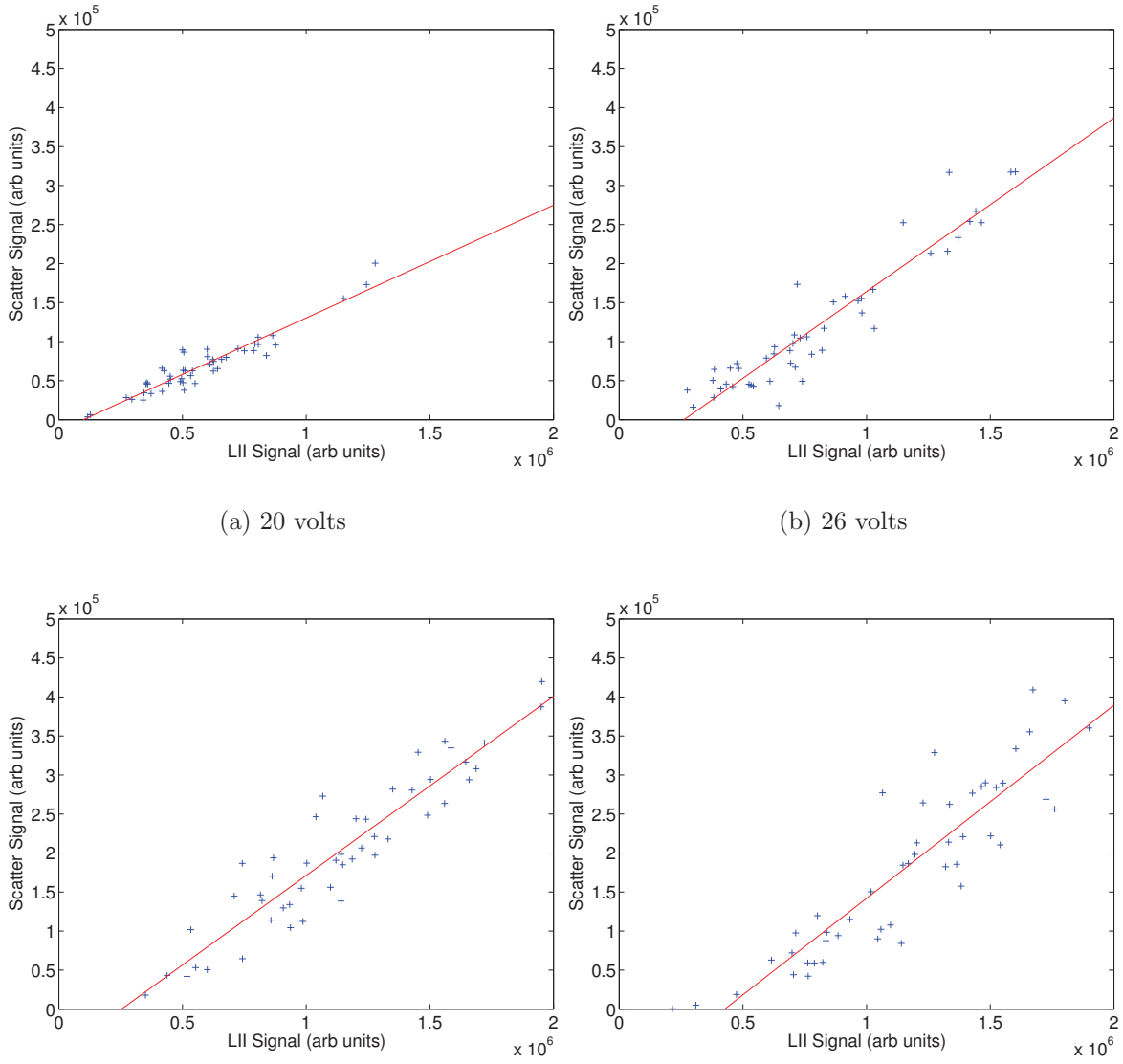

(a) 20 volts

(b) 26 volts

(c) 30 volts

(d) 33 volts

Figure 5.7: Laser scatter intensity versus LII intensity for different welding voltages

In the four plots presented here the trend between the two processes is similar. Since a similar trend exists between the scattering and the LII it would suggest that the optical properties of the particles remain fairly constant across the voltages. Significant changes in optical properties would demonstrate a departure in the relationship between the techniques as each is based on a separate optical process. This further supports the validity of laser scattering for the measurement of welding fume.

5.2.5 Laser extinction calibrated images

In Section 5.2.1.5 it was determined that the laser scatter could provide relative images of particulate fume concentration. However without a calibration reference the images collected with laser scattering only provide relative light intensity. Assuming that laser extinction can indeed be used to determine particle concentration then a calibration

factor can be determined.

Making all the relevant assumptions Equation 5.7 can be used to determine the particulate fume volume fraction from extinction measurements. The path length L can be taken as the width of the scattered image to provide the mean fume volume fraction across the image. A series of laser scatter images for the same welding variables can be averaged and the mean pixel intensity across the image determined. A calibration factor can then be determined by dividing the mean fume volume fraction by the mean image pixel intensity along the same path. This calibration factor can them be multiplied by the image intensity to produce a calibrated particulate fume volume fraction image. The calibration factor can be used as long as the optical configuration remains constant and the optical properties of the fume can be assumed similar.

As a demonstration extinction will be used to calibrate laser scattering images of the base GMAW welding variable Table 4.2. Photodiodes voltages of 4.317V and 3.888V were recorded before and after passing through the plume. The mean particulate fume volume fraction across the image can be calculated using Equation 5.7. In this case the refractive index m was assumed to be $1.96i + 0.2$ the wave length of the laser λ is 632.8nm and the path length L used was the width of the image 0.3m.

$$\upsilon = \frac{-632.8 \times 10^{-9}}{6\pi \times imag\left(\frac{(1.96i+0.2)^2-1}{(1.96i+0.2)^2+2}\right)} \times \frac{ln\left(\frac{4.317}{3.888}\right)}{0.3} \tag{5.9}$$

The mean particulate fume volume fraction υ through the plume 140mm above the arc was calculated to be 173.58 parts per billion. The average of 150 sequential laser scatter images was determined and corrected for beam divergence. Mean pixel intensity χ_{pix} across the image 140mm above the arc was calculated to be 25.11 counts. From the mean particulate fume volume fraction and the mean pixel intensity a calibration factor Υ was determined to be 6.91 parts per billion volume per pixel count.

$$\Upsilon = \frac{\upsilon}{\chi_{pix}} \tag{5.10}$$

This calibration factor was then multiplied by pixel intensity to produce a quantified image. Figures 5.8 and 5.9 present calibrated images of particulate fume distribution for the base GMAW welding variables. The colour scale to the side represents the particulate volume fraction in parts per billion. The matlab code used is included as Appendix E.4.

5.2.6 Summary

Laser scattering as expected proved very successful for imaging the particulate fume plume. While further research is required, the results presented here would suggest that

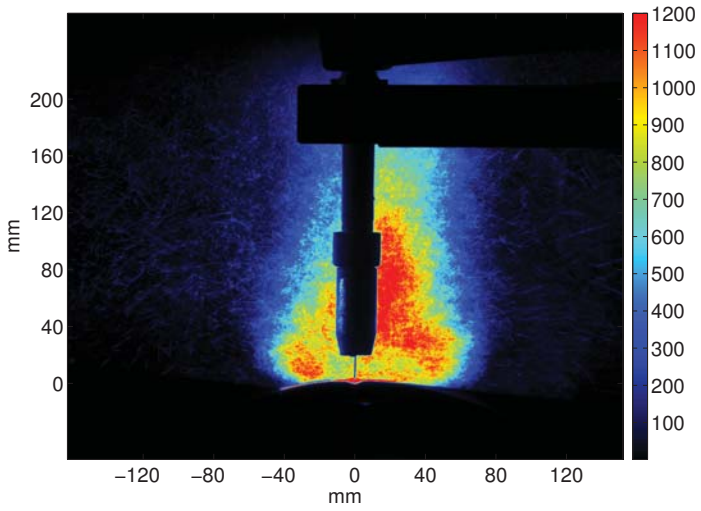

Figure 5.8: Calibrated average laser scatter image for the base welding variables in parts per billion volume

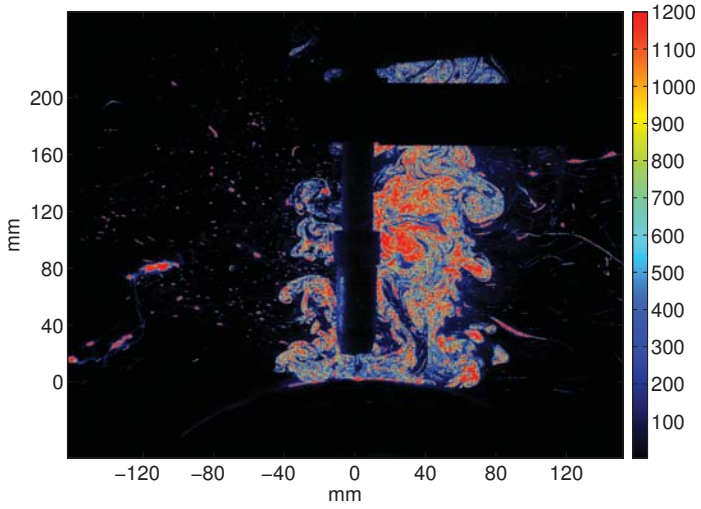

Figure 5.9: Calibrated instantaneous laser scatter image for the base welding variables in parts per billion volume

the optical properties of fume from GMAW remain constant across a range of welding variables. This being the case the intensity of scattered light can be used for a relative fume concentration measurement with acceptable accuracy. With some reference these relative measurements can also be quantified as demonstrated.

Laser Induced Incandescence proved less successful than laser scattering for a number of reasons. One of these reasons was the difficulty to conclusively differentiate LII from LIE and background light. No obvious advantage exists however in undertaking LII if the optical properties of the fume particles remain constant throughout the plume being imaged.

Laser extinction would appear a useful tool for determining fume concentration and as a calibration reference for laser scattering. For this to be conclusive further research is required to determine actual optical properties of welding fume.

5.3 Fume box

Fume box measurements were undertaken as the traditional measurement technique to determine a quantitative FFR from the actual process. These measurements proved relatively simple to undertake compared to laser measurement. The results are also more easily interpreted being the established method and not requiring extensive consideration of the physics behind the measured result.

5.3.1 GMAW

Figure 5.10 displays the FFR measured with the CSIRO fume box versus that measured by Quimby & Ulrich (1999) for a similar welding process. The FFR for the 4.5m/min electrode feed speed measured with the fume box here did not demonstrate the characteristic trend due to expected changes in droplet transfer. However the 7.6m/min electrode feed speed measured here demonstrated a much larger change between the onset of globular transfer at about 27 volts and spray transfer at around 31 volts then that found by Quimby & Ulrich (1999) or the laser scatter measurements. This difference is probably a combination of the multiple variations in the welding variables. The reduction in FFR at spray transfer is most likely due to improved arc stability. This could be as a result of change in power supply characteristics and or electrode feedability.

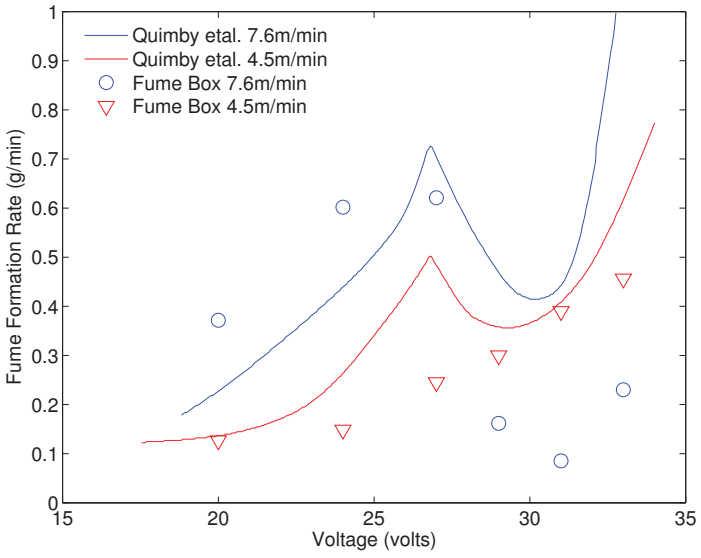

Figure 5.10: Measured FFR of GMAW for different voltages and wire feed speeds

It should also be noticed that while every attempt was made to operate at the same welding variables as used in the laser diagnostics experiments differences did exist. Of particular interest is that for the same welding voltage and wire feed speed setting the measured current was higher for the fume box work than it was for the laser measurements. Initially this was assumed to be due to the change in shielding gas

composition necessitated by the change in facilities. However the increase in current was also evident for unshielded FCAW. The difference therefore could be due to wire feedability, contact tip condition, torch angle or a combination of these. It was certainly the case that due to the extra space available the torch lead was much straighter for the fume box measurements than during the laser measurements. This would have reduced the force necessary to push the electrode along the torch lead and improved wire feedability. What ever the reason for spray transfer during the fume box measurements the arc stability was audibly and visibly smoother than that while undertaking laser measurements. The fume box measurements therefore not only collected qualitative data on the FFR but it also highlighted the sensitivity of the welding process to variable changes including those that are not easily measured.

5.3.2 FCAW

Figure 5.11 displays the FFR measured for FCAW at different shielding gas flow rates. The measurements indicate that the addition shielding gas leads to the slight reduction in FFR. The reduction in FFR with the additional shielding provided by shielding gas has been noted by other research groups. Figure 5.11 also indicates that at unrealistically high shielding gas flow rate the FFR is increased. Presumably this due to additional entrainment of metal vapour from the arc at higher gas flow rates and reduction of arc stability.

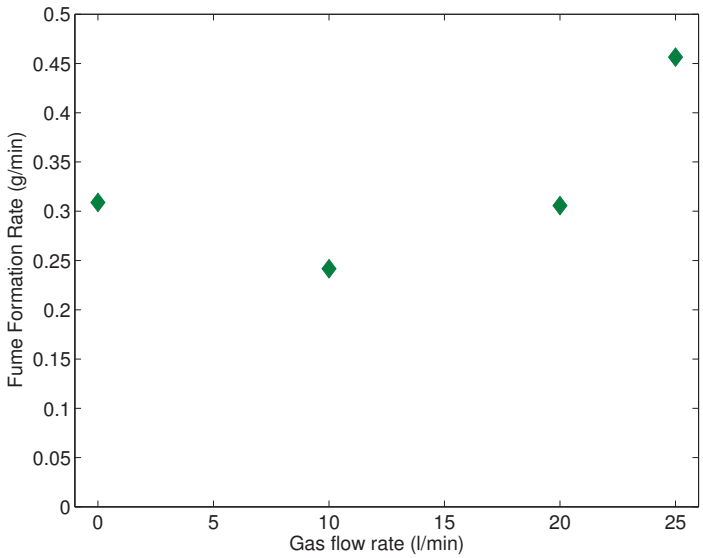

Figure 5.11: Measured FFR of FCAW for different gas flow rates

5.4 Plume dispersion

Previous research into welding fume plume dissipation has involved direct imaging and analogous water models. Direct imaging of plumes is obscured by the lighting of

the plume by the arc. As a result the inner plume structure is obscured by both the intense arc light and the outer fume plume. Water models while sufficient to investigate fundamental fluid dynamics of buoyant impinging jets have limitations arising from their simplification and scaling to represent the welding process. The introduction of liquid to replicate the plume produces a jet and mass transfer at the nozzle. This is a reasonable assumption for GMAW which has the introduction of shielding gas but could not be used to model unshielded FCAW which is a purely thermally driven plume. Water models also assume a homogeneous plume source which is not necessarily the case underneath or very close to the welding torch. Laser scattering provides a way to observe the plume structure from actual welding plumes. This allows for the influence of welding parameter changes on the plume shape to be observed.

Laser scattering images from GMAW collected as part of this work demonstrate plumes structures expected from the previously water modelling, in particular that described by Slater (2004) and Cooper & Hunt (2004). That is a jet of shielding gas that impinges the parent material and spreads radially. At the detachment of the boundary layer the fume rolls upwards and back towards the torch as shown in Figure 5.12. The fume from this roll is periodically released into the buoyant plume and rises into the environment. Slater (2004) investigated a number of plume variables including the radial spread and virtual origin.

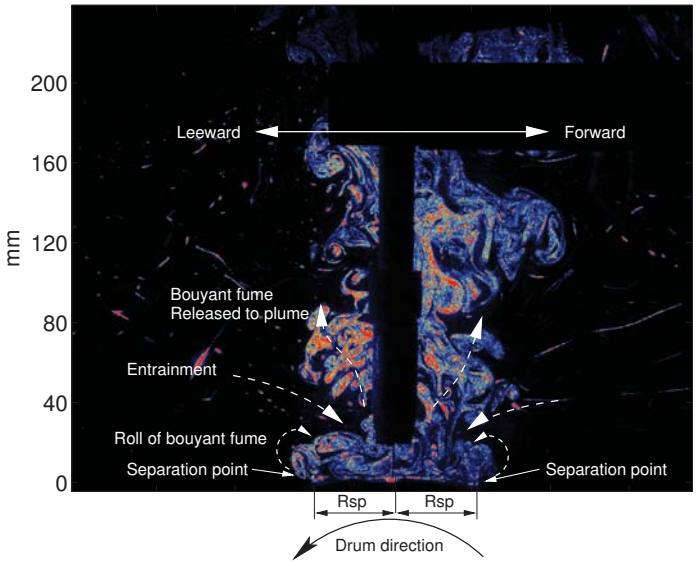

Figure 5.12: Plume features

5.4.1 Radial spread

The radial spread is the distance at which the radial jet boundary layer separates from the parent material. The separation point, and therefore the radial spread, can be directly identified from the laser scatter images. Figure 5.13 displays the radial spread measured from laser scatter images for different gas flow rates depicted in Figure 4.5.

The welding variables are reproduced here as Table 5.1. Since the parent material is moving the radial spread is non symmetric forward and leeward of the welding torch. Separation points at higher gas flow rates were more difficult to identify due to dilution of the fume concentration and increased distance from the welding torch. Further from the welding torch the separation point is not illuminated due to the shape of the laser sheet and the shadow cast by the drum. For this reason the radial spread for the highest gas flow rate of 35l/min is not identified. This would be avoided if the experiment was undertaken with a linear traverse and flat parent material.

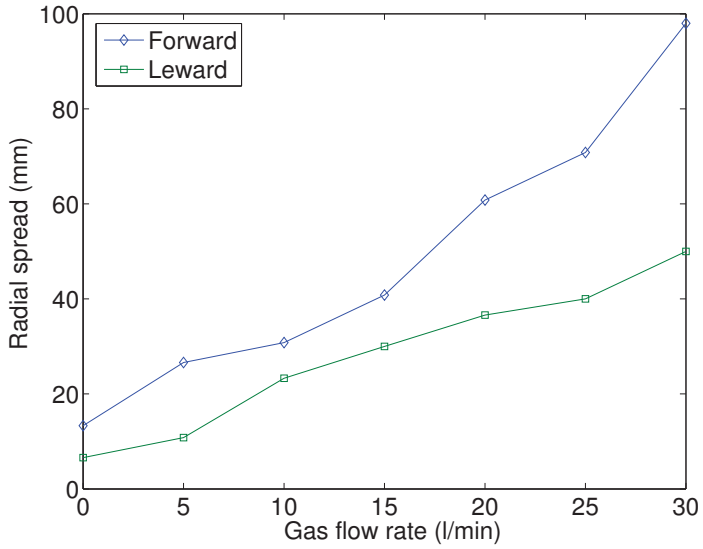

Figure 5.13: Radial spread measured from laser scatter images for different gas flow rates

	GMAW	Units
Electrode Wire	1.2mm ER70S6	
Voltage	26 (DCEP)	Volts
Wire Feed	7.6	m/min
Current	230	Amps
Shielding gas	Ar 81.25, CO_2 16, O_2 2.75	%
Gas Flow rate	0,5,10,15,20,25,30,35	l/min
Weld traverse rate	360	mm/min
Standoff	19	mm

Table 5.1: GMAW variables

From observing a series of images the point of detachment is surprisingly consistent for any particular gas flow and nozzle configuration. Figure 5.13 shows that radial spread increases with gas flow rate as suggested by Slater (2004). Figure 5.13 also demonstrates that the radial spread forward of the torch is greater than that leeward as was suggested by the cold flow modelling done by Johnson et al. (2006). This non symmetry is a result of the parent material having a velocity relative to the welding torch. The parent material movement being counter that of the radial jet flow forward of the welding torch and in the same direction leeward of the torch. Differential velocity between the

shielding gas and the parent material is therefore greater forward of the welding torch than it is in the leeward direction. Since the differential velocity is responsible for the boundary layer attachment, via Coanda effect, the radial jet forward of the torch remains attached for longer due to the higher initial relative velocity. Presumably at the respective points of detachment the differential velocity is similar being that which is insufficient to produce a retention force to counter the buoyancy and tendency for the plume to rise.

Slater (2004) developed an equation for fume plume radial spread from water modelling. This work was discussed in Subsections 2.4.3 and 2.4.4 with the final equation reproduce here as Equation 5.11. Using the welding variables from Table 5.1 the radial spread was calculated numerically and plotted in Figure 5.14. The code used for this calculation is included as Appendix E.5.

$$R_{sp} = \psi l_s \left(1 - \frac{c_2 B_o^{\frac{2}{3}} H^{\frac{4}{3}}}{M_o}\right)^{\frac{3}{4}} \tag{5.11}$$

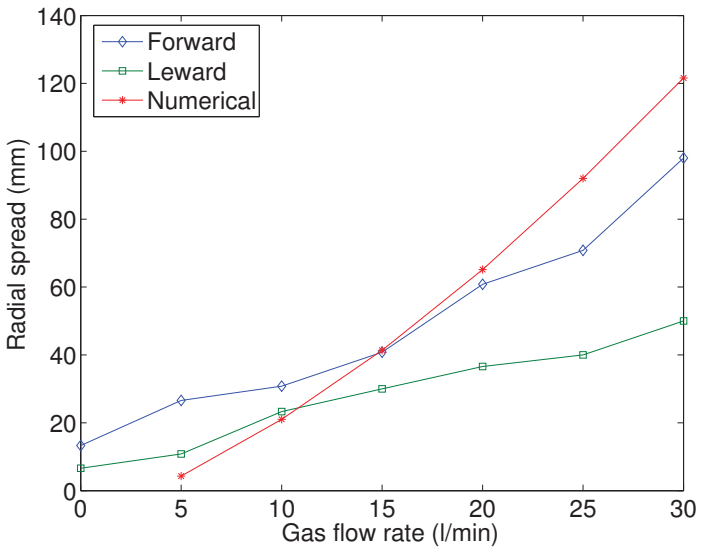

Figure 5.14: Radial spread measured from laser scatter images for different gas flow rates

Given the number of variables involved the equation is quite reasonable but would seem to over exaggerate the influence of shielding gas flow rate.

5.4.2 Plume dispersion

From the work undertaken there is reasonable cause to assume that the laser scatter intensity, when corrected for the vertical divergence of the illumination sheet, is in good correlation with the particulate concentration. This being the case then the scatter can be used to display more than just the extent of the plume but also the particulate concentration changes across the plume. This can be viewed as an image

with a colour map relative to the concentration as has been presented up to now. However it may be clearer to display this concentration as a plot. Figure 5.15b display a plot of relative laser scatter intensity across the plume shown in Figure 5.15a. This was obtained by accumulating the pixel columns from 0mm to 160mm above the drum then normalising with the maximum column. The silhouette produced by the welding torch features predominately as a reduction in intensity about 15mm horizontally either side of the origin.

Pure plumes at any particular height should demonstrate a normal distribution of concentration. While it is hard to statistically determine variables for such a function given the torch silhouette such a proposition would seem valid particularly for the lower shielding gas flow rates. Figure 5.16 displays the distribution across the plume for the different gas flow rates between 0 and 160mm above the arc.

Figure 5.16 demonstrates that increasing the shielding gas flow rate dilutes the plume, reducing the peak particulate concentration while increasing the plume width. The increase in plume width however actually increases the fume concentration at some points further away from the torch at some gas flow rates. This has some significance as far as welding operator exposure. That is while increased shielding gas flow, or other on torch dilution mechanism, decreases the peak particulate concentration the plume is wider making it harder to either avoid or extract.

Interestingly at very high gas flow rates there is a tendency for the plume to tend towards the leeward side of the torch. This is most obvious at the highest gas flow rate of 35l/min where a peak occurs at -80mm and a trough at -50mm. Its not clear why the high gas rates tend leeward when the lower gas flow rates and the cold flow modelling done by Johnson et al. (2006) tended in the forward direction. Potentially this could just be some asymmetry in the gas shroud.

The distribution for the higher gas flow rates would suggest the influence of a boundary layer as the plume rises against the welding torch. At the higher gas flow rates some of the plume is actually expelled beyond the torch boundary layer due to the increased radial spread. This results in the trough at -50mm for the gas flow rate of 35l/min.

5.4.3 Virtual origin

Another plume variable investigated by Slater (2004) was virtual origin, being the distance below the parent material to an imaginary ideal plume point source. Picking such a point directly from the laser scatter images is difficult given uncertainty involved in determining the outer limits of the plume given the turbulent nature. Some of this uncertainty can be removed by looking at the mean plume distribution at two different heights. Figure 5.17 displays normalised laser scatter intensity across the plume at two different heights above the arc for the lowest 6 gas flow rates. The higher shielding gas

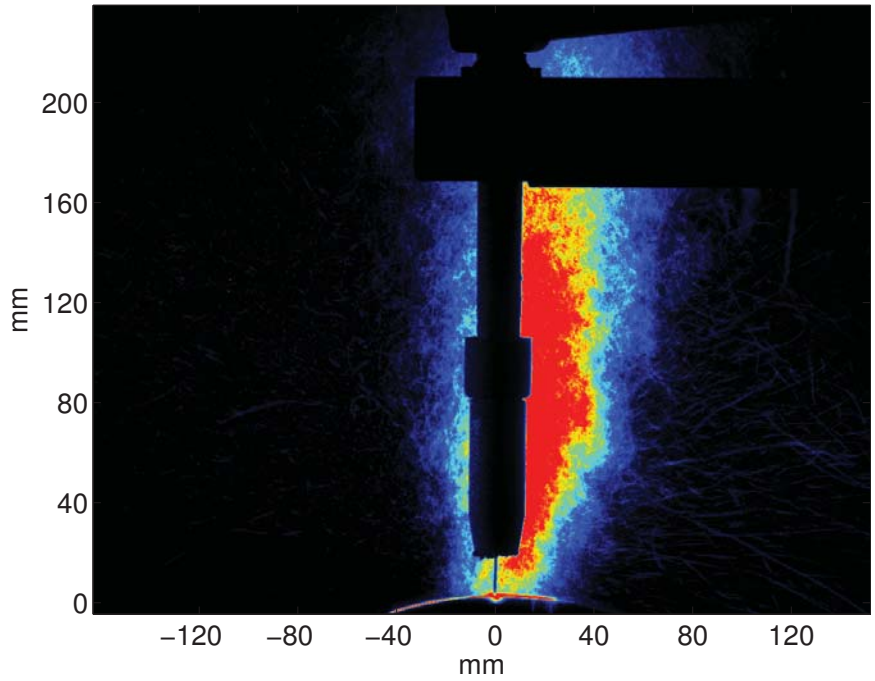

(a) Laser scatter image

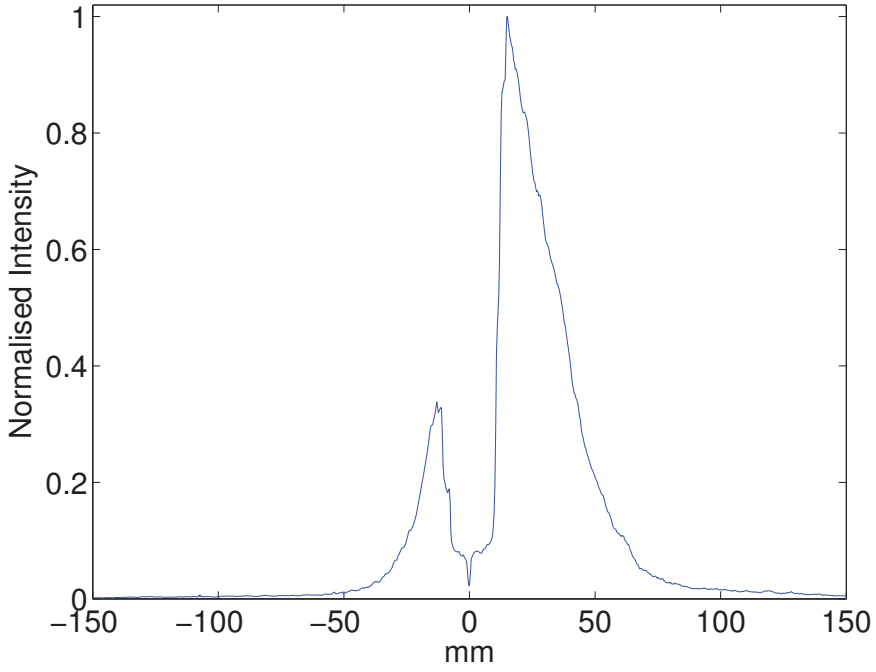

(b) Fume concentration profile

Figure 5.15: Normalised particle concentration profile across the GMAW plume between 0 and 160mm above the arc of no shielding gas flow

flow rates of 25, 30 and 35l/min not exhibiting a Gaussian shaped plume distribution. The lowest distribution was taken at 45mm above the arc to avoid the radial jet caused by impingement.

The extent of the plume for each gas flow rate was taken to be 0.1 of the peak and

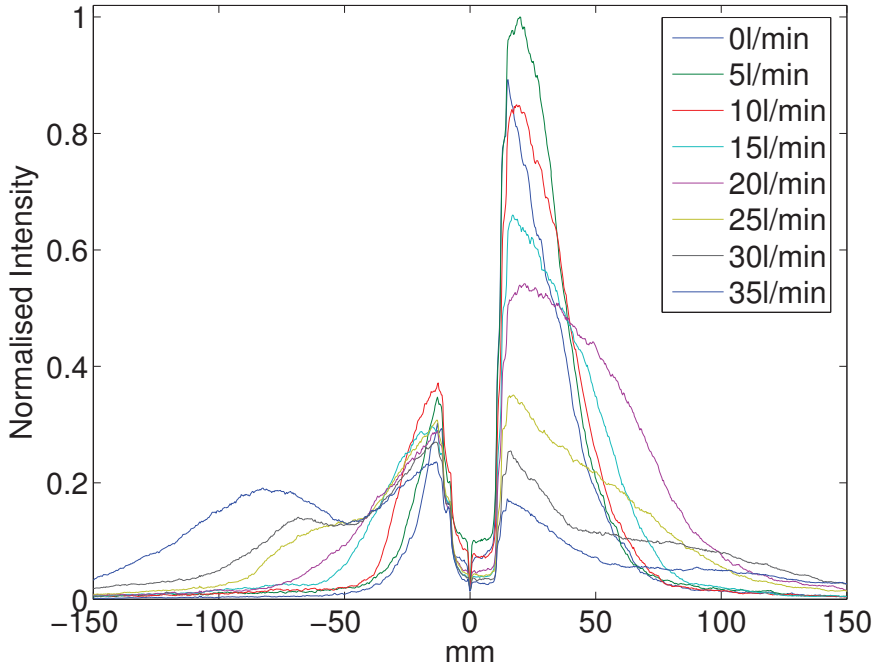

Figure 5.16: Concentration profile across the plume between 0 and 160mm above the arc for eight different gas flow rates

used to determine the plume widths displayed in Table 5.2. Linear extrapolation of the plume widths at the two different heights was used to determine the virtual origin.

Gas flow rate (l/min)	0	5	10	15	20
Plume width at 155mm (mm)	95	94	105	128	161
Plume width at 45mm (mm)	64	77	95	120	179
Entrainment constant α	0.141	0.077	0.046	0.036	-0.082
Virtual origin (mm)	-182	-453	-1000	-1605	+1139

Table 5.2: Plume widths at different heights above the arc for different gas flow rates based on 10% of the peak concentration

As expected increasing the gas flow rate moved the virtual origin further below the arc. However the results would indicate that increasing the gas flow rate decreased the rate of plume divergence represented as the entrainment constant. Indeed at a gas flow rate of 20l/min the plume converges between 45 and 155mm. This could well be related to previously discussed boundary layer along the welding torch. As a comparison using theory Slater (2004) estimated the virtual origin for similar welding variables with a shielding gas flow rate of 15l/min to be -2950mm. The virtual origin in the results obtained here were approximately half that found by Slatter at 15l/min. Unlike the theoretical modelling work undertaken by Slatter there is a number of external factors involved in actual welding. These include air movement both environmental and caused by thermal convection from the heated welding drum. From the data sets collected here is is difficult to determine what influence convection from drum heating had on the plume shape and whether this was responsible for plume collimation.

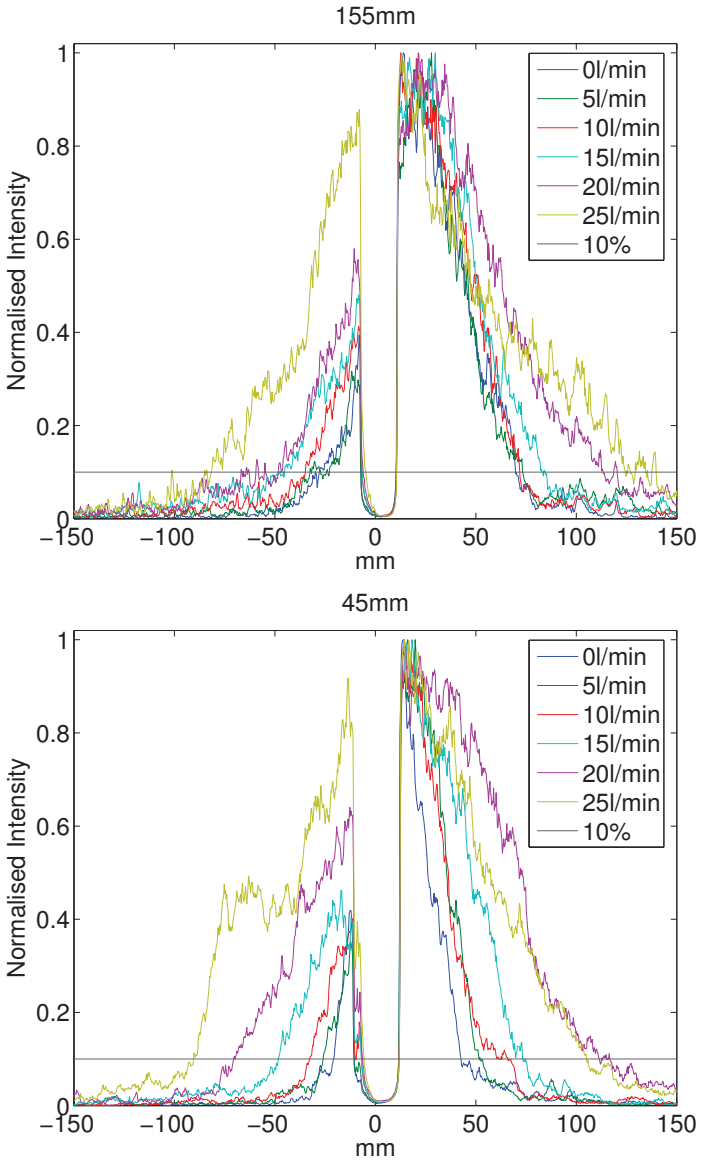

Figure 5.17: Concentration profile across the plume at 45mm and 155mm above the arc for the lowest six gas flow rates

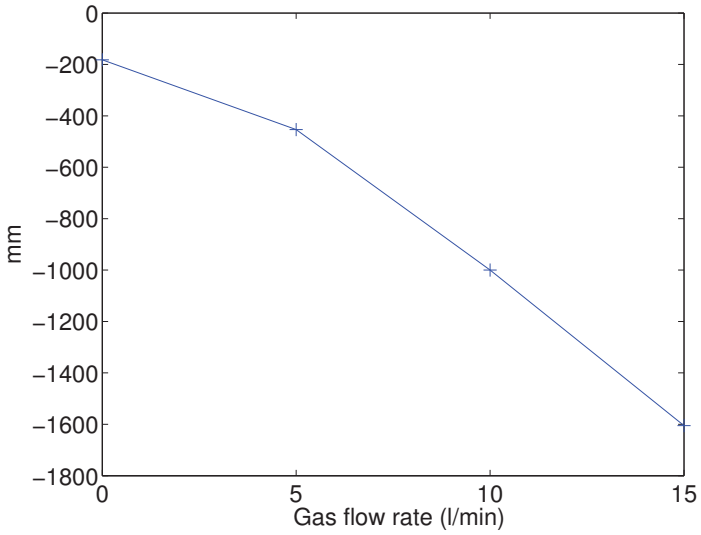

Figure 5.18: Virtual origin for the lowest four gas flow rates

Chapter 6

Conclusions

Several different laser diagnostic techniques were investigated for analysing fume plumes from GMAW and FCAW. The application of these laser techniques to arc welding plumes has not previously been reported in the literature.

Laser scattering was applied to successfully visualise the structure of welding fume plumes from GMAW and FCAW close to the arc. The combination of high laser illumination and optical filtering was found to overcome background light problems experience by other researchers imaging the plume close to the welding arc.

The results indicated that a linear correlation between laser scatter intensity and particulate concentration exists. Laser scattering results from next to the arc were found to agree well with FFR obtained from fume box measurements across dip, globular and spray droplet transfer modes referenced in the literature. Such a relationship makes laser scattering useful for generating images of particulate concentration within the plume in situ.

Laser Induced Incandescence was found not to be appropriate for the imaging of welding plumes. Reasons for this finding include the inability to differentiate the laser incandescence from other other optical emissions, the consistency of the fume size and the apparent success of laser scattering in producing images relative to fume concentration.

Laser extinction is a viable method to quantify particulate fume concentration and calibrate laser scatter images. The best available refractive index from the literature for Iron oxides of similar geometry was used to determine mean particulate volume fraction. The particulate volume fraction was then used to demonstrate how laser scatter images could be calibrated. However further research into the optical properties of fume particulates is required to obtain confidence in any quantitative result.

Fume box measurements were undertaken for GMAW and FCAW to determine actual fume formation rates. Fume formation rate was measured for a range of shielding gas flow values for FCAW. This showed that the addition of shielding gas reduced the FFR

as has been noted by other researchers. High gas flow rates were found to increase FFR above that of the unshielded case. This is presumed to be due to increased entrainment of metal vapour from the arc into the plume and a reduction in arc stability, both of which would result in more fume. The results suggest that an optimum shielding gas flow rate exists which could be used to reduce welder exposure to fume.

Fume box measurements for GMAW were undertaken across a range of voltages at two different wire feed speeds and showed general agreement with results obtained by Quimby & Ulrich (1999). These results demonstrated the complexity and variance found when trying to compare fume formation rates between different methods and research groups. Considering this, fume box measurements, laser scattering, laser extinction and results from the literature showed reasonable agreement.

For fixed traverse rates the radial spread along the parent material surface was found to be dominated by shielding gas flow rate for GMAW. Higher shielding gas flow rates moved the point of radial wall jet detachment further from the welding torch.

Differences in radial spread were measured forward and aft of the welding torch. For a given gas flow rate the detachment of the radial wall jet occurred further from the welding torch in the forward direction. This corresponded with greater differential velocity between the shielding gas and the parent material forward of the welding torch. Numerical equations generated from water modelling presented by Slater (2004) while not accounting for parent material velocity were in reasonable correlation with the experimental results recorded here.

Due to the greater radial spread in the forward direction the fume plumes were found to be asymmetric even when the torch was located vertically. The plume had a tendency to dissipate forward of the welding torch at typical shielding gas flow rates. Plume profiles were presented which showed higher shielding gas flow rates diluted the plume which decreased the peak concentration and increased the plume width.

The fume plume virtual origin was experimentally found to be approximately half the distance below the parent material surface than that determined by Slater (2004) from water modelling.

Chapter 7

Recommendations for further work

The work undertaken as part of this thesis was primarily focused on the application of laser techniques to the diagnostics of fume plumes. From this point further work in both improving laser diagnostics and applying the developed techniques can be suggested.

The presented work demonstrates that laser scattering can be used to image fume plume structure in GMAW and FCAW with very high resolution. Difficulty however is encountered when trying to relate scattered light intensity to the particulate concentration. Results would indicate that the optical properties of GMAW fume are constant across a range of variables. Even then difficulty is encountered in quantifying the scattered images to display particulate concentration. Using laser extinction as a calibration, as done with soot, would appear to be a viable method in fume. In the presented work, optical properties from particles similar to that of welding fume were used to determine mean fume volume fraction from extinction. Optical properties obtained for actual welding fume plumes would assist in validating laser extinction and laser scattering. Further work is required to measure the optical properties across a range of welding variables and processes. Ideally this would involve the determination of Stokes' matrices to classify the interaction between a light source and the particles from a particular process. From this point a Mie solution, or appropriate approximation, could be made to interpret light scattering or extinction through a plume. While requiring special optical equipment the process of measuring the optical properties of particulates would appear well documented in literature. Difficulty may be encountered in generating a consistent and controllable fume source for data collection.

Considering the number of variables involved with welding processes there is significant scope for further investigation of plume structure and concentration. The work presented in this thesis concentrated towards laser diagnostics. Research dedicated to welding fume plume distribution would optimise equipment and welding variables to the investigation of plume phenomena. For example the use of traverse to lay weld deposits onto a flat surface would coincide better with previous research and modelling than the round drum used here. Imaging the plume structure at a higher speed than

the 10 frames per second used in the work undertaken here would be advantageous.

Further research using laser scatter could be used to determined the dissipation into the wider work space and the effectiveness of ventilation strategies. The demonstrated ability to image the fume plume structure so close to the arc has specific application to the optimisation of on torch fume extraction. Further research into improving the extraction rate while minimising torch size would have direct benefits to industry.

While undertaking this research the influence of uncontrollable welding factors on fume formation was noticed. That is seemingly similar welding variables resulted in significant changes in arc stability and fume formation. Further fundamental research needs to be conducted into how things such as wire feedability influences arc stability and fume formation. For example Slater (2004) found that non-copper coated wire produced less fume. However the mechanism by which this reduction occurred isn't clearly understood and may have more to do with wire feedability then the lack of copper cladding.